NASA CONTRACTOR REPORT

NASA CR-1596

ASSESSMENT OF SPACE VEHICLE AEROACOUSTIC-VIBRATION PREDICTION, DESIGN, AND TESTING

by

Harry Himelblau
Space Division of North American Rockwell Corporation

C. Myron Fuller
McDonnell Douglas Astronautics Company - Western Division

Terry D. Scharton
Bolt Beranek and Newman Inc.

Prepared by
McDONNELL DOUGLAS ASTRONAUTICS COMPANY
Huntington Beach, Calif.
for Langley Research Center

NATIONAL AERONAUTICS AND SPACE ADMINISTRATION • WASHINGTON, D. C. • JULY 1970

NASA CR-1596

ASSESSMENT OF SPACE VEHICLE AEROACOUSTIC-VIBRATION PREDICTION, DESIGN, AND TESTING

By Harry Himelblau

Space Division of North American Rockwell Corporation

C. Myron Fuller

McDonnell Douglas Astronautics Company - Western Division

and

Terry D. Scharton

Bolt Beranek and Newman Inc.

Prepared under Contract No. NAS 1-6024 by
McDONNELL DOUGLAS ASTRONAUTICS COMPANY - WESTERN DIVISION
Huntington Beach, Calif.

for Langley Research Center

NATIONAL AERONAUTICS AND SPACE ADMINISTRATION

For sale by the Clearinghouse for Federal Scientific and Technical Information
Springfield, Virginia 22151 – CFSTI price $3.00

ABSTRACT

This document provides a general survey of the field of space-vehicle structural vibration, which is induced by acoustic and aerodynamic noise and certain mechanical excitation. The fundamental sources and mechanisms of the vibration are identified; analytical methods of vibration prediction are described. Laboratory, field, and flight testing are discussed, including problems of qualification- and acceptance-test selection. Although the advantages and limitations of the various analytical and experimental methods are assessed, specific methods are seldom recommended because selection of the methods is often influenced by the circumstances of the particular application, and by economic and scheduling factors.

A list of program objectives is furnished outlining a general procedure for ensuring the structural integrity and operational performance of launch vehicles and spacecraft exposed to structural vibration. Then, to ensure that these objectives are satisfied, general recommendations are made for implementing the various design, analysis, and testing techniques during various phases of vehicle development.

5.1.1.2 Applicability to Space-Vehicle Structures 54
5.1.1.3 Assessment 60
5.1.2 Vibration Tests 61
5.1.2.1 Test Classification and Philosophy 61
5.1.2.2 Test Facilities 65
5.1.2.3 Qualification-Test Requirements and Their Selection 70
5.1.2.4 Alternatives for Insufficient-Force Capacity 79
5.1.2.5 Acceptance-Test Requirements and Their Selection 80
5.1.2.6 Design-Development Test Selection 81
5.1.2.7 Assessment 81
5.1.3 Acoustic Tests 81
5.1.3.1 Test Facilities 81
5.1.3.2 Comparison with Vibration Tests 83
5.1.3.3 Test Requirements and Their Selection 85
5.1.3.4 Assessment 87
5.1.4 Combined Environmental Testing 89
5.2 Field Testing 90
5.3 Flight Testing 93

6. OBJECTIVES OF SPACE-VEHICLE DESIGN DEVELOPMENT FOR VIBRATION 97

7. RECOMMENDATIONS FOR IMPLEMENTING VARIOUS DESIGN, ANALYSIS, AND TESTING TECHNIQUES 99

7.1 Preliminary Design Phase 99
7.2 Early Development Phase 102
7.3 Last Development Phase 102
7.4 Flight-Test Phase 103

8. CONCLUDING REMARKS 105

APPENDIX Internal Force-and-Moment Vibration-Response Equations for Structures Exposed to Aeroacoustic Noise 107

REFERENCES 115

FIGURES

1	Vibration measured on the S-IVB stage of the uprated Saturn I space vehicle during Apollo-Saturn flight SA-203	2
2	Rocket-engine acoustic noise sources and directivity patterns to the space vehicle during liftoff or static firing	13
3	Schlieren shadowgraph of the aerodynamic flow field of an Apollo-Saturn model in a wind tunnel, showing turbulence, shock waves, and separated flow	15
4	A lumped-parameter model of a section of a space vehicle	18
5	Longitudinal cross-correlation of aerodynamic noise during the transonic period for two microphones located 40 in. apart on the external surface of the Apollo service module	21
6	Material-damping properties for various aerospace structures	23
7	Diagrammatic for determining vibration response to multiple sources	25
8	Fatigue curve for a typical aerospace material under sinusoidal loading	26
9	Ratio of the incomplete to the complete gamma function ($0 \leq \tilde{q} \leq 5$)	28
10	Ratio of the incomplete to the complete gamma function ($0 \leq \tilde{q} \leq 50$)	29
11	Plot of exponential constant α_o to be used in determining threshold crossing probability	31
12	Idealized representation of a simple space-vehicle structure used for predicting the space-average response of external and internal structure at higher frequencies by statistical-energy analysis	34
13	Space-average acoustic acceptance for an idealized representation of space-vehicle external structure	35
14	Vibration-transfer function between external and internal structure for an idealized representation of a space vehicle	36
15	Sound-pressure-level contours for the B-58 in the 300- to 600-Hz octave band	38
16	Vibration-prediction curves for Mahaffey-Smith and Brust-Himelblau methods in the 300- to 600-Hz octave band	39
17	Comparison of narrow-band, one-third octave-band, and octave-band spectral analyses of the same random-vibration measurement	41
18	Contribution to the rms acceleration from multimodal response as measured on several missiles	42
19	Vibration-prediction curves for Franken and Winter methods	44
20	Vibration efficiency of aerodynamic noise relative to acoustic noise	45
21	Vibration-reference spectra for Barrett method on 50 flight measurements on the aft skirt of Saturn I fuel tanks	50

22	Comparison of vibroacoustic-transfer functions for Snark missile structure and two one-quarter scale models	60
23	Structural details of the Apollo boilerplate service module	62
24	Comparison of Apollo boilerplate service module vibration-strain spectra	63
25	Comparison of Apollo boilerplate service module vibration-acceleration spectra	63
26	Comparison of vibration-strain spectra for prototype and model panels excited by jet noise	64
27	Laboratory vibration test of the Ranger spacecraft	66
28	Laboratory vibration tests of the Gemini spacecraft in the vertical and horizontal directions	67
29	Laboratory vibration test of the Surveyor spacecraft	68
30	Laboratory vibration-test facility of the thrust structure and aft skirt of the S-II stage, Saturn V launch vehicle	69
31	Simplified schematic diagram of a typical system for performing sinusoidal-vibration tests	70
32	Simplified schematic diagram of a typical system for performing random vibration tests	71
33	Comparison of spectral envelope for 8 and 180 vibration measurements made on the external panels of the Apollo service module during acoustic testing	76
34	Predicted vibration spectrum and a five-segment spectral envelope	78
35	Random vibration-test spectrum consisting of high-level narrow band ''spikes'' superimposed on lower-level wideband spectrum	79
36	Acoustic test of the OGO spacecraft near the discharge nozzle of a large blowdown wind tunnel	82
37	Laboratory acoustic test of the thrust structure, aft skirt, and interstage of the S-II stage, Saturn V launch vehicle in a reverberant test facility	83
38	Laboratory acoustic test of the Apollo spacecraft in a progressive test facility	84
39	Comparison of vibration spectra from acoustic test with flight and with original design and test requirement	88
40	Laboratory test facility for combined sustained acceleration-vibration-acoustic noise-altitude environmental testing of space-vehicle hardware	91
A-1	Forces and moments on a shallow shell element	107

ASSESSMENT OF SPACE VEHICLE AEROACOUSTIC-VIBRATION PREDICTION, DESIGN, AND TESTING

By Harry Himelblau, Space Division of North American Rockwell Corporation; C. Myron Fuller, McDonnell Douglas Astronautics Company - Western Division; and Terry D. Scharton, Bolt Beranek and Newman Inc.

1. INTRODUCTION

Various load and environmental conditions are applied to a space vehicle, its subsystems, or assemblies during a mission – conditions that must be considered in design and test to avoid mission failure or degradation. Mechanical vibration of the structure is an extremely important condition to be considered, since it may cause overstress or fatigue of the structure and equipment, or may cause malfunctions of the equipment. This report restricts itself to consideration of the integrity of structure; the performance and structural integrity of equipment will not be discussed herein. This document does however include a discussion of vibration design and test requirements for this equipment.

Structural vibration is often most predominant during the launch-and-ascent phase of flight, and, depending upon the mission parameters and the structural configuration, may be critical during space flight and/or atmospheric entry and flight. For example, figure 1 shows the time history of the instantaneous vibration and the time-averaged rms vibration of a point on the S-IVB stage of the uprated Saturn I space vehicle, measured during the launch-and-ascent phase. Significant vibration is observed during liftoff (T + 0 sec), the transonic period (T + 47), the supersonic period near the occurrence of the maximum aerodynamic pressure q_{max} (T + 63), and during S-IVB powered flight (from T + 147 to T + 434). Vibration spectra, in the form of acceleration spectral density vs frequency plots, are also shown for liftoff, transonic, and two periods during the S-IVB powered flight. Depending upon the structural and aerodynamic configuration of the vehicle and the location of the vibration-monitoring points on the structure, the relative magnitude of the vibration during these periods will vary considerably from that shown in figure 1. Locations near rocket engines, for example, may undergo high vibration during propulsion operation, and relatively low vibration at other time periods. Locations near the forward end of the vehicle, such as spacecraft structures, may undergo high vibration during transonic and/or supersonic periods, and relatively low vibrations at other times. Before flight, vibration may be applied to the vehicle, its subsystems, or assemblies during transportation from the manufacturer to the launch pad, or during the static firing of propulsion subsystems. Table I lists the mission phases and time periods where significant vibration may possibly be observed.

Usually, the attempt is made to integrate these environments into the vehicle development program by means of design and test requirements. The selection of these requirements can be vital to mission success and cost, and is therefore one of the subjects of this report. Requirements which are too low,

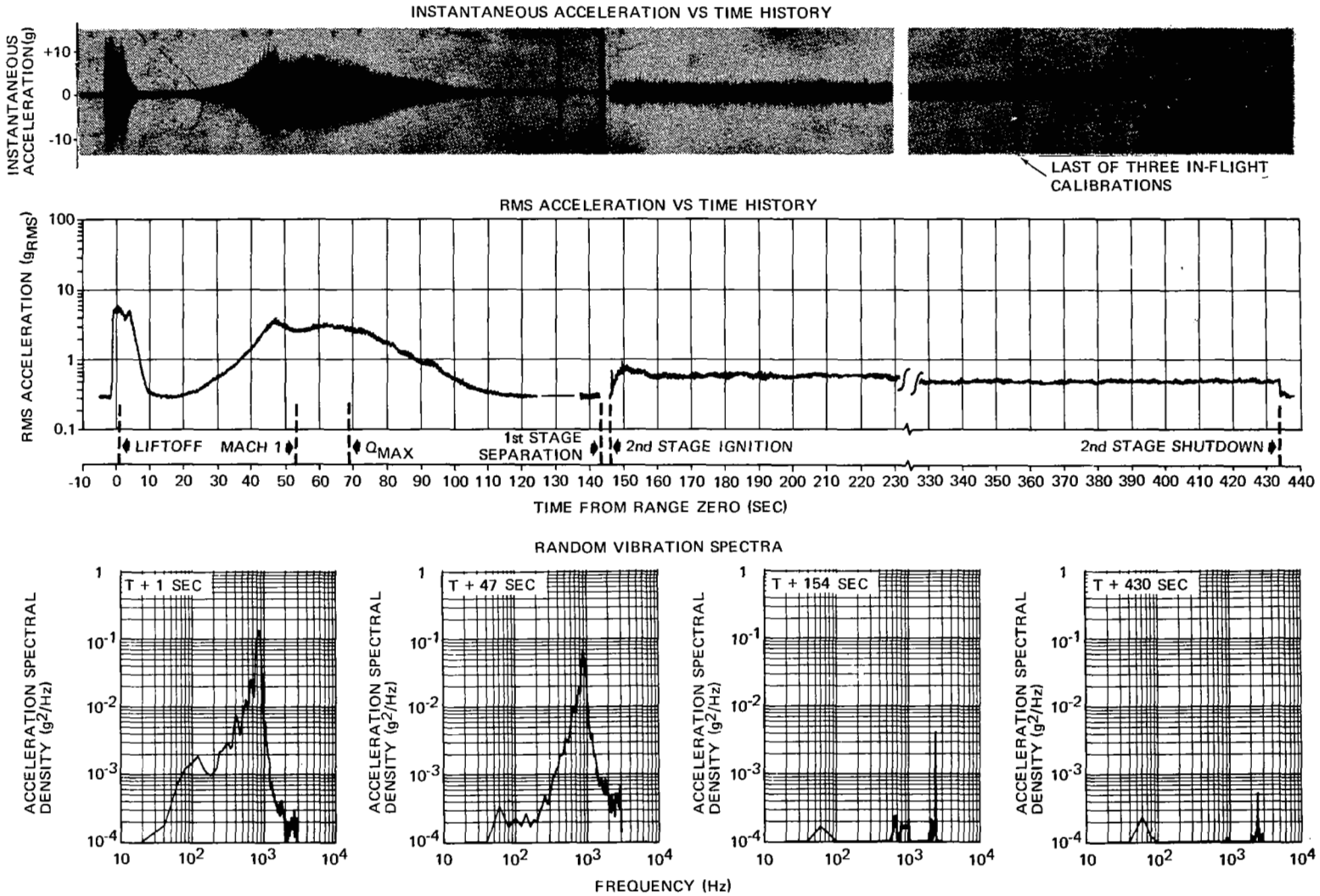

Figure 1.–Vibration measured on the S-IVB stage of the uprated Saturn I space vehicle during Apollo-Saturn flight SA-203.

TABLE I.—SIGNIFICANT STATIONARY VIBRATION ENVIRONMENTS

Mission phase	Source of vibration	Type, source, and magnitude of vibration
Prelaunch	Acceptance testing	Random and/or periodic vibration from laboratory vibration and/or acoustic test, if used. Often high magnitude.
	Transportation	
	Land	Random vibration from truck or inplant dolly. Periodic vibration also possible. Random and periodic vibration from railroad transportation. Usually (but not always) low magnitude and long duration.
	Air	Random vibration from jet aircraft. Periodic vibration also possible adjacent to jet engines. Periodic vibration from propeller aircraft. Random and periodic vibration from turboprop aircraft. Random vibration from gust loading on all aircraft at low frequencies. Usually (but not always) low magnitude and long duration.
	Sea	Random and periodic vibration from ships. Almost always low magnitude (except near fantail) and long duration.
	Static firing	Random vibration from engine-induced acoustic noise. Often high magnitude. Directly transmitted random and/or periodic vibration from engines, turbopumps, and auxiliary equipment. Often high magnitude near source.
	Ground wind loads	Random and/or periodic vibration at low frequencies. Large limit-amplitude self-excited oscillation may exceed limit stresses if system is unstable.

TABLE I.–SIGNIFICANT STATIONARY VIBRATION ENVIRONMENTS – Continued

Mission phase	Source of vibration	Type, source and magnitude of vibration
Launch and ascent	Liftoff	Same as ''static firing,'' except vibration spectra may be different.
	Wind loads – engine interaction	Transient or periodic vibration at low frequencies. Divergent vibration if system is unstable.
	Aeroelastic interaction and flutter	Transient or periodic vibration of structural assemblies exposed to aerodynamic flow. Divergent motion or limit amplitude if system is unstable.
	Pogo interaction	Transient or periodic vibration along the longitudinal vehicle axis, from engine-thrust oscillations, causing structural vibration of propulsion assemblies, and in turn causing propellant-flow and engine-thrust oscillations. Divergent motion or limit amplitude if system is unstable.
	Propellant sloshing	Transient or periodic vibration at low frequencies. Divergent if slosh-structure-control system is unstable.
	Transonic buffeting	Random vibration from aerodynamic turbulence, sometimes ''amplified'' by unstable shock waves. May cause local or overall vehicle vibration. Often high magnitude, usually at forward end of vehicle, and sometimes transient.
	Supersonic flight	Random vibration from aerodynamic turbulence in relatively stable q_{max} boundary layer. Often high magnitude, usually at forward end of vehicle.
	Booster or upper-stage operation	Directly transmitted random and/or periodic vibration from engines, turbopumps, and auxiliary equipment. Often high magnitude near source.

TABLE I.-SIGNIFICANT STATIONARY VIBRATION ENVIRONMENTS – Concluded

Mission Phase	Source of vibration	Type, source and magnitude of vibration
Launch and ascent (concluded)	Abort	If abort rocket is aft, same as 'Booster or upper-stage operation.'' If abort rocket is forward, random vibration from exhaust flow. Possible interaction with or increased transonic buffeting or boundary layer turbulence. Often high magnitude.
Space flight	Booster or upper-stage operation	Same as under ''Launch and ascent.''
Entry and atmospheric flight	Hypersonic flight	Random vibration from aerodynamic turbulence. Usually lower magnitude due to low density of boundary layer and, in some cases, separated base flow.
	Deceleration loads	Random vibration from retrorocket exhaust flow. Possible interaction with hypersonic turbulence. Random vibration from aerodynamic turbulence on parachute. Usually low magnitude.

compared to the vehicle environment, may jeopardize the mission because of failure to discover design or fabrication inadequacies. On the other hand, excessive requirements may obtain unnecessarily high reliability, and will usually cause excessive costs, schedule slippage, and/or excessive vehicle weight.

By definition, structural vibration is an oscillatory motion of a mechanical system relative to a frame of reference, and is described by certain parameters which are considered to be stationary or steady state. This vibration may be periodic or random, or both. In space vehicles, this vibration occurs only for definable periods of time, and therefore it is theoretically transient. However, there are several phases of the mission where the significant parameters defining the vibration (such as the rms value) are invariant or are slowly changing with time, as observed in figure 1. During these periods, the effects of the vibration on vehicle integrity and performance may be determined adequately through the use of stationary or steady-state assumptions in the

vibration analysis and test. The minimum period that a vibration may be considered as stationary is usually dependent on the characteristics of the source, the structural characteristics (especially the damping), the failure and malfunction parameters, the accuracy desired, and sometimes common aerospace practice or the investigator's judgment. Vibration not considered sufficiently stationary or steady state should be considered as transient, and is not discussed in this report.

The sources of space-vehicle vibration discussed in this report are acoustic noise, aerodynamic noise, and mechanically induced excitation. The predominant frequencies of these sources usually cover a wide range, often from 10 Hz to 10 kHz. In most locations on the vehicle, however, vibration above 2 kHz is seldom a cause of failure, so that the main emphasis is devoted to the range from 10 Hz to 2 kHz. In this frequency range, subsections of the vehicle often vibrate independently of other subsections (e.g., entire stages, individual skin panels, longerons, stiffeners, or frames, or equipment items on structure). At lower frequencies, the vehicle usually vibrates ''as a whole'' in its various lateral, longitudinal, and torsional modes. Often, this behavior begins to disappear before the 10th lateral mode, whose resonant frequency usually varies inversely with the size of the vehicle. In the larger space vehicles, this resonant frequency usually occurs below 25 Hz.

It should be emphasized that the initial design of the space vehicle is almost never made considering structural vibration. Most vehicle structures are initially designed to static and sometimes thermal loads, with some overdesign factors specified for such additional loads as structural vibration. It will be necessary to ascertain whether enough overdesign has been incorporated to obviate the need to redesign, considering structural vibration and other loads and environments.

2. SYMBOLS

A	area of structure exposed to spatially distributed applied loading, $in.^2$
a	radius, in.
$B_p(x,\tilde{x})$	transfer function between internal force or moment at location x and applied force at location $\tilde{x}$
$[C]$	damping matrix, lb-sec/in.
$C_p(\xi,\xi',f)$	cospectral density function of fluctuating pressures at frequency f and locations ξ and ξ', $(psi)^2/Hz$
$C_r(f)$	ratio of vibration response to applied loading at frequency f
c	specific heat (subscripts denote medium), $in.^2/sec^2\ ^oF$ or Btu in./lb $sec^2\ ^oF$
c_a	speed of sound in acoustic medium, in./sec
c'_L	speed of longitudinal waves in a plate or shallow shell (subscripts denote structural system), in./sec
D	fatigue damage; vehicle diameter, in.; flexural rigidity, in.-lb
$\mathcal{Q}$	inplane rigidity, lb/in.
E	Young's modulus, psi
F, $F(\tilde{x},t)$	instantaneous external force (subscripts denote single amplitude or source), lb
f	frequency, Hz
f_c	acoustic-structure coincidence frequency, Hz
f_i, f_n	natural frequency in i^{th} mode, Hz
f_r	ring frequency, Hz
$G_{IK}(f)$	cross-spectral density functions for sources I and K at frequency f

$G_p(\xi,\xi',f)$	cross-spectral density function of fluctuating pressures at frequency f and locations ξ and ξ' of the structure exposed to the pressure field, $(psi)^2/Hz$
$G_{pr}(f)$	reference pressure spectral density function at frequency f, $(psi)^2/Hz$
G (x,f)	spectral density function of parameter at location x and frequency f (subscript denotes parameter), $(...)^2/Hz$
G ($\tilde{x},\tilde{x}'$,f)	cross-spectral density function of parameter at locations $\tilde{x}$ and $\tilde{x}'$ (subscripts denote parameter), $(...)^2/Hz$
g	acceleration due to earth gravity, $in./sec^2$
$H_i(f)$	frequency response function in i^{th} mode (asterisk denotes complex conjugate)
$\underline{H}_{Ix}(f)$	transfer function between any response parameter at location x and any applied loading parameter I (asterisk denotes complex conjugate)
h(x)	thickness of structure at location x (subscripts denote core half-thickness and face-sheet thickness for sandwich shell), in.
I_{sp}	specific impulse of engine, sec
$I(u,\tilde{q})$	ratio of incomplete to complete gamma function
$j_{ik}^2(f)$	cross-joint acceptance function of pressure field with the i^{th} and k^{th} structural mode shapes.
[K]	stiffness matrix, lb/in.
K_d	ratio of stress to displacement, lb $sec/in.^3$
K_f	stress-concentration factor in fatigue
K_ϕ	mode-shape factor
$\mathscr{K}$	sine-to-random fatigue conversion factor
k	thermal conductivity (subscripts denote medium), lb/sec ^oF or Btu/in. sec ^oF

ℓ	length, in.
M	moment-per-unit length (subscripts denote directions), lb
[M]	mass or inertia matrix, lb-sec^2/in.
M_i	modal or generalized mass in i^{th} mode, lb sec^2/in.
m	mass of structure, lb-sec^2/in.
N	number of modes; number of measurements; number of engines; inplane-force-per-unit length (subscripts denote directions), lb/in.
N_i	number of cycles to failure at stress amplitude s_i
n_i	number of applied cycles at stress amplitude s_i; scale factor
P_o	static or absolute ambient pressure, psi
$P_T(\beta \geq \beta_o)$	probability that stress peak s_i will exceed threshold stress s_u^* during exposure time T
p, $p(\xi,t)$	instantaneous pressure at location ξ, psi
$p_p(s_i)$	probability density of stress peaks, $(psi)^{-1}$
{Q}	column matrix of applied generalized forces in i^{th} normal modes, lb or in. lb
Q, Q_i, Q_n	quality factor or resonant magnification in i^{th} mode; transverse force-per-unit length (subscripts denote directions), lb/in.
$Q_p(\xi,\xi',f)$	quad-spectral density function of fluctuating pressures at frequency f and locations ξ and ξ', $(psi)^2$/Hz
q	aerodynamic pressure, lb/ft^2
{q}	column matrix of coordinate displacements in i^{th} normal modes, in. or radians
$R_p(\xi,\xi'\tau)$	cross-correlation function of fluctuating pressures at locations ξ and ξ' and time delay τ, $(psi)^2$

R_{rad}	radiation resistance of structure in acoustic medium, lb-sec/in.
S	total area of structure, $in.^2$
s	stress (subscripts denote type), psi
T	time at liftoff; exposure time, sec; engine thrust, lb
T_f	time-to-failure, sec
t	time, sec
u, u(x,t)	instantaneous displacement in X_1 direction at location x (subscripts denote partial spatial derivatives), in.
v, v(x,t)	instantaneous displacement in X_2 direction at location x (subscripts denote partial spatial derivatives), in.
W	weight, lb
w, w(x,t)	instantaneous displacement in Z direction at location x (subscripts denote single amplitude or partial spatial derivatives), in.
X_i	rms value of i^{th} measurement, g
x,x',$\tilde{x}$,$\tilde{x}'$	locations on structure (underline denotes dummy variable to be integrated)
Z(f)	mechanical driving point impedance of system at frequency f
z	distance from neutral plane in Z direction, in.
α	logarithmic slope of s_i vs N_i curve
α_3	coefficient of skewness for statistical distribution
$\Gamma(\tilde{q} + 1)$	complete gamma function of parameter $\tilde{q}$
γ	mass-attenuation factor
δ^2	multimodal-response factor
ζ_i	viscous damping ratio in i^{th} mode

η	structural damping-loss factor or coefficient; coupling-loss factor between systems (subscripts denote structural or acoustic systems)
Θ	phase, rad; time-average modal energy for structural and acoustic modes, in.-lb
μ	coefficient of viscosity, lb-sec/in.^{2}
ν	Poission's ratio (subscripts denote sandwich shell)
ξ, ξ'	locations on part of structure exposed to spatially distributed applied loading (underline denotes dummy variable to be integrated)
π_i	i^{th} dimensionless group of parameters
ρ_a	mass density of acoustic medium, lb-sec^2/in.^{4}
ρ, $\rho(x)$	mass density of structure at location x, lb-sec^2/in.^{4}
σ	standard deviation of parameter (subscript denotes parameter); rms value when mean value is zero or can be ignored
τ	time delay for cross-correlation analysis, sec
$\phi_i(x)$	mode shape at location x in Z direction and i^{th} mode
$\varphi_i(x)$	mode shape at location x in X_2 direction and i^{th} mode
$\psi_i(x)$	mode shape at location x in X_1 direction and i^{th} mode
$\lvert \ldots \rvert$	absolute value of parameter
$\langle \ldots \rangle$	spatial average of parameter
$\overline{\ldots}$	time average of parameter
$\underline{\ldots}$	dummy variable to be integrated

SUBSCRIPTS

a	acoustic medium (usually air); accelerometer
cr	criteria
e	endurance limit; external structure; equipment

F	external force
f	fluid, failure
i	i^{th} mode; i^{th} measurement; internal structure; peak value
k	k^{th} mode; number of frequency band
m	model or subscale structure
max	maximum
min	minimum
n	n^{th} mode; new vehicle
o	single amplitude
P	internal force or moment
p	pressure; prototype or full-scale structure
r	reference vehicle
s	structure
u	ultimate; displacement in X_1 direction
v	displacement in X_2 direction
w	displacement in Z direction
1,2,3	system numbers; directions; partial spatial derivatives

3. FUNDAMENTAL SOURCES OF VIBRATION

3.1 ACOUSTIC NOISE FROM PROPULSION-SYSTEM OPERATION

The fundamental sources of structural vibration are many and varied. Rocket engines emit high-velocity exhaust gases which mix with the ambient air, causing turbulence in the process. The pressure fluctuations of the turbulence are transmitted to the surroundings, including the space vehicle, as acoustic noise at the speed of sound. The distributed acoustic field progresses over the vehicle surface and causes the structure to vibrate. Since the turbulent mixing is a random process, the acoustic noise and the structural vibration are also random. Observations show that most of the higher-frequency noise is generated by smaller-scale mixing near the engine, while most of the lower-frequency noise is generated by larger-scale mixing further downstream.

If the launch pad or the test stand has a flame deflector, the exhaust gases are caused to mix differently with the ambient air than they would if no flame deflector were present, and the directivity of the acoustic noise changes relative to the surroundings, including the space vehicle, as shown in figure 2. Thus, the acoustic field changes, causing a change in the structural vibration. The launch pad or test stand, the surrounding terrain, and climatic conditions may have similar influences on the acoustic field by providing varying degrees of sound reflection and shielding.

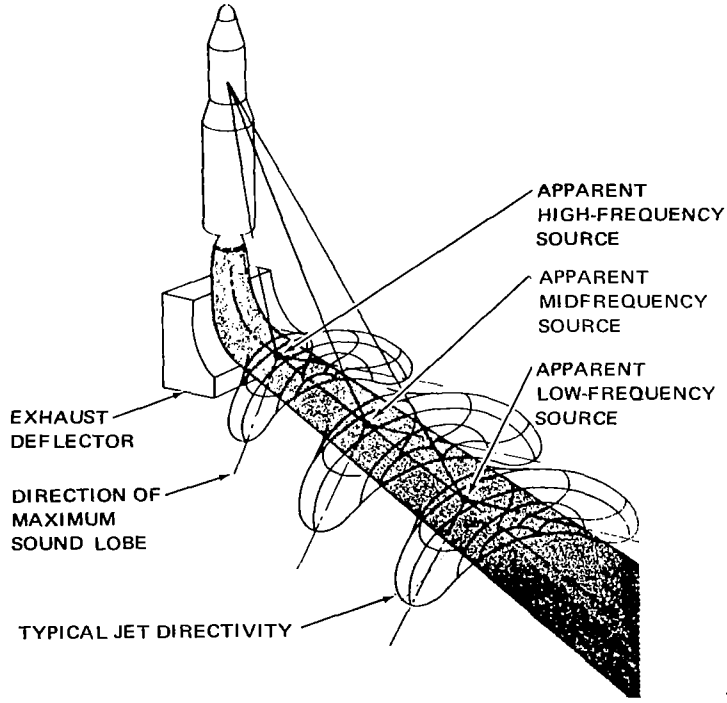

Figure 2.–Rocket-engine acoustic noise sources and directivity patterns to the space vehicle during liftoff or static firing.

Some space vehicles use multiengine arrangements. These have effects on the turbulence generation and the acoustic noise transmission that are different from single-engine effects. Rocket-engine noise characteristics are summarized in references 1 through 7, which also reference other pertinent documents.

3.2 MECHANICAL VIBRATIONS FROM PROPULSION-SYSTEM OPERATION

The mixing of propellant gases inside the rocket-engine combustion chamber generates fluctuating pressures (as well as static pressures) on the engine wall. The wall vibrations may be transmitted throughout the vehicle, but are often rapidly attenuated with distance from the source. In addition, acoustic resonances may occur in the combustion chamber. For a liquid-propelled rocket engine, these resonances may occur at fixed frequencies, while for a solid-propellant rocket motor, these resonances may occur at progressively lower frequencies as the propellant burns and the size of the combustion chamber increases. These resonances are substantially attenuated or eliminated during the design or development of the rocket engine. Failure to do so is one cause of engine explosion (refs. 8 through 11).

Turbopumps and other equipment often have rotating parts operating at high speed. Turbine-blade resonance and unbalance of rotating parts may cause periodic vibration throughout the vehicle, but this vibration is often rapidly attenuated with the increase of distance from the source.

3.3 AERODYNAMIC FLOW FIELD

As a space vehicle moves at high speed through the atmosphere, turbulence is generated by mixing in the boundary layer. The resulting pressure fluctuation is applied over the vehicle surface and causes the structure to vibrate. This pressure field, often called aerodynamic noise or buffeting, is transported down the vehicle surface at a speed which is somewhat less than the free-stream velocity of the vehicle. The speed of the aerodynamic flow seldom equals the speed of sound in air. As the vehicle cross-sectional area changes from fore to aft, shock waves occur in the aerodynamic flow, causing increases in the turbulence and fluctuating pressures. Examples of these shock waves and typical effects on the pressure field are shown in figure 3. Note that separated flow may occur on a conical section of the vehicle aft of a cylindrical section, and vice versa.

In the transonic regime, the shock waves, which have just formed at various locations, are often unstable and tend to move aft. During the launch-and-ascent phase, the vehicle speed is increasing in the transonic regime, so that a non-stationary or transient pressure field exists, causing a vibration of the structure.

In the supersonic regime, the shock waves are generally stable and less susceptible to speed or attitude changes. Thus, the fluctuating pressure field and structural vibration are more nearly stationary. Aerodynamic noise characteristics are summarized in references 6, 7, and 12 through 20, which also reference other pertinent documents. However, much research on aerodynamic noise is still needed before this environment can be adequately predicted.

SUPERSONIC (M = 1.10)

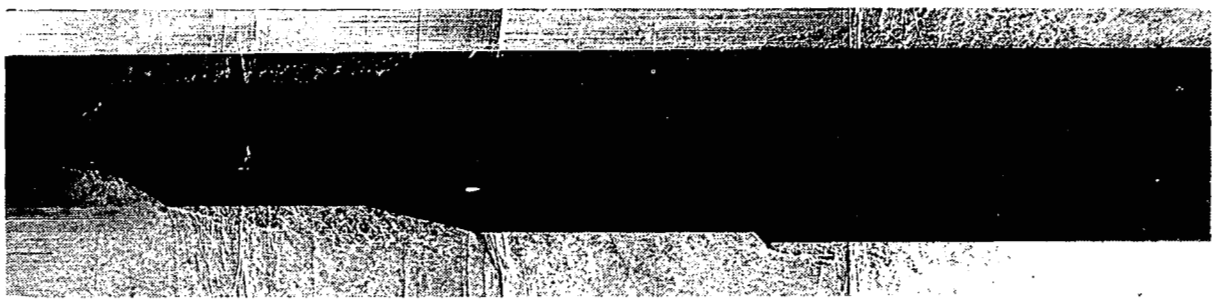

SUBSONIC (M = 0.90)

Figure 3.–Schlieren shadowgraph of the aerodynamic flow field of an Apollo-Saturn model in a wind tunnel, showing turbulence, shock waves, and separated flow.

Less information is available on fluctuating pressure fields in the hypersonic regime (important though they are during atmospheric entry), other than that they tend to cause less structural vibration (refs. 21 and 22). The exception is atmospheric entry of low-drag vehicles, where high vibration is observed at the lower altitudes (ref. 23).

Structural protuberances into the aerodynamic flow should also be considered, because they can cause added turbulence and fluctuating pressures. These protuberances may include ullage, control and retro-rockets, stabilization fins, electrical cabling and propellant lines or their shrouds, and communication antennas.

4. ANALYTICAL DETERMINATION OF VIBRATION

Various methods and combination of methods are available for determining structural integrity and predicting equipment-vibration requirements, especially during the early phases of vehicle development. These methods may be divided into the following three categories: (1) classical analysis, (2) statistical energy analysis, and (3) extrapolation.

4.1 CLASSICAL ANALYSIS

Deterministic or classical analyses are those in which (a) the vehicle structure or one of its sections is represented by a mathematical model; (b) the applied loading is described by its time history or loading spectrum, and in the case of aeroacoustic loading, by its spatial distribution over the exposed surface; and (c) the resulting vibration at various locations of the structure is calculated by the solution of equations of motion derived from the model. Descriptions of analytical methods may be found in references 24 through 29.

4.1.1 Selection of Mathematical Model

The selection of the mathematical model is influenced by the desired accuracy and frequency range, the details to be employed in describing the loading and the structure, and the cost of computation and model formulation. The mathematical model is an important element in vibration calculations. Careful consideration is usually given to stiffness and mass distributions, and boundary considerations in the synthesis of the model.

Basically, two types of models are available: (a) continuous - or distributed-parameter representations and (b) lumped- or discrete-parameter representations. Distributed representations are mostly used for fairly simple structures for which classical solutions are known, such as domes, conical and cylindrical shells, plates, and beams, all with simple boundary conditions (refs. 28 through 30). In addition, parametric studies of structural vibration often use a distributed representation (ref. 31). It is often found, however, that composite construction, complex boundaries (including joints and cutouts), and attached masses make a distributed analysis difficult to formulate, often inaccurate, and expensive or impossible to solve. Thus a lumped-parameter representation is usually preferred to model the structure. In addition, one form of lumped-parameter modeling, called finite-element modeling, is gaining wide usage, mainly because of its adaptability to matrix notation and high-speed digital computation (refs. 26, 32, and 33). Figure 4 shows a typical lumped-parameter model of a space-vehicle section. Rigid or lumped masses, whose weights are selected on the basis of the mass distribution of the structure, are not shown, but are placed at all connecting points of the model.

The accuracy of the resonant frequency, mode shape, and vibration stress and motion calculations will generally be highly dependent upon the number and location of these masses and the frequency considered. For the lower-order modes, some of the structural details may be compromised, while others may not. For example, a structure represented by a lumped-parameter model requires fewer lumped masses for the lower-order modes without significantly influencing the

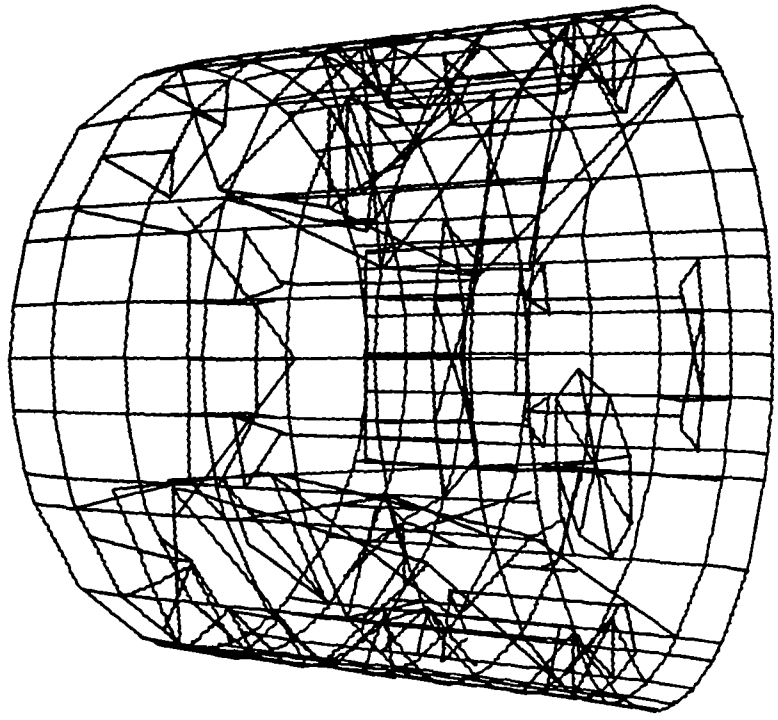

Figure 4.–A lumped-parameter model of a section of a space vehicle.

proper estimation of the resonant frequencies and mode shapes. At locations of high vibration stress (and thus, possible failure), however, the local details are vital for proper estimation. On the other hand, the structure requires more lumped masses for the higher-order modes to preserve resonant frequency and mode-shape accuracy, but there is often less likelihood of high stress points and thus fewer of these local details to consider. If many masses are used for the higher-order modes, the cost of computation is almost always unusually large and often overwhelming. Thus, the details of the lumped-parameter model should be selected with great care.

All real structures vibrate nonlinearly, so that the transfer function (i.e., the ratio of the response to the applied loading) varies with the magnitude of the loading. Unfortunately, there have been almost no nonlinear vibration analyses of mathematical models that approach the complexity of nearly all space-vehicle structures (ref. 34). However, as pointed out by Lyon (ref. 35), nonlinearities need not be considered unless their effects rival the uncertainty of the linear estimate. When sufficiently severe nonlinear behavior is expected, it is common practice to assume a linear model and perform the classical analysis using the linear values of structural stiffness and damping which represent the expected, or the minimum, effect of the nonlinearity on the response. The linear response is then scaled, using results of nonlinear vibration studies performed on simple models, such as those reviewed in reference 34, to provide an approximate or conservative estimate of the nonlinear

response. It is assumed hereafter that the nonlinearities are sufficiently small to permit the use of linear models.

4.1.2 Formulation and Solution of Equations of Motion

Regardless of the specific method of analysis used, such as those described in references 24 and 25, for a linear structure the mathematical formulation of the problem will lead to a set of equations of the form

$$[M]\{\ddot{q}\} + [C]\{\dot{q}\} + [K]\{q\} = \{Q\} \qquad (1)$$

where [M], [C], and [K] are the square matrices of mass (or inertia), damping, and stiffness coefficients, respectively (and are called the mass, damping, and stiffness matrices); and {q} and {Q} are the column matrices of the coordinate displacements and the applied forces, respectively. If the damping matrix can be diagonalized by the same transformation that uncouples the undamped system, classical normal modes exist [i.e., in each normal mode, the various locations of the structure vibrate in phase or 180 degrees out of phase (ref. 36)]. A well-known special case of classical normal modes is Rayleigh's proportional damping, where the damping matrix [C] is a linear combination of the stiffness matrix [K] and/or the mass matrix [M]. Otherwise, nonclassical normal modes exist, requiring special treatment (refs. 25 and 37). For classical normal modes, the solution of equation (1) will yield the resonant frequencies, mode shapes, and the vibration displacement to a given loading, which can then be used to determine structural adequacy and the motions and forces applied to equipment. For nonclassical normal modes, it is usually assumed that they are classical in order to avoid certain mathematical complexities in obtaining a nonclassical solution.

4.1.2.1 Natural Frequencies and Mode Shapes

The solution of the homogeneous form of equation (1) without damping (i.e., [C] = {Q} = 0) provides the resonant or natural frequencies and mode shapes which characterize the mathematical model and thus the structure. There are many methods available for calculating resonant frequencies and mode shapes. It is common to group them into three categories, depending upon their mathematical formulation: (1) energy methods, (2) differential equation methods, and (3) integral equation methods. Energy methods include Rayleigh's method (for the fundamental mode) and the Rayleigh-Ritz method (for higher-order modes).

Differential equation methods include the Holzer, Myklestad, and Thomson methods. Integral equation methods include the collocation, Galerkin and Stodola methods. These methods have their relative advantages and limitations as to their accuracy and their ease or cost of implementation, which are discussed in references 24, 25, and 33.

The principal use of modal data is the determination of the vibration response. The resonant frequencies and mode shapes are, however, also useful in selecting mounting locations for equipment and guidance sensors, such as gyros and accelerometers. This is especially important when known critical frequencies will cause detrimental effects to the equipment, structure, or control system.

4.1.2.2 Vibration Response

The response of a structure at various frequencies, or at desired intervals throughout the frequency range of interest, is usually calculated by summing the response in each of the orthogonal modes which characterize the structural vibration. Since the applied loading is generally random in nature, the response is also random. The vibration at location x of the structure is therefore expressed in terms of its spectral density function G(x,f). Extending the work of Wang and Uhlenbeck (ref. 38), references 25, 34, and 39 show that the displacement spectral density for location x at each frequency f due to a spatially-distributed applied loading is

$$G_w(x,f) = A^2 G_{pr}(f) \sum_{i=1}^{\infty} \sum_{k=1}^{\infty} \frac{\phi_i(x)\phi_k(x)H_i^*(f)H_k(f)j_{ik}^2(f)}{(2\pi)^4 f_i^2 f_k^2 M_i M_k} \tag{2}$$

where the cross-joint acceptance function is given by

$$j_{ik}^2(f) = \left[A^2 G_{pr}(f)\right]^{-1} \iint_A G_p(\underline{\xi},\underline{\xi}',f)\phi_i(\underline{\xi})\phi_k(\underline{\xi}')d\underline{\xi}d\underline{\xi}' \tag{2a}$$

the frequency response function by

$$H_i(f) = [1 - (f/f_i)^2 + i2\zeta_i f/f_i]^{-1} \tag{2b}$$

and the modal or generalized mass by

$$M_i = \int_S \phi_i^2(\underline{x})[\rho(\underline{x})h(\underline{x})]d\underline{x} \tag{2c}$$

and where f_i, ζ_i, and $\phi_i(x)$ are resonant frequency, viscous damping ratio, and mode shape (at location x) in the i^{th} mode and Z direction, respectively; $H_i^*(f)$, the complex conjugate of $H_i(f)$; A, the area of the surface exposed to the fluctuating pressure field; $[\rho(x)\ h(x)]$, the surface density (i.e., mass per unit area) of the structure at location x; S, total area of structure; and $G_{pr}(f)$, the reference fluctuating-pressure spectrum (often the spatial average over the exposed surface). The cross-spectral density function of the fluctuating pressures for locations ξ and ξ', of the exposed surface is

$$G_p(\xi,\xi',f) = C_p(\xi,\xi',f) - iQ_p(\xi,\xi',f) \tag{3}$$

where the cospectrum and the quadspectrum are

$$C_p(\xi,\xi',f) = 2\int_0^{\infty} [R_p(\xi,\xi',\tau) + R_p(\xi,\xi',-\tau)] \cos 2\pi f\tau d\tau \tag{3a}$$

$$Q_p(\xi,\xi',f) = 2\int_0^\infty [R_p(\xi,\xi',\tau) - R_p(\xi,\xi',-\tau)] \sin 2\pi f\tau d\tau \qquad (3b)$$

respectively (ref. 40). Thus, the pressure cross-correlation $R_p(\xi,\xi',\tau)$ must be measured or assumed as a function of the time delay τ for every combination of location points ξ and ξ'. References 7, 34, 39, 41, and 42 describe and discuss several distributions of cross-correlation functions that might be assumed for various aeroacoustic-noise loadings. Figure 5 shows the measured cross-correlation coefficients, $R_p(\xi,\xi',\tau)/\sigma_p(\xi)\sigma_p(\xi')$, in various frequency bands for a pair of points during flight, where $\sigma_p(\xi)$ is the rms pressure at location ξ.

Substitution of equation (3) into equation (2) will determine the displacement spectral density of the vibration response. Computer programs have been developed recently to calculate this response (refs. 43 through 46). The acceleration spectral density, usually preferred in specifying design and test requirements for equipment, can be found from $G_{\ddot{w}}(x,f) = (2\pi f)^4 G_w(x,f)$. Spectral density equations for moments and forces, from which the stresses throughout the structure can be calculated, are generally more complicated than equation (2) for displacement and appear in the appendix.

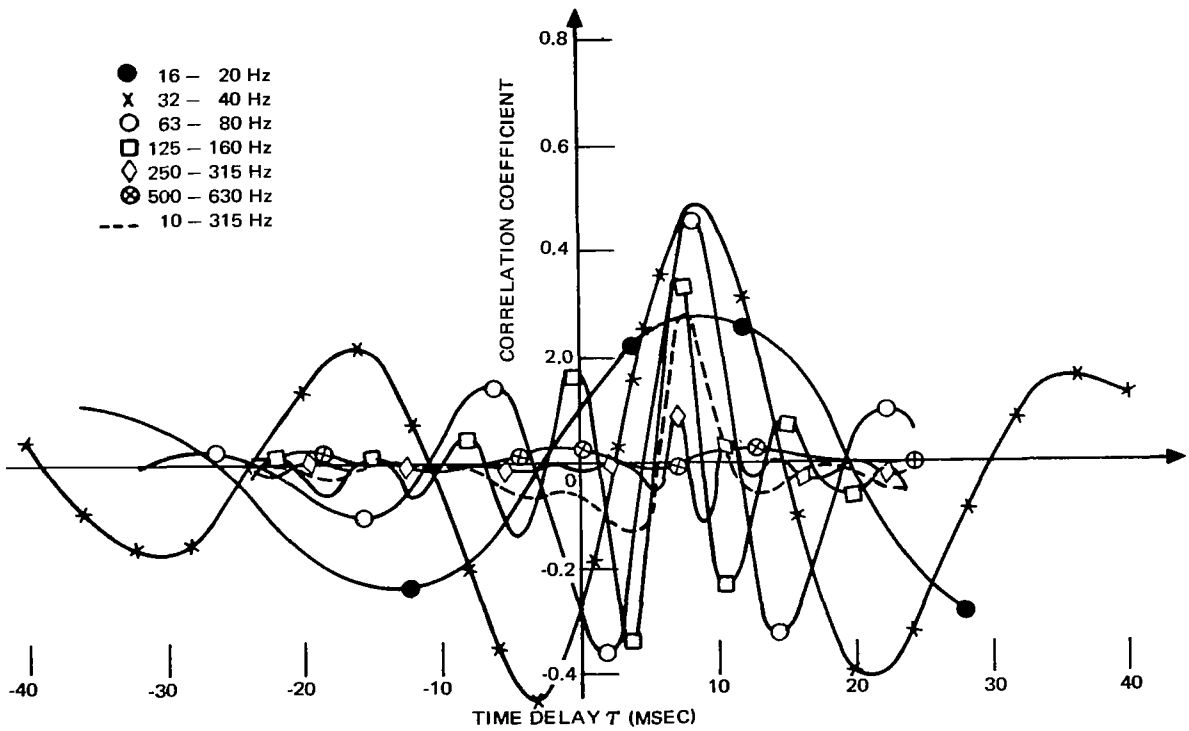

Figure 5.–Longitudinal cross-correlation of aerodynamic noise during the transonic period for two microphones located 40 in. apart on the external surface of the Apollo service module.

Considerable simplification of equation (2) can be achieved if the viscous damping ratio ξ_i in each mode is small, and the resonant frequencies f_i are well separated. Then at the resonant frequencies

$$G_w(x,f_i) \approx A^2 G_{pr}(f_i)\phi_i^2(x)Q_i^2 j_i^2(f_i)/(2\pi f_i)^4 M_i^2 \qquad (4)$$

where $Q_i = \frac{1}{2\zeta_i}$ = resonant magnification or quality factor in the i^{th} mode.

The analyst is confronted with two major problems in achieving an accurate prediction using equation (2) or (4). The first problem is the proper determination of the pressure cross-spectral density $G_p(\xi,\xi',f)$ or cross-correlation $R_p(\xi,\xi',\tau)$, used in calculating the joint acceptance. If the cross-correlation is assumed, the assumption may be invalid. If it is to be measured, it will be necessary to use a large number of wideband measurement channels during wind tunnel or flight test. Also, there will be an additional cost to provide accurate relative phase characteristics throughout the data acquisition and reduction process. Wind tunnel measurements may require the use of a low-noise wind tunnel. Otherwise, high tunnel noise may mask more moderate aerodynamic noise over the wind tunnel model. Also, the microphone size must be scaled. Since flight testing usually occurs late in the vehicle-development program and to avoid the cost of telemetered flight data, the cross-correlation is usually assumed, often inaccurately.

The second problem is the proper determination of the viscous damping ratios in the various modes. In equations (2) and (4), viscous damping is assumed because of its compatibility with the assumption of linear vibration and the subsequent ease in solving equation (1). Unfortunately, the damping of real aerospace structures is not viscous, but usually occurs in one or more of the following three forms: (1) material damping, (2) friction damping, and (3) acoustic radiation. Material damping is the inelastic behavior of the structure caused by internal friction during microscopic slip between interfaces within the nonhomogeneous material. Lazan has shown experimentally that the damping in a mode of vibration is dependent on the stress distribution through the material, i.e., on the maximum stress, as shown in figure 6, and the mode shape $\phi_i(x)$ (refs. 47 and 48). If the maximum vibration stress s_{max} is less than the endurance limit stress s_e of the material ($s_{max} < 0.7\ s_e$ in fig. 6), the damping changes only slightly with stress. If the maximum stress (from the contribution of all modes) exceeds the endurance limit, the damping increases significantly for most materials; but how it is distributed in the various modes is presently unknown. However, because of the increased damping, the life of the structure is prolonged. Friction damping is energy dissipation caused by slip or sliding between mated surfaces. Slip is relative motion within a region of the mated surface, whereas sliding occurs over the entire surface. Since most aerospace structures are comprised of parts that are

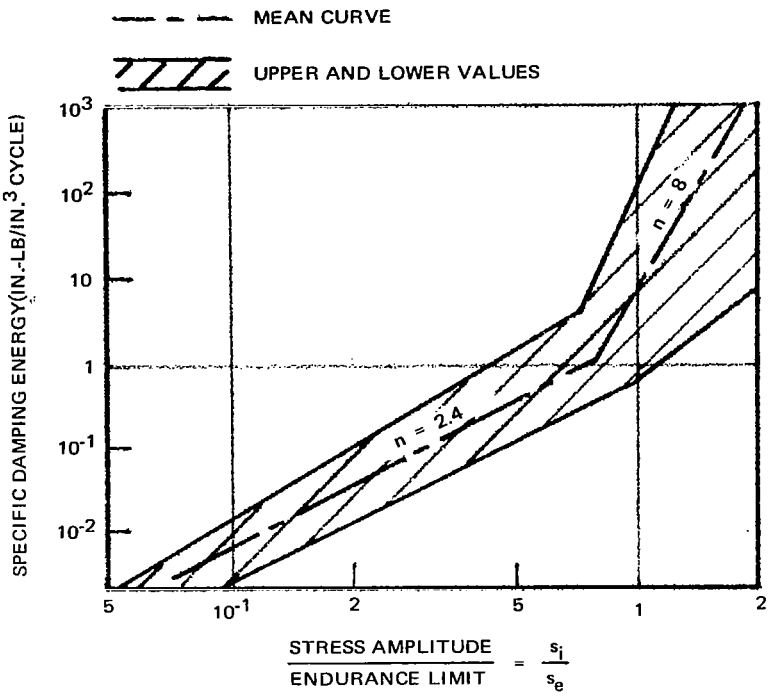

Figure 6.–Material-damping properties for various aerospace structures.

bolted or riveted together, friction damping is usually the dominant source of damping. The friction force per unit area during slip or sliding is approximately constant and is controlled by the pressure normal to the mated surfaces (refs. 47, 49, and 50). Because the friction force is not proportional to velocity, as is the viscous-damping force, a significant nonlinearity exists. Since it is approximately constant, friction damping is unfortunately less effective for controlling high vibration. Also, the static friction must be overcome for slip or sliding to occur. Thus, there is little or no friction damping at low vibration. The proper estimation of friction damping and its distribution in the various modes is very difficult. This is because of the distribution of the normal pressure over the mated surfaces between the fasteners, the variations between the forces exerted by the fasteners (due to the lack of control during manufacturing and fabrication), and the spatial variations in the static and kinetic coefficients of friction.

Acoustic radiation (i.e., air damping) is the generation of acoustic waves by the vibration of the structure and its propagation to other structures and the surrounding space. Radiation can be an appreciable form of damping for structures with low surface densities, such as panels, unless the structure vibrates at high altitude (where the radiation is reduced) or the surrounding space is reverberant. For simple cases, such as acoustic radiation from a rectangular panel into a free field, or a reverberant space with known surface characteristics, radiation damping in the various modes can be properly estimated with relative ease (refs. 51 through 56). In the more complex cases, the estimation can be quite involved.

There are also other forms of damping. One of them is viscoelastic, which damps by the inelastic behavior of certain rubber-like materials caused by nonlinear distortion of long-chain molecules. These materials are sometimes bonded as a layer or sheet to the surface of structural panels (often in combination with foil backing as a tape), or are sandwiched between adjoining structures in the joints or interfaces. References 47 and 57 may be used to estimate the contribution of viscoelastic damping.

Adjacent structures that have small spaces between facing surfaces, as might be found in joints that connect panels with stiffeners or other panels, can exhibit damping in the form of air ''pumping.'' (This dissipation is in addition to the friction, radiation, and viscoelastic damping discussed previously.) The contribution of air-pumping is described by Maidanik (ref. 58).

From this discussion it should be obvious that the proper estimation of the damping in the various modes will be difficult or impossible, except for the simplest structural configurations. Thus, to determine damping, there is usually great reliance on data from previous tests of similar structures. Even then, the data must be extrapolated to account for the differences between the structural configurations and the test and flight conditions. A conservative value is usually selected for the ''equivalent viscous'' damping ratio to be used in equation (2) or (4). Sometimes an iteration procedure is used to modify the damping selection after the vibration displacement and stress are calculated in the various modes. Nonlinear representation of damping in complex structures is considered to be beyond the present state of the art.

Vibration response is often caused by excitation from more than one source (e.g., aeroacoustic noise applied to the external vehicle surface, and mechanically transmitted vibration direct from the engines). During a particular phase of the mission, if only one source is dominant, as illustrated in figure 1, then only the response to that source need be considered. On the other hand, if two or more sources are effective during the period, multiple-input analysis may be used, as illustrated in figure 7. Reference 40 shows that the response spectral density for location x at each frequency f due to multiple loading is

$$G(x,f) = \sum_{I=1}^{N} \sum_{K=1}^{N} \underline{H}^{*}_{Ix}(f)\, \underline{H}_{Kx}(f)\, G_{IK}(f) \qquad (5)$$

where $\underline{H}_{Ix}(f)$ is the transfer function between the response (displacement, acceleration, moment, stress, etc.) at x and the applied loading (force, pressure, acceleration, etc.) at I; and $G_{IK}(f)$, the cross-spectral density between sources I and K. The units of $\underline{H}_{Ix}(f)$ will, of course, differ for each type of loading and response.

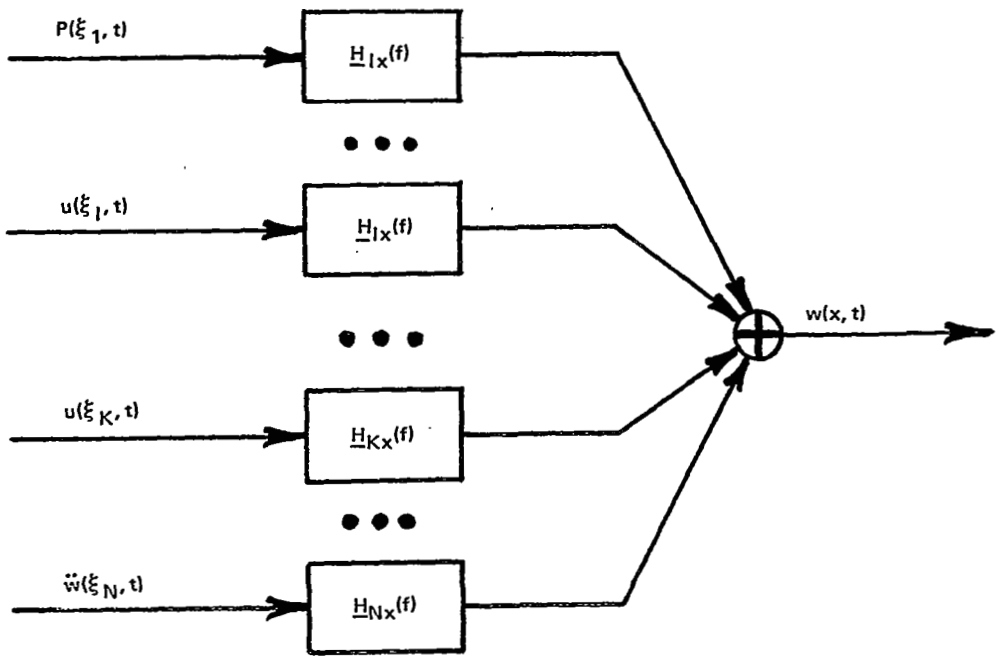

Figure 7.–Diagrammatic for determining vibration response to multiple sources.

Usually, the sources are independent of each other. Then equation (5) reduces to

$$G(x,f) = \sum_{I=1}^{N} |\underline{H}_{Ix}(f)|^2 G_I(f) \tag{5a}$$

Values of the transfer function may be determined analytically or experimentally. As shown in references 34, 39, and 59, the rms response σ (really the standard deviation) can be obtained from the variance

$$\sigma^2(x) = \int_{f_{min}}^{f_{max}} G(x,f)\, df \tag{5b}$$

When the applied loading is sinusoidal, which it is occasionally, the displacement at location x and frequency f of the sinusoid is

$$w(x,t) = w_o(x) \cos(2\pi ft + \theta) = \underline{H}_{Ix}(f)\, F_o(\xi) \cos 2\pi ft \tag{6}$$

where w_o and θ are the amplitude and phase of the response displacement, respectively; and $F_o(\xi)$, the amplitude of the applied loading at location ξ.

4.1.2.3 Failure Modes

Despite the fact that most space vehicles undergo relatively short exposure time to high vibration during flight, the most common cause of structural vibration failures is fatigue. The major factor is the relatively high frequency of the vibration. A great deal of experimental data are available on fatigue under conventional single-stress amplitude single-frequency sinusoidal stresses, and combined static and sinusoidal stresses (refs. 60 through 63). Some fatigue data are available for multistress amplitude single-frequency (''programmed'') stresses, but little for multifrequency or random stresses (ref. 64). In most cases, therefore, sinusoidal fatigue data must be extrapolated for use in estimating damage and possible failure under random vibration stress, as found in space vehicles.

Sinusoidal fatigue data are conventionally plotted as s_i vs N_i curves, as shown in figure 8, where s_i, s_u, and s_e are stress amplitude, ultimate tensile stress, and endurance limit, respectively; and n_i and N_i, the number of applied cycles and number of cycles to failure at stress amplitude s_i, respectively. The s_i vs N_i curve is dependent on the static stress, temperature, and frequency, since they affect the fatigue properties. If the stress contribution from one of the modes is much greater than the contribution from all other modes, the resulting narrow-band random stresses are quite similar to multistress amplitude single-frequency stresses. In these cases, it is possible to make two assumptions which are useful in calculating fatigue

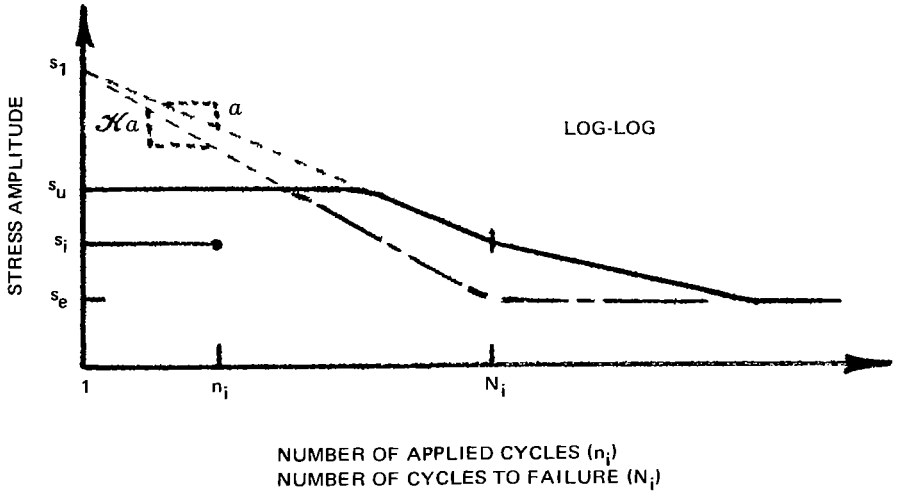

Figure 8.–Fatigue curve for a typical aerospace material under sinusoidal loading.

damage. First, it can be assumed that the damage D accumulates as in the Palmgren-Langer-Miner hypothesis, which states that $D = \sum (n_i/N_i)$. Using this hypothesis, fatigue failure will occur when D = 1. Second, it can be assumed that the stress peaks vary in accordance with the Rayleigh distribution:

$$p_p(s_i) = (s_i/\sigma_s^2) \exp [-s_i^2/2\sigma_s^2] \tag{7}$$

where σ_s is the rms stress. All of the various damage-accumulation hypotheses produce errors, the magnitude of which varies with the material and the sequence of the stress amplitudes applied. The Palmgren-Langer-Miner hypothesis is commonly used because it is no worse than the others, such as the Corten-Dolan hypothesis (ref. 65), and it is easy to apply. The actual distribution of random peaks generally approximates the Rayleigh up to fairly high stresses ($s_i < 3\sigma_s$), beyond which the Rayleigh assumption is almost always conservative. Applying a modification to the analysis first performed by Miles (ref. 66), the damage under narrow-band random stresses is

$$D = [f_n T/(s_1/\sigma_s)^{2\tilde{q}}][2^{\tilde{q}}\ \Gamma(\tilde{q}+1)][I(u_u,\tilde{q}) - I(u_e,\tilde{q})] \tag{8}$$

where f_n is the resonant frequency of the mode which has the dominant stress contribution; T, the exposure time of the applied loading; $\tilde{q} = \mathcal{K}\alpha/2$ (defined in the next paragraph); $\Gamma(\tilde{q}+1)$, the complete gamma function (ref. 67); and $I(u,\tilde{q})$, the ratio of the incomplete to the complete gamma function shown in figures 9 and 10 (ref. 68), $u_u = (\tilde{q}+1)^{-1/2}\ s_u^2/2\sigma_s^2$, and $u_e = (\tilde{q}+1)^{-1/2}\ s_e^2/2\sigma_s^2$. Crandall (ref. 59) has shown that the damage variability due to this randomness is usually small.

Material fatigue properties s_1 and α are shown in figure 8 as the ordinate intercept and slope of the s_i vs N_i curve. The sine-to-random fatigue conversion factor $\mathcal{K}$, necessary to provide random fatigue failure when D=1, varies with the material. Its value has been observed to vary over a wide range $(1/2) < \mathcal{K} < 2$, and is the subject of some disagreement (refs. 66 and 69). If more than one mode contributes to the stress, the distribution of peaks is a combination of the Rayleigh and the Gaussian distributions (ref. 70). Unfortunately, no widely acceptable damage theory has been developed for this case (ref. 64). However, the use of equation (8) will provide a conservative estimate of damage (ref. 71).

Another possible failure mechanism is the exceedance of the ultimate dynamic stress of the material by a single stress peak. This is a special case of the random-vibration problem, commonly called the threshold-crossing or first-passage problem, and specifically the probability $P_T(\beta \geq \beta_o)$ that a single

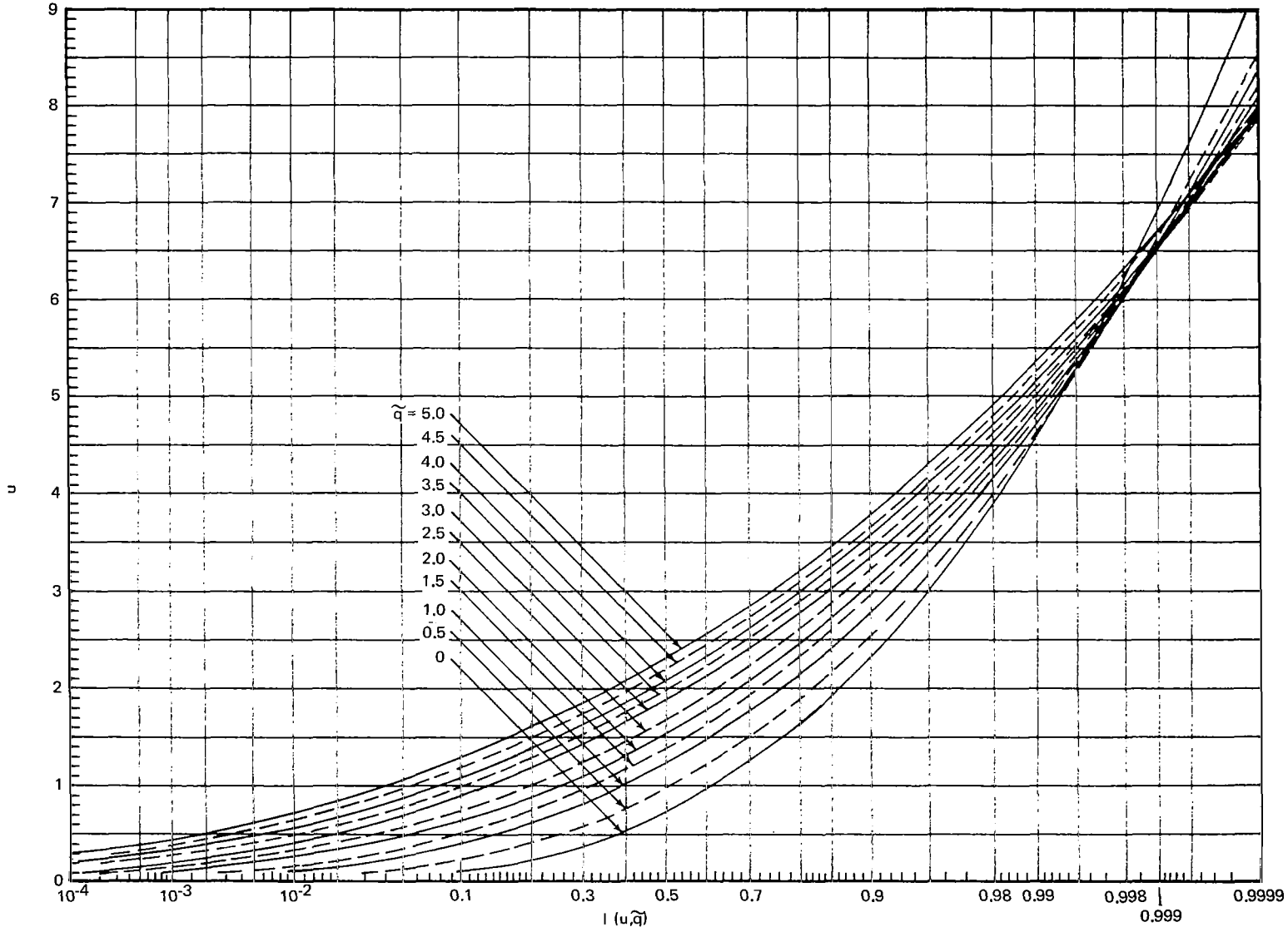

Figure 9:–Ratio of the incomplete to the complete gamma function ($0 \leqslant \tilde{q} \leqslant 5$).

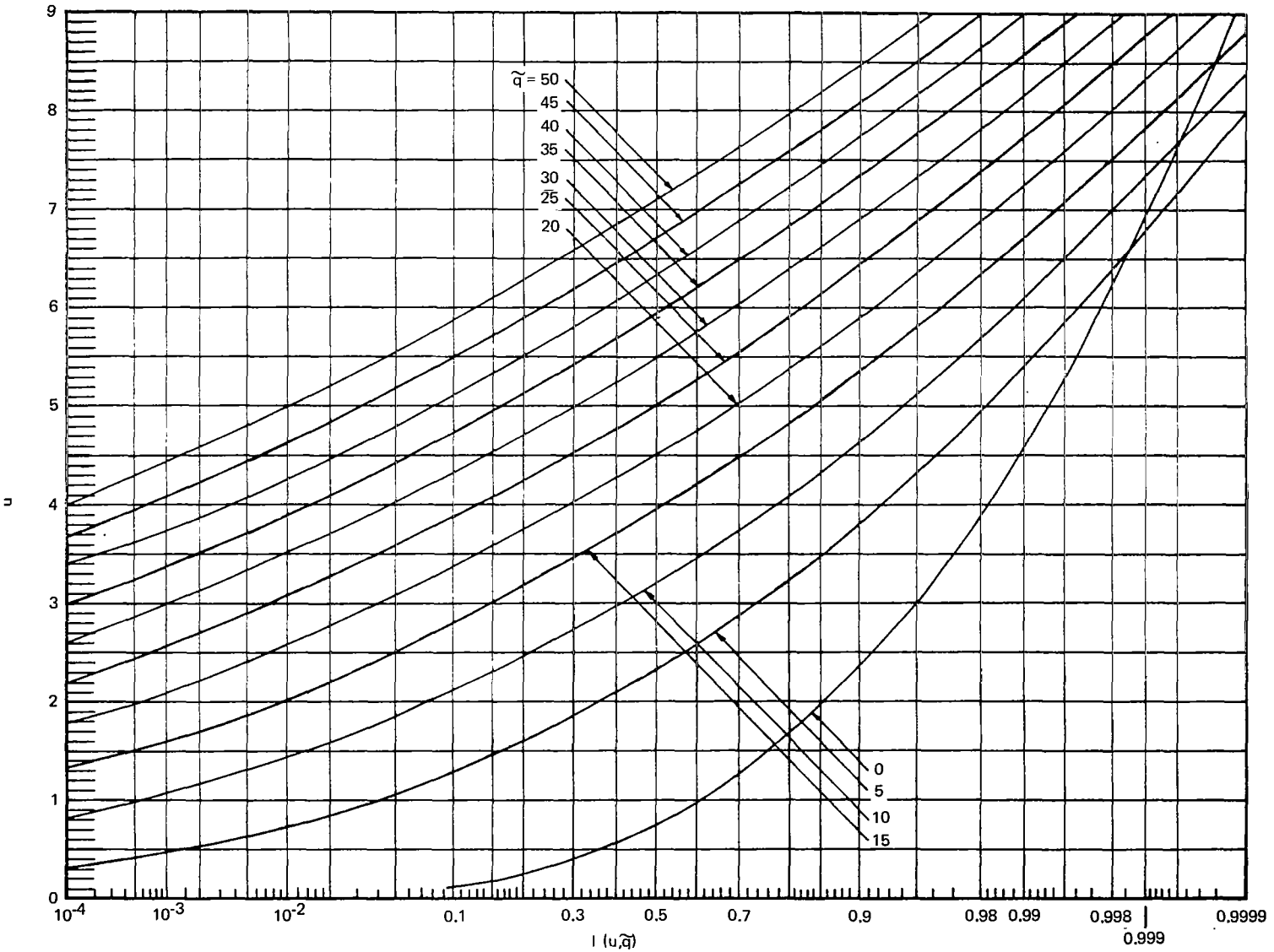

Figure 10.–Ratio of the incomplete to the complete gamma function ($0 \leqslant \tilde{q} \leqslant 50$).

stress peak s_i exceeds or equals the threshold (or ultimate dynamic stress) s_u^* during the exposure time T, where $\beta = s_i/\sigma_s$, $\beta_o = s_u^*/\sigma_s$, and σ_s is the rms stress. If the stress contribution in one of the modes is much greater than the contribution from the other modes, the probability may be approximated by

$$P_T(\beta \gtrsim \beta_o) \approx 1 - \exp\left[-2\pi\alpha_o f_n Q_n T\right] \tag{9}$$

where f_n and Q_n are the resonant frequency and resonant magnification of the dominant mode, respectively, and α_o is as given in figure 11 (refs. 72 and 73), in which $\beta = \beta^+$ should be used when failure may occur in tension only (i.e., a one-sided threshold), and $\beta = |\beta|$ should be used when failure may occur in either tension or compression (i.e., a two-sided threshold). It is important to note that the ultimate dynamic stress s_u^* usually is greater than the ultimate static stress s_u, since most materials can withstand a higher stress when the duration of application is short (ref. 74). Unfortunately, if more than one mode contributes substantially to the stress, no experimental data are presently available on the probability of threshold exceedance in a given time period.

There are other possible failure mechanisms under vibration, including collision between adjacent structures, wear, and operational drift. Collision between adjacent structures is another case of the threshold-crossing problem and is usually only of concern to elements within equipment rather than to primary or secondary vehicle structure. Wear is seldom a failure mechanism in space vehicle structures and operational drift is usually associated with guidance equipment (refs. 75 and 76). Thus, neither will be discussed in this report.

To determine the adequacy of the structure for all potential failure modes, the effects of vibration must be assessed in combination with other loads existing simultaneously and sequentially. As an example, high vibration may be expected near the q_{max} period of flight. During this period, high static stresses may be induced by the sustained acceleration and differential pressure resulting from venting lag. Since all of these act simultaneously, their combined effect must be considered.

In certain cases, the combined effects may be readily determined. For example, s_i vs N_i curves are available for many common metals under combined static and sinusoidal stresses and various temperatures, which may be used in figure 8 and equation (8) when one mode dominates the random response. Also, the probability of exceeding a threshold under combined static and random stresses, which may be calculated when one mode dominates by substituting $\beta = (s_i \pm s_{st})/\sigma_s$ into figure 11, where s_{st} is the static stress and the $\pm$ sign indicates that the static acceleration causes a tensile or compressive stress, respectively. If the static stress is large enough, the threshold

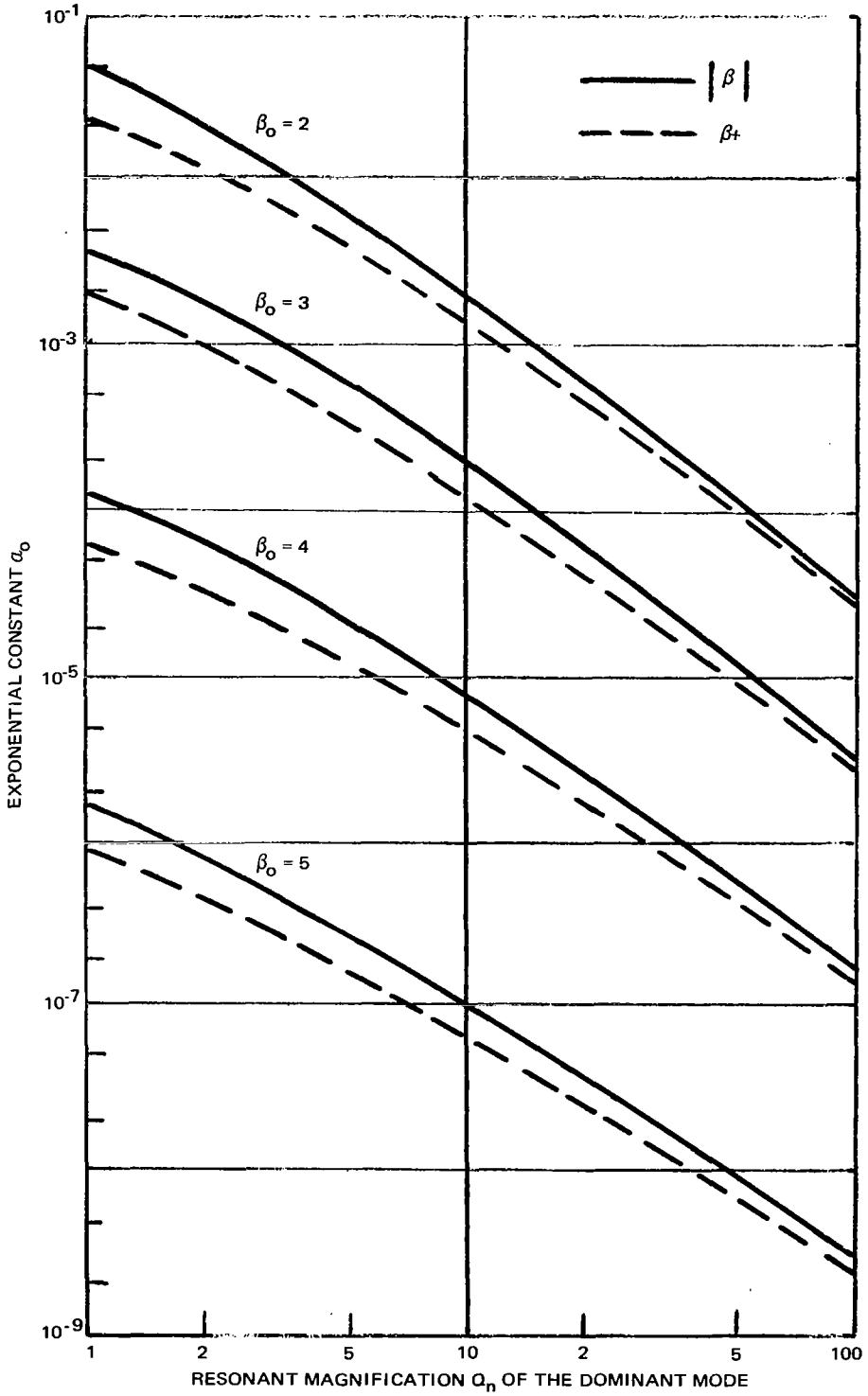

Figure 11. – Plot of exponential constant α_0 to be used in determining threshold-crossing probability.

exceedance is predominantly one-sided, so that $\beta = \beta^{+}$ should be used. Unfortunately, in many cases, state-of-the-art advances are required before combined effects can be predicted (ref. 77).

In the preceding discussion, it is assumed that single-point structural failures must be avoided. However, under certain circumstances, structural redundancy allows one or more of these failures without loss of the complete structure. These circumstances are described in reference 78.

4.1.3 Assessment

Classical analysis can be the most accurate method of predicting vibration stresses and motions in the lower-frequency range. Typically a rigorous analysis is restricted to that range which encompasses the lower 50 modes of the structure or section. The lack of structural detail in the model of simplifications made in describing the loading often further reduces the useful frequency range.

4.2 STATISTICAL-ENERGY ANALYSIS

Acoustic and aerodynamic noise cause the vehicle structure to vibrate in many modes over a broad frequency range. As noted in Section 4.1, classical methods often provide results which are inaccurate and/or expensive in the higher-order modes. An alternate approach, statistical energy analysis (SEA), has been developed by Lyon and his associates (refs. 79 through 84) to estimate the vibration of complex structure subjected to random loading at high frequencies. SEA can be used at the high frequencies to provide upper-bound and broad-brush estimates of vibration response and transmission with few calculations (relative to those required for classical methods), using only gross structural properties. However, SEA and classical methods both suffer from the lack of accurate information on the structural damping (material and friction) of the various modes.

4.2.1 General Statistical-Energy Analysis Formulation

The primary variables in statistical energy analysis (SEA) are power flow and modal energy (i.e., the vibration energy per mode). A fundamental principle of SEA states that under wideband random loading:

- The time-average power flow between two coupled dynamic systems is proportional to the differences in the time-average modal energies of the systems.
- The power flows from the high-modal-energy system to the low-energy system (ref. 52).

When system 1 is excited by wideband random loading and system 2 is excited only through coupling, the relationship between the time-average modal energies θ_1 and θ_2 of the two systems is

$$\theta_2/\theta_1 = \eta_{21}/(\eta_{21} + \eta_2) \tag{10}$$

where η_2 and η_{21} are the damping of systems 2 and the coupling loss factor from system 2 to system 1, respectively. Since $\eta_2 > 0$ and $\eta_{21} > 0$, it results that $\theta_2 < \theta_1$. From this result, a rule can be formulated for estimating an upper bound on the vibration of unexcited structures that are coupled in cascade to the directly excited structure; namely, the time-average modal energy of these unexcited structures cannot exceed the time-average modal energy of the directly excited structure.

SEA is used to predict the space-average response of a system, rather than the response at particular locations. The modal energies are simply related to common dynamic parameters. For a flat plate, the modal energy θ_{p1} is related to the space-average acceleration spectral density $\langle G_{\ddot{w}}(f) \rangle$ by

$$\theta_{p1} = [\rho h^2 c_L'/3^{\frac{1}{2}}(2\pi f)^2] < G_{\ddot{w}}(f) > \tag{10a}$$

where ρ, h, and c_L' are mass density, thickness, and speed of longitudinal waves of the plate, respectively. For a reverberant acoustic field, the modal energy θ_{ac} is related to the space-average pressure spectral density $\langle G_p(f) \rangle$ by

$$\theta_{ac} = [c_a/\rho_a(2\pi f)^2] < G_p(f) > \tag{10b}$$

where ρ_a and c_a are mass density and speed of sound in the acoustic medium (i.e., air), respectively (ref. 81).

4.2.2 Applicability to Simple Vehicle Structures

SEA calculations are quite simple for many vehicle configurations. Figure 12 shows an idealized representation of a simple structural configuration often found in space vehicles. Acoustic noise from the rocket engine causes the external structural section to vibrate. Because of the spatial distribution of the noise sources and the sound-reflection effects of the launch pad or test stand and the surrounding terrain (discussed in Sec. 3.1), the acoustic field adjacent to the external structure may be represented by a reverberant field with a space-average pressure spectral density $\langle G_p(f) \rangle_\xi$. The external structure, represented here as a flat plate, responds as a reverberant

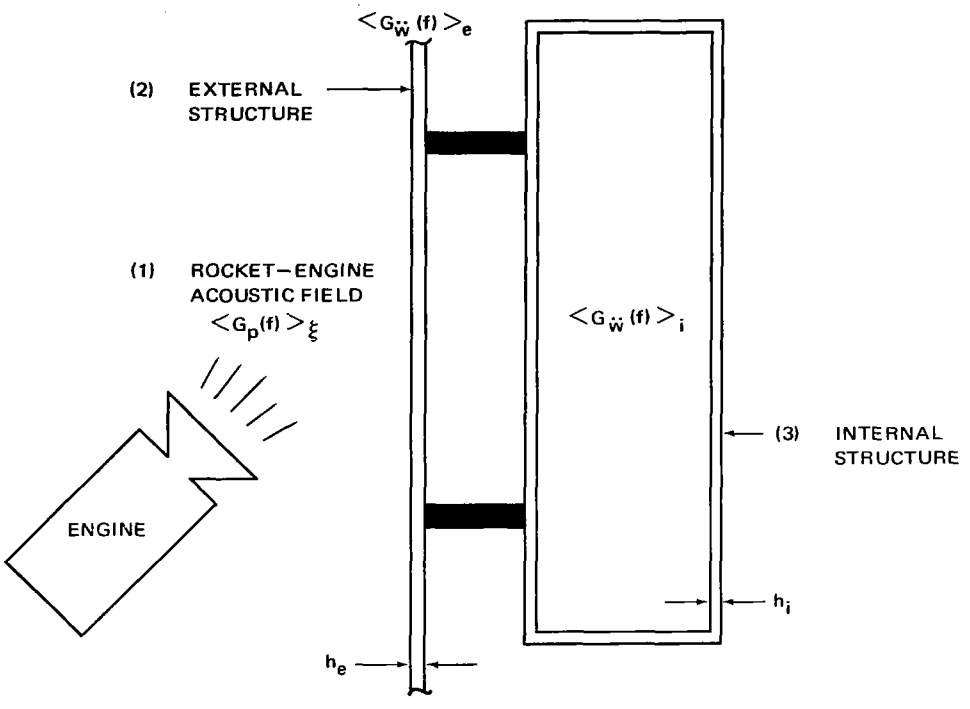

Figure 12.–Idealized representation of a simple space-vehicle structure used for predicting the space-average response of external and internal structure at higher frequencies by statistical-energy analysis.

vibration field with a space-average acceleration spectral density $<G_{\ddot{w}}(f)>_e$ and transmits vibration to the internal structure (or equipment), which has a space-average acceleration spectral density $<G_{\ddot{w}}(f)>_i$. (Since most external vehicle sections are cylindrical shells rather than flat plates, curvature effects must usually be considered below the ring frequency $f_r = c_L'/2\pi a$, where a is the radius of the cylinder.)

If the vibration power transmitted from external to internal structure is small, compared with the total power dissipated and radiated by the external structure, the last three equations may be used to determine the resonant-motion acoustic acceptance (or vibroacoustic transfer function) of the external structure:

$$\frac{< G_{\ddot{w}}(f) >_e}{< G_p(f) >_\xi} = \frac{2}{(\rho_e h_e)^2} \frac{3^{\frac{1}{2}} \rho_e c_a}{2\rho_a c_L'} \frac{\eta_{ea}}{\eta_{ea} + \eta_e} \tag{12}$$

The upper bound of the acceptance is obtained by assuming $\eta_{ea} >> \eta_e$ (i.e., the acoustic radiation damping exceeds the structural damping of the external structure). This upper bound is shown in figure 13 for an 0.125-in. thick aluminum plate. The coupling loss factor can be calculated from

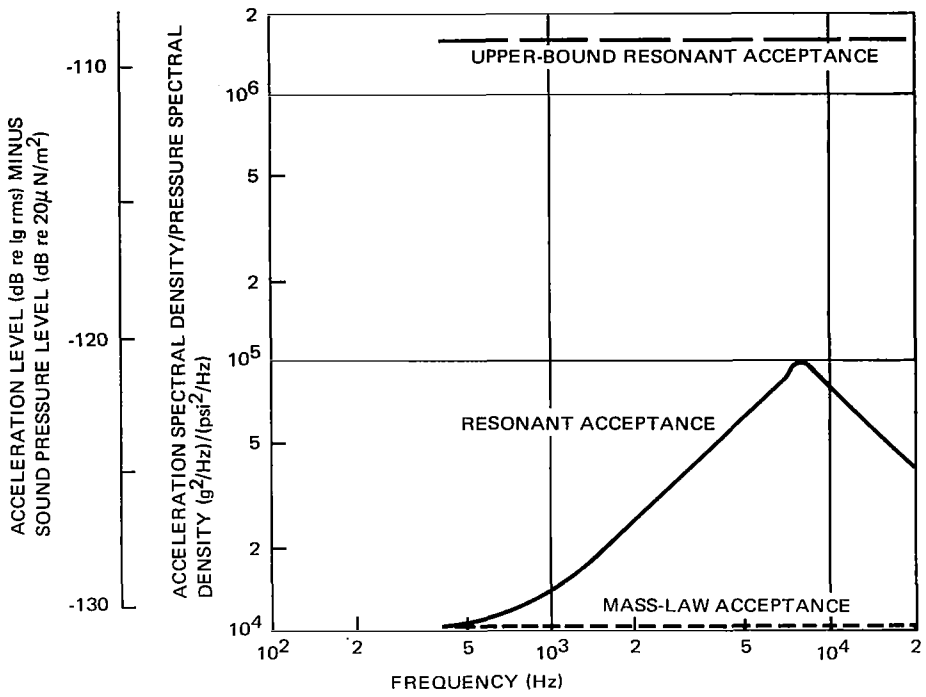

Figure 13. – Space-average acoustic acceptance for an idealized representation of space-vehicle external structure.

$\eta_{ea} = R_{rad}/2\pi fm$, where R_{rad} is the radiation resistance, and m, the mass of the plate (ref. 82). Figure 13 also shows the resonant acceptance of an assumed structural damping of $\eta_e = 10^{-2}$ and the calculated coupling loss factor η_{ea}. In this case, the acceptance peaks at the acoustic-structure coincidence frequency $f_c = 3^{1/2} c_a^2/\pi h_e c_L'$.

The off-resonance behavior of the external structure is controlled by its mass. The mass-controlled acoustic acceptance for the flat plate is $2/(\rho_e h_e)^2$ and is also shown in figure 13. The total acceptance is the sum of the resonant and mass-controlled acceptances.

The vibration-transfer function from external to internal structure, obtained from equations (10) and (10a), is

$$< G_{\ddot{w}}(f) >_i / < G_{\ddot{w}}(f) >_e = (\rho_i h_i^2/\rho_e h_e^2)\ \eta_{ie}/(\eta_{ie} + \eta_i) \qquad (12)$$

when the internal structure is represented by a box comprised of six plates, as shown in figure 12, and where ρ_i, h_i, and η_i are mass density, thickness, and structural damping of these plates, respectively. If the internal

structure is attached to the external structure by four rigid studs, the coupling loss factor is $\eta_{ie} = 2h_i c'_{L_i} / 3^{1/2} f A_i$, where A_i and c'_{L_i} are total surface area and speed of longitudinal waves of the internal structure, respectively (ref. 83). The vibration transfer function is shown in figure 14 for $\rho_i = \rho_e$, $h_i = h_e$, $\eta_i = 10^{-2}$ and the calculated value of η_{ie} using $A_i = 12$ ft^2. This example demonstrates the application of SEA relationships and calculations to simple vehicle configurations.

4.2.3 Applicability to Complex Vehicle Structures

SEA techniques have also been applied to large complex vehicle configurations. Sections of the Saturn V launch vehicle have been analyzed to predict vibration for a variety of fluctuating pressure fields: acoustic noise at liftoff, subsonic and supersonic boundary-layer turbulence, shock-induced separation, and disturbed flow at various times during the ascent phase of the mission (ref. 84). The launch vehicle was represented as an orthotropic cylindrical shell with ring frames and longitudinal stiffeners. The vibration acceleration and strain were calculated for each loading condition. It was observed that the time-average power from the aerodynamic-pressure field was relatively insensitive to the details of the correlation field used to represent the pressure source.

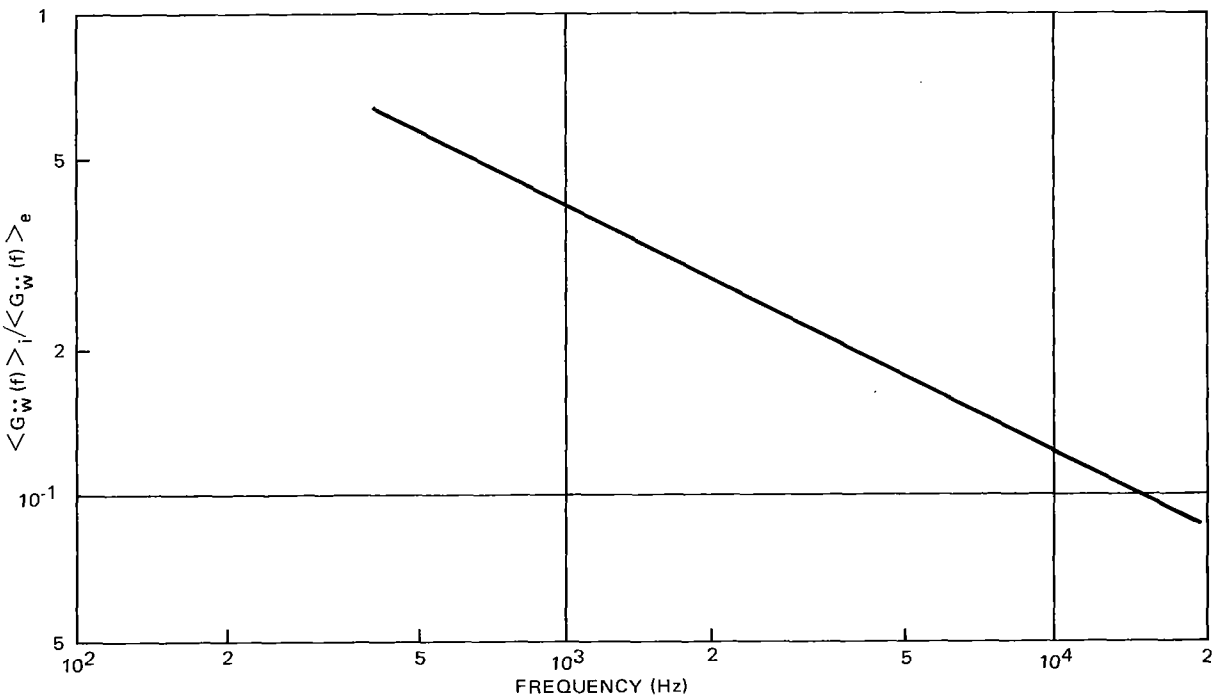

Figure 14.– Vibration-transfer function between external and internal structure for an idealized representation of a space vehicle.

Acoustical and mechanical vibration transmission has been investigated for a simplified physical model of the OGO spacecraft (ref. 81). The external acoustic field was again represented as a reverberant field, which excited vibration of the payload shroud. The vibration was transmitted to the spacecraft by way of two paths. The acoustic path was comprised of the shroud, which radiates acoustic noise into the interior space; the internal reverberant acoustic field; and the spacecraft. The mechanical path was comprised of the shroud, a ring frame, four mounting trusses, and the spacecraft. The analysis showed that the acoustic path was more efficient at low frequencies, and the mechanical path at high frequencies. An experimental study confirmed this conclusion.

SEA calculations for both the Saturn V and OGO cases were longer than those shown previously for simple structures. However, they still represented a small fraction of the calculations that would have been required if classical methods had been used to provide similar estimates.

4.2.4 Assessment

Although still in its early development, SEA is already a valuable tool for providing physical interpretation and rough estimates of vehicle vibration for frequencies sufficiently above the lower resonant frequencies. Future developments are likely to produce improved accuracy and/or greater simplifications for complex structures. However, it is unlikely that the simplicity of the extrapolation methods discussed in Section 4.3 will be challenged.

4.3 EXTRAPOLATION METHODS

Extrapolation or empirical methods utilize experimental data obtained on a vehicle, usually called a reference vehicle, to predict the vibration of a new vehicle. Certain assumptions must be made for the extrapolation method to be used. Often these assumptions are only partially valid, so that errors may be expected. Also, presently available extrapolation methods are generally used to predict vibration motion (usually in terms of acceleration vs frequency for sinusoidal excitation, or acceleration spectral density vs frequency for random excitation) rather than vibration stress. Thus, these methods are used only to determine vibration requirements for equipment, rather than to determine the integrity of structure. The methods may be further divided into two subcategories: frequency response methods and scaling methods. The relative merits and limitations of these methods, as well as the classical and SEA analyses previously described, are discussed in references 85 and 86 in detail.

4.3.1 Frequency-Response Methods

Frequency response methods use measurements obtained on the reference vehicle to determine $C_r(f)$, the ratio of the resulting vibration to the magnitude of the fundamental source, as a function of frequency or bandwidth. For all these methods, the fundamental source is acoustic noise or aerodynamic noise applied to the vehicle surface, or both.

All frequency response methods use statistical analysis to determine a sufficiently conservative value $C_r(f)_{cr}$ to be used as vibration criteria for the new vehicle:

$$G_{\ddot{w}n}(f) = C_r(f)_{cr} G_{pn}(f) \tag{13}$$

where $G_{\ddot{w}n}(f)$ is the acceleration spectral density of the structural vibration, $G_{pn}(f)$ the pressure spectral density of the aeroacoustic noise as measured on the external structure, and the subscript cr denoting criteria based on the reference vehicle.

4.3.1.1 Mahaffey-Smith Method

Mahaffey and Smith (M-S) (ref. 87) were the first to apply this method, using data obtained on B-52 and B-58 aircraft. First, acoustic measurements were made at a sufficient number of locations to define adequately the distribution of fluctuating pressures over the vehicle surface, and were analyzed in octave bands to determine their frequency content. Figure 15 shows the resulting distribution of sound-pressure levels for the octave band from 300 to 600 Hz over the surface of the B-58 during ground runup of its turbojet engines. Vibration measurements were then made at various locations throughout the vehicle, including structure adjacent to points of equipment attachment, and

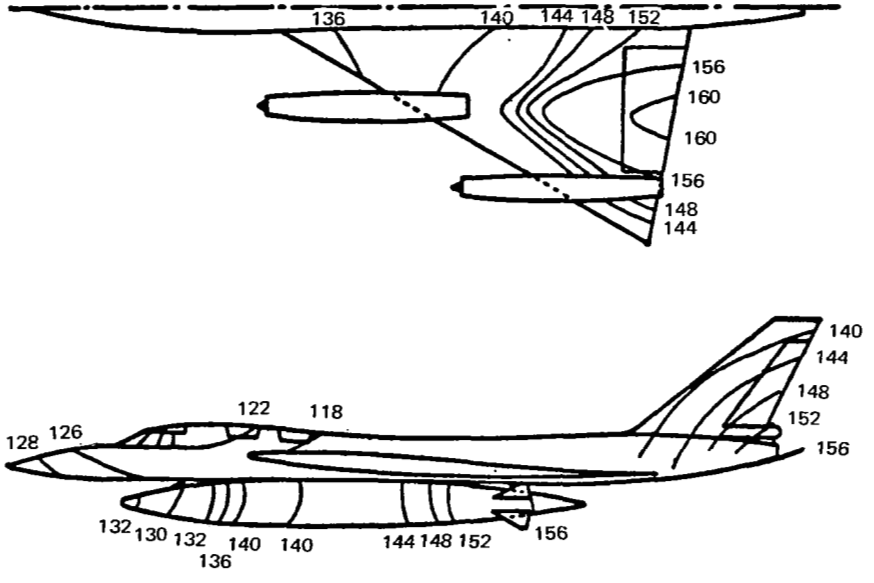

Figure 15.—Sound-pressure-level contours for the B-58 in the 300- to 600-Hz octave band.

were similarly analyzed in octave bands. These data were next used to plot vibration magnitude vs sound pressure level, as measured on the vehicle surface closest to the vibration measurement, in each of the octave bands throughout the frequency range of interest, (i.e., a lower limit of 37.5 Hz and an upper limit of 2.4 kHz). Figure 16 shows this plot for the 300- to 600-Hz octave band.

As seen from the first ordinate in figure 16, the vibration data are plotted in terms of peak rather than rms values, even though acoustically-induced vibration from jet engines is invariably random. M-S were required to present their data in peak values to derive sinusoidal design and test specifications, as required on the B-58 by the Air Force. However, M-S stated that generally the ratio of the peak value to the rms value was about 3.3. Because the vibration varied considerably throughout the vehicle, even for the same sound pressure level, the remainder of the octave band plot showed a considerable dispersion of data (fig. 16). This would be expected since there was no effort made to categorize the vibration data according to sections of the vehicle (called zones), the type of structure, or direction monitored. Thus, higher vibration would be expected for external panels, wing locations, unloaded structure, and directions normal to the nearest vehicle surface, than for internal structure, fuselage locations, equipment-loaded structure, and directions tangent to the nearest vehicle surface. M-S handled this dispersion statistically, using the plotted data to establish the regression line, and, assuming a log-normal distribution, the standard deviation.

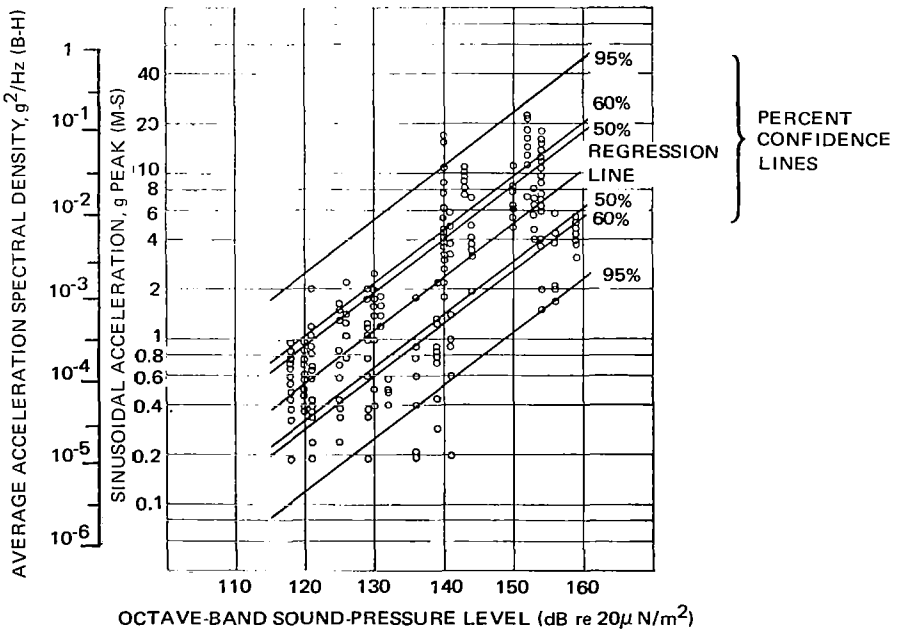

Figure 16.—Vibration-prediction curves for Mahaffey-Smith and Brust-Himelblau methods in the 300- to 600-Hz octave band

Figure 16 shows the regression and various confidence lines for the 300- to 600-Hz octave band. It is also noted that for any of these lines, the vibration increases by a factor of about 4 (rather than 10) for a 20-dB increase in sound-pressure level. This demonstrates that, statistically speaking, the B-58 structure is nonlinear.

To use the M-S method for a new vehicle, it is necessary to assume, among other things, that (a) the vibration is primarily acoustically induced, (b) the new vehicle and the B-58 are dynamically similar statistically, (c) the lack of data categorization has no particular disadvantage, and (d) the desired unit of vibration magnitude is the peak acceleration in an octave band. Then the acoustic noise spectra at the locations of interest on the surface of the new vehicle must be established, using the references noted in Section 3.

4.3.1.2 Brust-Himelblau Method

Brust and Himelblau (B-H) (ref. 88) reconverted the M-S vibration measurements from peak values to the original rms values (a factor of 3.3), then squared them and divided by the octave bandwidths to express the random vibration in more suitable units, the (mean square) acceleration spectral density (ASD) averaged over the octave band. The second ordinate of figure 16 shows this conversion. Following a M-S suggestion, B-H used the upper 60% confidence line to derive vibration design and test requirements for equipment locations. However, it is common knowledge that random vibration measured in narrow bands varies considerably from that averaged over an octave band.

Using the narrow-band, one-third-octave band, and octave-bandd analyses of random vibration measured on the Titan I missile, shown in figure 17, B-H concluded that the ratio of narrow-band ASD to octave-band ASD was nearly always less than a factor of 5. Thus, if vibration requirements are to be derived by enveloping the narrow-band peaks, the octave-band-averaged ASD from figure 17 must be multiplied by five to provide the necessary correction.

To use the B-H method, it is necessary to make the assumptions used in the M-S method, except that the desired unit of vibration magnitude is either the octave-averaged or the narrow-band ASD. For the narrow-band ASD, the assumption relating the narrow-band ASD to octave-band ASD must be acceptable.

4.3.1.3 Eldred, Roberts, and White Method No. 1

Eldred, Roberts, and White (E-R-W) (ref. 4) analyzed vibration and acoustic measurements made on the Snark missile and plotted them in a manner almost identical to that of M-S. The random vibration was, however, plotted in terms of rms acceleration rather than peak acceleration in each octave band. Because fewer measurements were used, only the regression line was drawn. Converting to compatible units (a factor of 3.3), the E-R-W regression line was always found to be higher than the M-S regression line and usually varied between the M-S upper 50% and upper 95% confidence lines. Also, above 150 Hz,

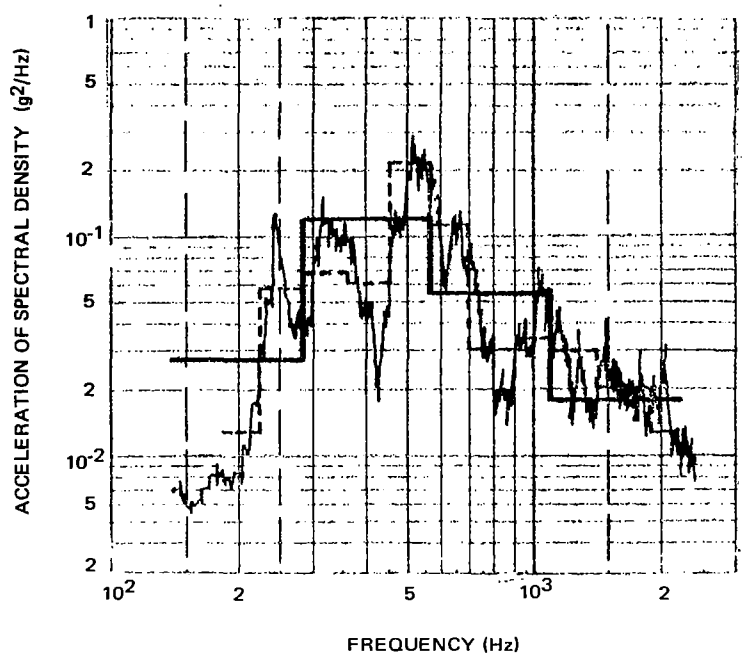

Figure 17. – Comparison of narrow-band, one-third octave-band, and octave-band spectral analyses of the same random-vibration measurement.

the rms vibration increased by a factor of 10 for a 20-dB increase in sound-pressure level, demonstrating that the Snark structure was linear on a statistical basis.

To use the E-R-W method, most of the assumptions mentioned under the M-S method must apply. In addition, the E-R-W restricts its use to the regression line. The E-R-W method could be revised to more suitable random-vibration units (i.e., ASD), using a conversion similar to that of B-H on the M-S method. Also, a narrow-band correction could be applied to the octave-band vibration, as mentioned by B-H.

4.3.1.4 Eldred, Roberts, and White Method No. 2

In addition to the method just described, Eldred, Roberts, and White devised a second method (refs. 4 and 89) based on the response of a simple mechanical oscillator (i.e., a single-degree-of-freedom system) to a random force applied to the mass

$$\sigma_{\ddot{w}}^2 \approx \pi f_n Q G_F(f_n)/2m^2 \qquad (14)$$

where $\sigma_{\ddot{w}}$ is the rms-acceleration response; f_n, Q, and m are resonant frequency, resonant magnification or quality factor, and mass of the oscillator,

respectively; and $G_F(f_n)$ is the force-spectral density of the random force at a frequency corresponding to the natural frequency of the oscillator. Great care must be exercised in the use of equation (14) because the rms acceleration is infinite when the random force has a white spectrum. However, as shown in reference 54, equation (14) generally provides a reasonable approximation when the random force has a band-limited white spectrum and the oscillator has a $Q \geq 20$.

To apply this equation to a multimodal structure which is typical of space vehicles, E-R-W suggested that the right-hand side of equation (14) be multiplied by a multimodal-response factor δ^2. To determine the value of this factor to be used, E-R-W examined vibration and acoustic data obtained on eight vehicles: the Corporal, Vanguard, Thor, Titan I, Talos, Polaris, Atlas, and Terrier. They assumed that (1) the effective mass m was the gross mass of the entire vehicle, (2) the effective random force $G_F(f_n)$ was the product of the average pressure spectral density (over the entire vehicle) times the square of the entire surface area, and (3) $Q = 15$.

Figure 18 shows δ^2 as a function of the normalized wave number $(\pi fD/c_a)$ where D is the vehicle diameter and c_a, the speed of sound in air (c_a = 1130 ft/sec at sea level and at 70°F). As seen from figure 18, $\delta^2 \approx 1.6$ on the average and did not exceed a factor of 50 for the vehicles surveyed. To use this method, it is necessary to assume that (a) the vibration is primarily

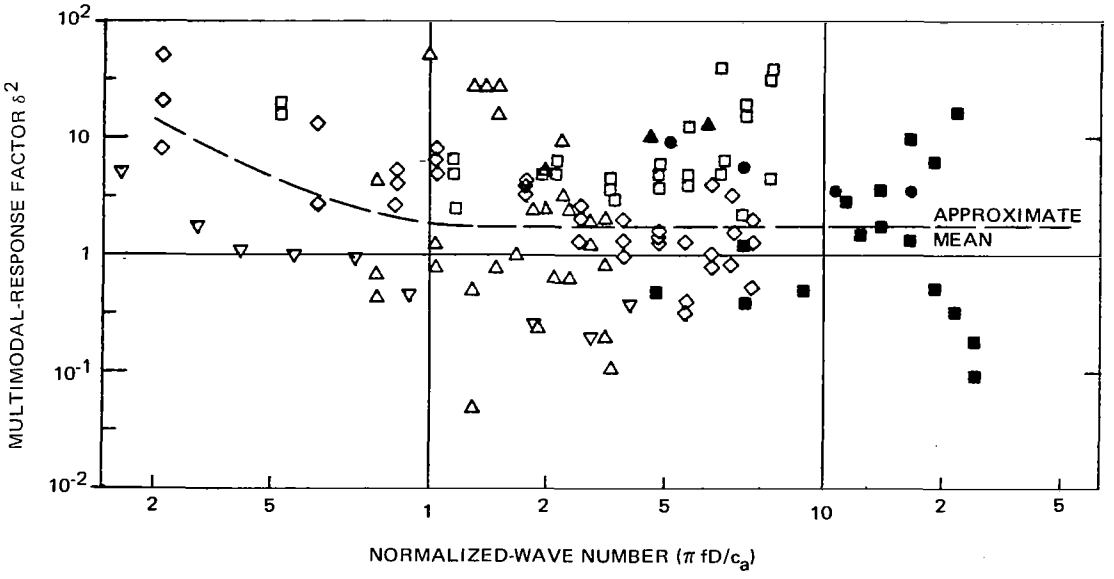

Figure 18. – Contribution to the rms acceleration from multimodal response as measured on several missiles.

acoustically induced, (b) the lack of data categorization is not a particular disadvantage, and (c) the desired unit-of-vibration magnitude is the rms acceleration over the entire frequency range of interest.

Since the eight reference vehicles have a wide dispersion of dynamic properties, the assumption of dynamic similarity between the new vehicle and the reference vehicles can generally be considered satisfied. However, on a theoretical basis, δ^2 should never be less than unity. Since $\delta^2<1$ was calculated from many data points, it must be assumed that the error was caused by the assumptions of the effective mass, random force Q, or other factors discussed in reference 4.

4.3.1.5 Curtis Method

Curtis (ref. 90) observed that the vibration (caused by flow-induced aerodynamic noise) measured on aircraft during high-speed flight was related to the aerodynamic pressure q. The values of q studied varied from 90 to 1760 psf. He performed a statistical analysis of vibration data obtained from F8U, B-59, F-101 and F-106 aircraft and concluded that the data approximated a Rayleigh distribution. Curtis established that

$$G_{\ddot{w}n}(f) = (q_n/2130)^2 \, G_{\ddot{w}r}(f) \qquad (15)$$

where $G_{\ddot{w}}(f)$ is the acceleration spectral density of the structural vibration and n and r the subscripts denoting new and reference vehicles, respectively.

For structure adjacent to internally located equipment, it was determined that the mean reference spectral density $\overline{G_{\ddot{w}r}(f)} = 0.006$ g^2/Hz, and that 98% of the reference narrow-band spectral peaks (based on a Rayleigh distribution) were less than the recommended criteria $G_{\ddot{w}r}(f)_{cr} = 0.11$ g^2/Hz, 20 Hz<f<2 kHz. For structure adjacent to equipment exposed directly to the aerodynamic flow (such as IR sensors and antennas), $\overline{G_{\ddot{w}r}(f)} = 0.011$ g^2/Hz, 20 Hz<f<150 Hz, and 0.020 g^2/Hz, 150 Hz<f<2 kHz. The 98-percentile $G_{\ddot{w}r}(f)_{cr} = 0.130$ g^2Hz, 20 Hz<f<150 Hz, and 0.235 g^2/Hz, 50 Hz<f<2 kHz. To use the Curtis method, it is necessary to assume that (1) the vibration is induced primarily by aerodynamic noise, (2) the acceleration spectral density of the random vibration is directly proportional to q^2, and (3) the new vehicle is dynamically similar to the four reference aircraft on a statistical basis. Only the aerodynamic pressure q_n of the new vehicle need then be established.

4.3.1.6 Franken Method

Franken (ref. 91) performed a similar study of vibration and acoustic measurements of Jupiter and Titan I external structures (stiffened cylindrical shells) exposed to acoustic noise from rocket engines during static firing,

analyzing the data in one-third-octave bandwidths. Vibration measurements were made in the radial direction only (i.e., normal to the surface). For each band, the rms vibration was multiplied by the average weight-per-unit area of the structure (called the average surface density) and then divided by the rms-acoustic noise, which is one form of a frequency-response function (FRF). The use of the weight-per-unit area is related to ''mass-law'' relationships in classical acoustics.

The vibration of a cylindrical shell can be related to the ratio of the excitation frequency to the isotropic ring frequency, that is, $(f/f_r) = (f\pi D/c_L')$, where D is the vehicle diameter and c_L', the speed of longitudinal waves in the material (approximately 17 000 to 18 000 ft/sec for most aerospace materials, and 40 000 to 50 000 ft/sec for beryllium and certain boron and carbon composites). Taking this as a cue, Franken plotted his FRF vs the product fD to obtain the dashed curve shown in figure 19. A maximum scatter of 6 dB is observed in this figure. Also, the maximum FRF occurs at fD = 6000, corresponding to the ring frequency. To use the Franken method for a new vehicle, it is necessary to assume that (a) the vibration is primarily acoustically induced, (b) the new vehicle and the Jupiter and Titan I external structures are dynamically similar within a 6-dB scatter, and (c) only the radial direction is of interest. Then the acoustic noise spectra at the locations of interest on the surface of the new vehicle, as well as its diameter, must be established. However, if vibration requirements are to be derived by enveloping the narrow-band peaks, then the one-third-octave band-averaged ASD must be multiplied by a factor to provide this correction. From the comparisons shown in figure 17, B-H suggested a correction factor of 2.5.

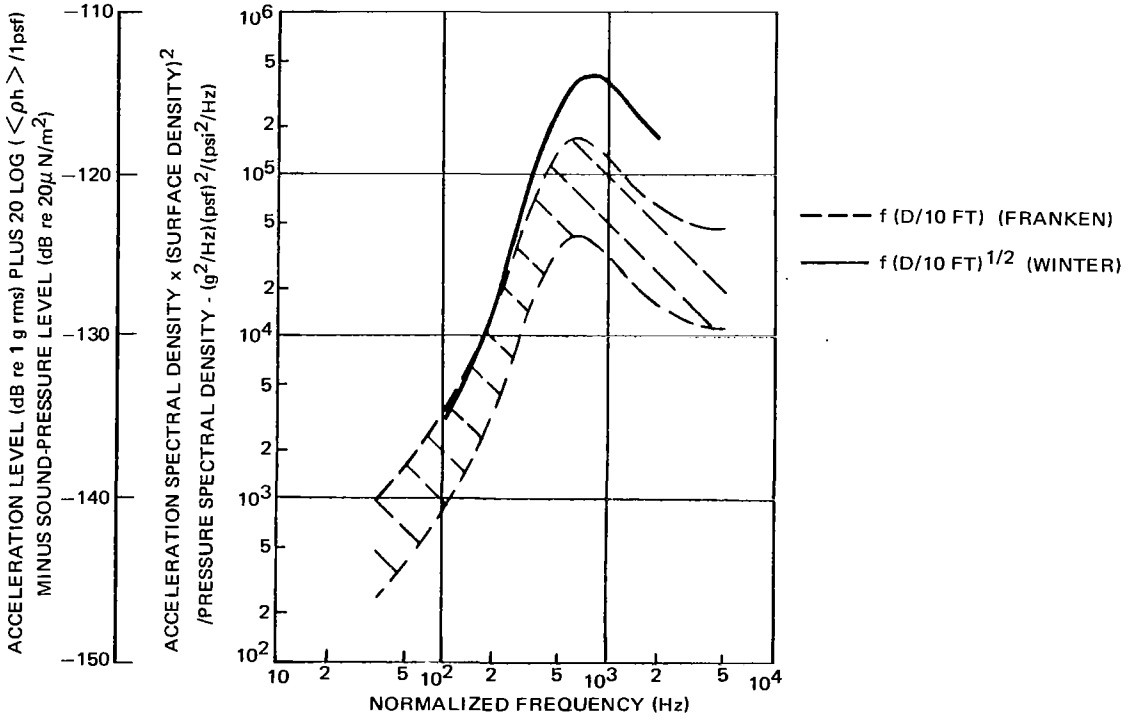

Figure 19. – Vibration-prediction curves for Franken and Winter methods.

4.3.1.7 Winter Method No. 1

Winter (ref. 92), who assisted in the development of the Franken method, has modified the method after adding Minuteman, Skybolt, and Genie data to the previously used Jupiter and Titan I data. As shown in figure 19 as the solid curve, the Winter FRF is directly analogous to the Franken FRF. However, the frequency scale has been changed since Winter observed a better comparison among data when the square root of the diameter was used in the abscissa. For internal structure not efficiently coupled to external structure (e.g., internal beams and truss structure), it is suggested that the acceleration spectral density be determined by (a) the solid curve in figure 19 for frequencies below 100 Hz, (b) 15% of the solid curve for frequencies above 500 Hz, and (c) a smooth curve connecting the points at 100 and 500 Hz.

Winter had added a mass-attenuation factor when heavy equipment is attached to the structure. This factor is identical to that described in the Barrett method and will be discussed in Section 4.3.2.2. Winter has also extended his method to include vibration induced by aerodynamic noise. This extension, suggested by Stewart (ref. 85), is in the form of the efficiency factor shown in figure 20. Aerodynamically induced vibration is predicted by multiplying the acceleration spectral density obtained from the solid curve in figure 19 (for acoustically induced vibration) by this factor. It is noted that aerodynamic noise is relatively ineffective at low frequencies (usually because of a low spatial cross-correlation coefficient) and may be quite effective at high frequencies (usually owing to aerodynamic coincidence).

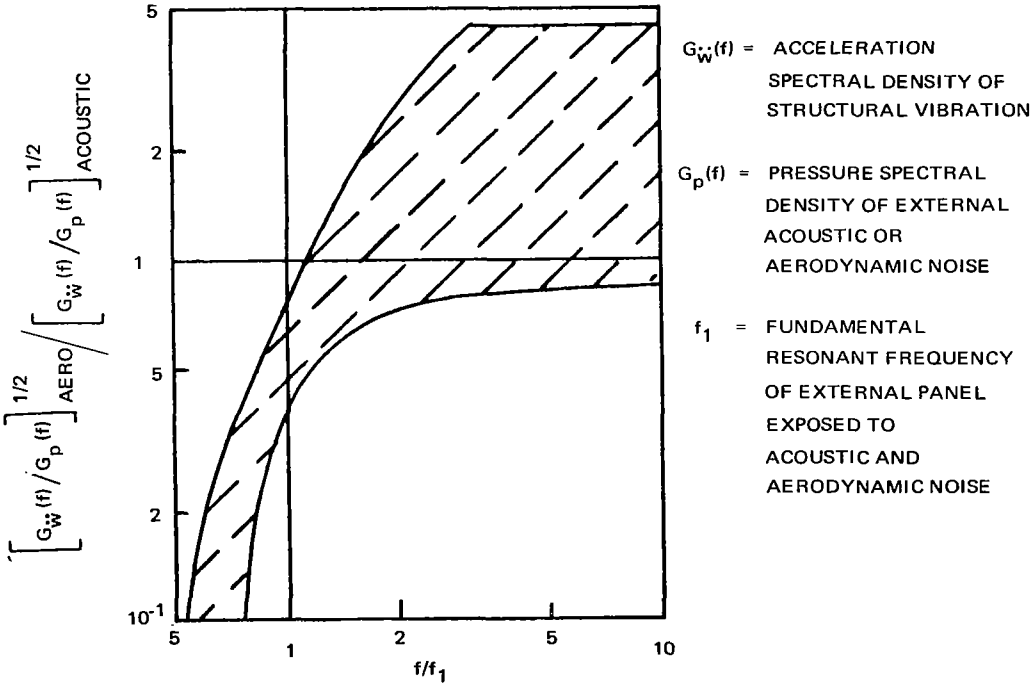

Figure 20. – Vibration efficiency of aerodynamic noise relative to acoustic noise.

4.3.1.8 Assessment and Extensional Applications

The major advantage of the frequency-response methods is the ease in calculating the vibration motion of the new vehicle without considering the detailed calculations of the structure. Obviously, these methods are highly desirable during the early development of a new vehicle, when the structure is sufficiently defined or when detailed calculations have not been made. The major deficiency of all these methods is their susceptibility to inaccuracy. In some cases the overall accuracy is fairly good, while in other cases considerable overprediction and underprediction have been found (refs. 88 and 91 through 95). However, inaccuracy should be expected because these methods intentionally ignore the very details that determine the response. In addition, in those methods which plot their data on a statistical basis, poor comparison between predicted and measured vibration is sometimes observed because of a too conservative selection of the statistical parameter. Although the various methods have not become standardized on the same unit for expressing the magnitude of random vibration, nor use the same bandwidth, they are all convertible to acceleration spectral density, the unit most preferred by workers in the field. (E-R-W Method No. 2 is the one exception.)

Although frequency response methods usually are not used to determine vibration stresses, certain modifications to presently available methods can be made for their prediction. First, consider a simple mechanical oscillator, where the rms stress σ_s in the spring can be related to the rms acceleration $\sigma_{\ddot{w}}$ of the mass:

$$\sigma_s = (K_d/4\pi^2 f_n^2)\sigma_{\ddot{w}} \tag{16}$$

where K_d is the ratio of the stress to the (relative) displacement. This relationship could be a logical extension of E-R-W Method No. 2, using the values of δ^2 presented in figure 18. Second, the derivations by Hunt (ref. 96), Ungar (ref. 97), and Crandall (ref. 98) can be used to establish the following relationship between rms velocity and rms stress for distributed structures:

$$\sigma_s = (EK_\phi K_f/c_L')\sigma_{\dot{w}} \tag{17}$$

where E is the modulus of elasticity, and K_ϕ and K_f, the mode-shape factor and stress-concentration factor, respectively. For a plate, Hunt shows that $1.2 < K_\phi < 1.8$; from reference 61, $1 < K_f < 4$. Using $K_\phi = \sqrt{3}$ and $K_f = 1$, Franken compared predicted strain with the strain measured in one-third-octave bands on the external structure of the Minuteman missile (ref. 91). The strain comparison was only marginal (i.e., measured strain exceeded predicted strain by as much as a factor of 5), even though the acceleration comparison was rather good. Further refinements will probably be made as interest grows in determining vibration stresses during the early phase of a vehicle-development program.

4.3.2 Scaling Methods

When a new vehicle has structural and configurational characteristics and fundamental sources of vibration that are similar to the reference vehicle, scaling methods make use of experimental data obtained on the reference vehicle to predict the vibration on a new vehicle. In general, the two vehicles must use the same design philosophy regarding structure, aerodynamics, and propulsion. Scaling, however, is not restricted to scale modeling, which attempts to duplicate all characteristics of the new vehicle. Because of the similarities of the vehicles, it would be expected that scaling methods are more accurate than frequency-response methods. This is not always the case, as is shown later in this section. General scaling methods have been used only to predict vibration motion. One reason these methods have not been extended to prediction of vibration stresses is that scaling with the more accurate scale models have shown only mixed results. These results are discussed in the section on model tests (Sec. 5.1.1).

4.3.2.1 Condos-Butler Method

Condos and Butler (C-B) (ref. 99) were the first to utilize data obtained on the Titan I missile and the following equation to predict vibration on Titan II:

$$G_{\ddot{w}n}(f) = [G_{pn}(f)/G_{pr}(f)][\langle \rho h \rangle_r / \langle \rho h \rangle_n]^2 G_{\ddot{w}r}(f) \qquad (18)$$

where $G_p(f)$ is the pressure spectral density of the acoustic or aerodynamic noise averaged over the applicable section of the vehicle; $\langle \rho h \rangle$, the average structural mass per unit of exposed area (surface density); and n and r are subscripts denoting new and reference vehicles, respectively. Because the structures were similar, but were not scale models, C-B did not attempt to predict the vibration on a point-to-point basis. Instead, the structures were divided into zones of similar location and type of structure. For each zone of the reference vehicle, the measured vibration spectra were grouped and a statistical analysis made.

It was observed that the data tended to follow a log-normal distribution, which was then used. (This distribution was confirmed later by statistical analysis.) To perform the analysis, C-B divided the frequency range of interest, 0 to 2 kHz, into 40 contiguous bands of 50 Hz each. In each band, the maximum ASD value of each measurement was selected for the analysis, rather than the average value. This tended to bias the analysis toward a distribution of spectral peaks rather than the distribution of complete spectra. Then, using all measurements for the zone, the log-normal mean value and standard deviation for each of the 40 bands were calculated, similar to the technique used by M-S for octave bands. Finally, the 95%-probability level in each band was selected to be used as $G_{\ddot{w}r}(f)$ in equation (18) for predicting the 95%-probability level for the new vehicle.

Since the goal of the investigation was the establishment of vibration design and test levels for equipment, only measurements on structure adjacent to equipment were used. C-B selected the following as zones: (1) external structure, a stiffened cylindrical shell exposed directly to the pressure field; (2) ''outside'' structure, secondary structure adjacent to external structure but inside the vehicle; and (3) truss structure, a ''space frame'' consisting of welded beams segments used to attach internal equipment to the external stiffeners. The analysis showed no significant differences between the three orthogonal directions (supposedly including external structure), so that all directional measurements in a zone were combined.

To determine the average surface density $\langle \rho h \rangle$, C-B used the total mass of external and internal structure for the equipment section of the vehicle and the exposed area for the section. To use the C-B method, it is necessary to establish the similarity (although not the identity) of the two vehicles, and to determine the required values in the right-hand side of equation (18). The zones, type of statistical analysis (or lack thereof), spectral division, directions, etc., need not correspond to the parameters used by C-B.

4.3.2.2 Barrett Method

Barrett (ref. 100) used a method almost identical with that of C-B to predict acoustically induced vibration on uprated Saturn I and Saturn V vehicles, using equation (18) and the vibration measurements from Saturn I. Barrett modified the C-B method by using (a) a mass-attenuation factor to reduce the predicted vibration when the weight of the equipment was large; (b) a normal distribution, modified by a skewness function whose coefficients were experimentally determined; and (c) a 97.5%-probability level based on the calculated distribution. The mass-attenuation factor, to be multiplied by the right-hand side of equation (18), is

$$\gamma = W_n/(W_n + W_e) \tag{19}$$

where W_n and W_e are weight of the structure and of the equipment of the new vehicle, respectively. The 97.5%-probability level for each zone of the reference vehicle was calculated using N zonal measurements and the overall rms value X_i of the spectral envelope of each (or i^{th}) measurement (ref. 101):

$$X_i^2 = (50\ \text{Hz}) \sum_{50}^{2050} G_{max}(f_k)_i \tag{20}$$

where $G_{max}(f_k)$ is the maximum value of the acceleration spectral density (g^2/Hz) measured in each of the 50-Hz bands (similar to the C-B method) from 50 to 2050 Hz, and where X_i should not be confused with the true standard

deviation $\sigma_{\ddot{w}i} = \left[\int_{f_{min}}^{f_{max}} G_{\ddot{w}i}(f)\, df\right]^{1/2}$ of the same measurement. Barrett calculated the 97.5%-probability level from

$$X_{cr} = \bar{X} + n_X \sigma_X \tag{21}$$

where $$\bar{X} = \frac{1}{N} \sum_{i=1}^{N} X_i \tag{21a}$$

$$n_X = A_o \exp\left[A_1\alpha_3 - A_2\alpha_3^2\right] \tag{21b}$$

$$\sigma_X = \frac{1}{N-1} \sum_{i=1}^{N} (X_i^2 - \bar{X}^2) \tag{21c}$$

$$\alpha_3 = \frac{N^2}{(N-1)(N-2)\sigma_X^3}\left[\left(\frac{1}{N}\sum_{i=1}^{N} X_i^3\right) - \left(\frac{3\bar{X}}{N}\sum_{i=1}^{N} X_i^2\right) + 2\bar{X}^3\right] \tag{21d}$$

Barrett found that $A_o = 1.64$, $A_1 = 0.2055$, $A_2 = 0.0155$ gave a good experimental fit to the 97.5% level. (For a normal distribution where $\alpha_3 = 0$, the 97.5% level would be determined at $n_X = 1.96$.) Then $G_{\ddot{w}r}(f)_{cr}$, to be utilized in equation (18), was determined on the basis that its spectrum would have the same general shape as

$$\overline{G_{max}(f_k)} = \frac{1}{N} \sum_{i=1}^{N} G_{max}(f_k)_i \tag{22}$$

but would have a standard deviation equal to X_{cr}; that is,

$$X_{cr}^2 = \int_{f_1}^{f_2} G_{\ddot{w}r}(f)_{cr}\, df \tag{22a}$$

Figure 21 shows a typical spectrum $G_{\ddot{w}r}(f)_{cr}$ based on this procedure and 50 vibration measurements made on the aft skirts of the Saturn I fuel tanks.

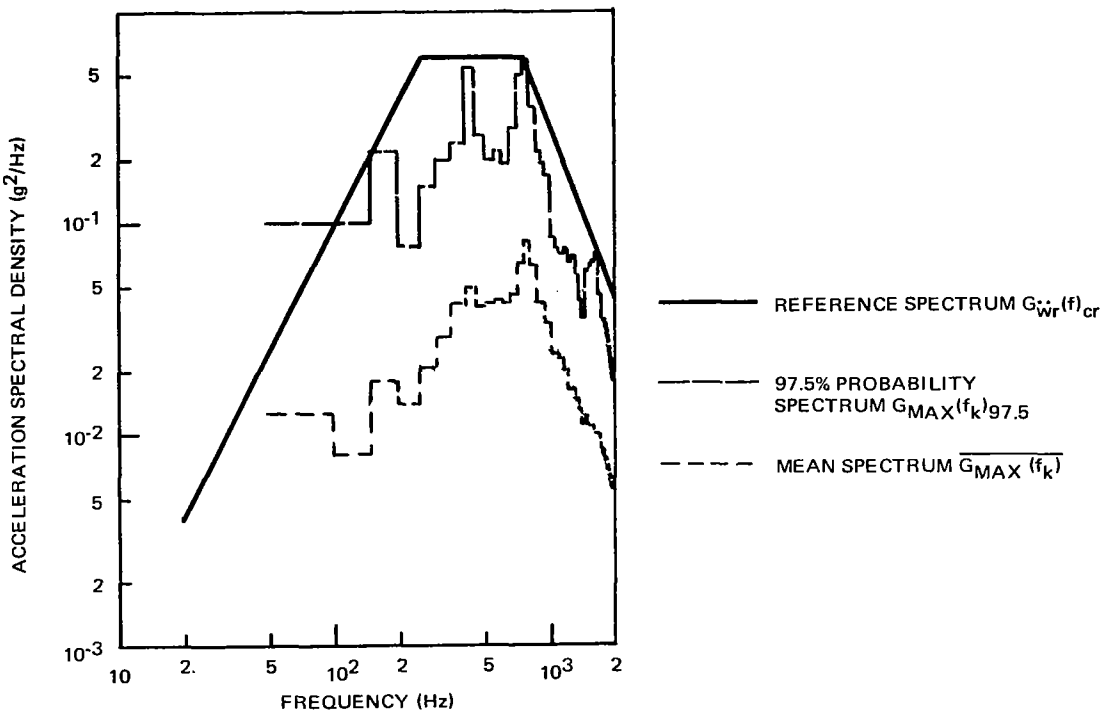

Figure 21. – Vibration-reference spectra for Barrett method on 50 flight measurements on the aft skirt of Saturn I fuel tanks.

Also shown in figure 21 is the mean spectrum $G_{max}(f_k)$ calculated from equation (22), and the 97.5 percentile $G_{max}(f_k)_{97.5}$, determined for each of the 50-Hz bands for these 50 measurements, as presented in reference 101. Reference 100 shows methods of calculating the average surface density $\langle \rho h \rangle$ for honeycomb and corrugated structures to be used in equation (18).

Barrett has also developed a scaling method for mechanically transmitted vibration from liquid-fueled rocket engines through structure that is not primarily excited by acoustic and/or aerodynamic noise. Engine components and structure near engines which do not have large exposed surface areas often fall into this category. A scaling equation adapted from Barrett's work is

$$G_n(f) = \frac{N_n T_n I_{sp_n} W_r}{N_r T_r I_{sp_r} W_n} \gamma \, G_r(f) \qquad (23)$$

where G(f) is the acceleration spectral density of the mechanically transmitted vibration; N, the number of engines; T and I_{sp}, the thrust and specific impulse of each engine, respectively; and W, the weight of the structure or engine component. The value of γ is defined in equation (19). Random vibration of the rocket engine or of engine-mounted components is however usually

influenced by that engine only. Thus, Barrett suggests that $N_n = N_r = 1$ be used for the combustion chamber, turbopump, and actuator structures and components.

For structure which is excited simultaneously by mechanically transmitted vibration and acoustic or aerodynamic noise, such as the structure near the engine compartment of the first stage of a launch vehicle, Barrett suggests using the following equation to determine the combined effect on the new vehicle:

$$G_{nt}(f) = C_1 G_{\dot{w}n}(f) + C_2 G_n(f) \qquad (24)$$

where $C_1 + C_2 = 1$, and $G_{\dot{w}n}(f)$ and $G_n(f)$ are determined from equations (18) and (23), respectively. Reference values to be substituted into these equations, based on measured Saturn I data appear in reference 100. Barrett also presents additional reference quantities for sinusoidal vibration, even though the measurements showed the vibration to be random. Sinusoidal vibration extrapolation to a new vehicle is performed by using the sinusoidal-reference quantities of reference 100 and the square root of equations (18) and (23), and, if applicable, equation (19) or (24), or both.

4.3.2.3 Winter Method No. 2

Winter (ref. 85) has suggested a scaling method similar to his frequency-response method discussed previously. In this method, curves for various zones are derived similar to those of figure 19, based on vibration and acoustic measurements from the reference vehicle. Once these curves are determined, the values of surface density and diameter and the predicted acoustic environment for the new vehicle are used with these curves to predict the vibration for the various zones.

4.3.2.4 Assessment

The major advantage and deficiency of the scaling methods are identical to those of the frequency-response methods, even though there are clear structural, configurational, and aerodynamic similarities between the reference vehicle and the new vehicle. For example, C-B observed as much as a 15-dB difference between the predicted and measured 95% levels for the new vehicle (Titan II) for the frequency range above 500 Hz, although the difference was usually less than 5 dB below 500 Hz. Fortunately, in this case, the prediction was almost always greater than the measured percentile. (Since C-B did not use a mass-attenuation factor, there was greater overprediction for heavy items of equipment.) Similar differences have sometimes been noted for later Saturn stages using earlier Saturn measurements and the Barrett method.

5. EXPERIMENTAL DETERMINATION OF VIBRATION

Various methods and combination of methods are available to determine design adequacy or to predict structural vibration during the various phases of vehicle development, or to refine earlier predictions, such as described in Section 4. These methods may be divided into the following three categories: (1) ground testing, (2) field testing, and (3) flight testing.

5.1 GROUND TESTING

Various ground tests may be performed which may have a significant contribution to the program. Often the results of these tests are not the sole source of data, but must be used in conjunction with the results of other tests or analyses, or both.

5.1.1 Model Tests

A wide variety of subscale models has been used to establish (1) acoustic noise and aerodynamic fluctuating-pressure fields, (2) stability and flutter boundaries, (3) propellant-sloshing behavior, (4) natural frequency and modal data, (5) structural response to specific dynamic loads, and (6) fatigue and other failure mechanisms. The first three uses of models will not be discussed in this report except as they may affect the last three uses. The primary advantages of using subscale models are the great saving in cost and schedule compared to full-scale testing, possible implementation early in the program, and often greater accuracy than may be achieved by analysis, especially when excessive oversimplification is used. (These physical models should not be confused with the mathematical model discussed in Sec. 4.1.1.)

Models may be divided into the following categories: (a) perfect, or true, models; (b) adequate models; (c) distorted models; and (d) dissimilar models.

5.1.1.1 Structural-Modeling Theories

A perfect model reproduces faithfully the significant characteristics of the full-scale prototype. Here, the prototype may be the new vehicle or a section of the vehicle. However, unless the prototype is quite simple in construction (or the scale factor for length is not too large) and no fluids are involved, it will probably be extremely difficult or impossible to achieve perfect modeling.

Adequate models give an adequate estimate of the performance of the prototype under a given set of conditions without correction, even though certain scaling parameters are violated.

A distorted model requires a correction; but if a correction does not produce an adequate estimate, then the model is useless. At present, most structural models in use are adequate or distorted. A dissimilar model bears no physical resemblance to the prototype, but provides an estimate of performance by analogy. An analog computer program set up to represent the prototype is such a model.

The theory of models requires the selection of certain fundamental units (refs. 24 and 102). In structural models, these units are always mass, length, and time. If heating effects are important, then temperature is added. Then certain independent dimensionless groups π_i are obtained by dimensional analysis or from mathematical equations which define the dynamics of the structure. For structural models, these dimensionless groups are usually one or more of the following: the Strouhal, Froude, Mach, and Reynolds numbers, or their modification by multiplication with dimensionless ratios.

The Buckingham pi theorem states that the number of dimensionless groups must be equal to the total number of variables (dependent and independent) minus the number of fundamental units (refs. 24, 102, and 103). If the problem has one dependent variable, the dimensionless group containing the dependent variable is a function of the dimensionless groups containing the independent variables; i.e.,

$$\pi_1 = \phi(\pi_2, \pi_3, \ldots \pi_m) \tag{25}$$

Complete similitude is achieved when model and prototype have identical values for each π_i.

There is often more than one dependent variable. In most of these cases, the dependent variables are interrelated (e.g., the displacement, acceleration, bending moment, and stress at a particular location on the structure), so that the remaining dependent variables may be readily determined after the first variable is established. In other cases, the dependent variables are not related; thus, a more sophisticated approach is required (ref. 104). Also, a dependent variable in one problem may be an independent variable in another. For example, the natural frequency would be a dependent variable when the resonance properties are determined, but would be an independent variable when vibration response to a specific loading is obtained. Obviously, the experimenter must be able to distinguish between the dependent and independent variables and must assume that the basic phenomenon is independent of structural size.

5.1.1.2 Applicability to Space-Vehicle Structures

For most structural models, scale factors n_i between the model and the prototype are selected for length, Young's modulus, mass density, and either pressure or force; i.e., $\ell_p = n_\ell \ell_m$, $E_p = n_E E_m$, $\rho_p = n_\rho \rho_m$, and $\tilde{p}_p = n_{\tilde{p}} \tilde{p}_m$ or $F_p = n_\ell^2 n_{\tilde{p}} F_m$, respectively. If model and prototype use the same material, then $n_E = n_\rho = 1$. If it is desired to keep the stress constant, then $n_{\tilde{p}} = 1$. The perfect model will have the same mode shape as the prototype in each mode. If the model and prototype have their elastic moduli and mass densities related by $E_p/\rho_p = E_m/\rho_m$ (i.e., the same speed of longitudinal waves), which is often found, then the frequency-scale factor is inversely proportional to the length-scale factor n_ℓ.

There are difficulties in achieving even a distorted model for most aerospace structures subjected to acoustic or aerodynamic noise and/or mechanically transmitted vibration. In many cases, it is extremely difficult to scale all length parameters adequately. Exceptionally thin skin may be required for the model; thus necessitating special fabrication and handling. The cost of scaled rivets and fasteners may be considerable. Since these elements often control resonant behavior and determine nonlinear effects, it is important that they be installed with great precision. Insufficient room for tools often makes this impossible. In addition, surface roughness effects that influence friction must also be scaled.

Problems may arise in producing scaled welded or brazed joints. Composites honeycomb, etc., may require special processing to achieve proper scaling. Compromises in construction usually have an appreciable effect on dynamic behavior in the higher-order modes, but often little effect in the lower-order modes (ref. 102). Unfortunately, for large prototype structures it is the higher-order modes that are usually excited by acoustic or aerodynamic noise and/or mechanically transmitted vibration.

If accelerometers are used to measure the vibration of the model, their mass loading may have an appreciable effect on the measured vibration magnitude, mode shape and natural frequencies, unless they are scaled or their impedance small, compared to the driving-point impedance of the structure. The spectral density G"(f) for the unloaded structure can however be calculated from the spectral density G'(f) measured by the accelerometer (refs. 105 and 106):

$$G''(f) = |[Z_1(f) + Z_2'(f)]/[Z_1(f) + Z_2''(f)]|^2 G'(f) \qquad (26)$$

where $Z_1(f)$ and $Z_2'(f)$ are the mechanical (driving point) impedance of the structure and the accelerometer at the accelerometer-mounting point, respectively; and $Z_2''(f) = 0$. For frequencies sufficiently below the resonant frequency of the accelerometer, $Z_2'(f) = i\,2\pi m_a f$, where m_a is the mass of the accelercmeter.

If propellant sloshing influences the structural vibration in the frequency range of interest, another problem is encountered. Slosh natural frequencies vary in accordance with $(\text{gravity/length})^{1/2}$, so that gravity should be scaled. To avoid using an accelerator or centrifuge, most experimenters substitute a model fluid which has a greater mass density (ref. 107). Fortunately, the frequency range where the effects of acoustic and aerodynamic noise and mechanically transmitted vibration are predominant is usually above the slosh natural frequencies that have an appreciable effect on the structure. However, the slosh natural frequencies for both model and prototype must be calculated to ascertain this observation.

When structural models are used to determine the vibration response to acoustic noise from rocket or jet engines, best results are obtained when model engines are used for generating the acoustic noise. For a perfect model, the

fluctuating pressures will be nearly identical to those of the prototype, if the model engines use the same propellants and thrust determined from $T_p = n_\ell^2 n_p T_m$ (refs. 108 and 109). When model engines are not feasible, a random acoustic-noise source may be substituted. The characteristics of the pressure field may be calculated for the prototype and then scaled to the model (ref. 108).

The vibration response to aerodynamic noise and buffet can be estimated by exposing the structural model to aerodynamic flow in a wind tunnel. The Mach and Reynolds numbers for the model must be identical with that of the prototype to achieve properly scaled flow conditions. However, no wind tunnel is capable of providing simultaneously the desired ranges of Reynolds number and Mach number experienced by actual space vehicles. For the forward parts of the vehicle, Reynolds-number distortion usually has only a minor effect on the spectrum of the fluctuating pressure field (refs. 14 and 15). However, little comparative data are available for the aft parts of the vehicle, where Reynolds-number differences and the model's shock reflections off the wind-tunnel walls may affect the pressure field appreciably. Unfortunately, most wind tunnels have inherently high noise levels, usually caused by general turbulence in the tunnel. Also, shocks in the expansion section of a blowdown wind tunnel or turbulence generated by the compressor and turning vanes of a continuous wind tunnel may add to these high noise levels. If the vehicle is aerodynamically ''clean,'' this noise can be a substantial contributor to the total fluctuating pressure field and the structural vibration of the model, thus invalidating the data. If the external shape of the vehicle is unfortunately conducive to severe aerodynamic-flow disturbances, such as described in Section 3 and shown in figure 3, the aerodynamic noise will probably mask the undesirable wind-tunnel noise.

Occasionally, in wind-tunnel tests, shock waves have been observed to oscillate in the transonic regime, as well as to generate increased aerodynamic noise. Under certain conditions, the subsonic boundary layer allows the higher pressure aft of the shock to feed forward under the shock. This in turn increases the pressure gradient at that point and tends to move the boundary-layer separation point upstream. The balance between the initial flow conditions that position the shock and the tendency of the shock to move forward is unstable. This causes the shock to move randomly about a small region of the vehicle so that the flow in this region alternates randomly between attached and separated conditions. Oscillating pressure changes as high as 0.8 q have been observed in wind-tunnel tests of Apollo and Dyna Soar (refs. 15 and 110). A dominant full-scale frequency range of 0 to 2 Hz has been observed. However, shock oscillations have not been observed during flight. The increasing speed of the vehicles does not permit the shocks to ''stabilize'' in the transonic regime, and causes the shocks to pass through those conditions conducive to shock oscillations. Thus, oscillating shocks could occur for a vehicle operating at constant speed in the transonic regime, such as in a wind-tunnel test, but would not for a vertically rising vehicle following a conventional trajectory.

Structural buckling of the model under static loading may be another problem if the prototype structure normally stands vertically and the model is tested

horizontally in the wind tunnel. Experimental data on the buckling of structures similar to the model may be used to determine if horizontal testing will be a problem (refs. 111 through 113). (Results of theoretical analyses on idealized structures should be used with great care because they often provide an unconservative estimate of critical buckling loads.)

Mechanically transmitted vibration is not often modeled. Best results can probably be expected using model sources for the excitation. If the source of mechanically transmitted vibration is the rocket engine, it will probably be difficult or expensive to obtain a model rocket engine with sufficient detail to provide proper dynamic-force scaling. Other sources, such as pumps and generators, can be expected to have similar difficulties.

If an electrodynamic or hydraulic shaker is substituted for the model source, it should apply a spectral density $G''_m(f_m)$, which can be calculated from equation (26) after certain vibration and mechanical impedance measurements are made on the prototype source and on the adjoining test structure (e.g., the full-scale rocket engine and its test stand), and on the model structure (ref. 105). The acceleration spectral density $G'_m(f_m)$ to be used in the right-hand side of equation (26) can be calculated from the acceleration spectral density $G'_p(f_p)$, which is measured at a location near what is normally the interface of the prototype source with the prototype structure, during excitation of the source (e.g., static firing of the rocket engine):

$$G'_m(f_m) = (n_\ell n_E^{\frac{1}{2}} n_\rho^{\frac{3}{2}} / n_p) G'_p(f_p) \tag{27}$$

The frequency should be scaled in accordance with

$$f_m = n_\ell (n_\rho / n_E)^{\frac{1}{2}} f_p \tag{28}$$

The mechanical impedance $Z_{1m}(f_m)$ and $Z'_{2m}(f_m)$, can be calculated from the driving-point impedance measurements $Z_{1p}(f_p)$ and $Z'_{2p}(f_p)$, made separately on the prototype source structure and the test structure, respectively, at the interface:

$$Z_{1m}(f_m) = Z_{1p}(f_p) / n_\ell^2 (n_E n_\rho)^{\frac{1}{2}} \tag{29}$$

$$Z'_{2m}(f_m) = Z'_{2}p(f_p) / n_\ell^2 (n_E n_\rho)^{\frac{1}{2}} \tag{29a}$$

The mechanical driving-point impedance $Z''_{2m}(f_m)$ can be determined by direct measurement of the model structure at the normal interface with the shaker which represents the model source. Impedance-measurement techniques are discussed in references 114 through 118.

The vibration response to acoustic or aerodynamic noise, or to mechanical transmission from the source, can be scaled correctly only if the structural

damping is not affected by the scaling. As discussed in Section 4.1.2.2, damping occurs in one or more of the following three forms: material damping, friction damping, and acoustic radiation. Material damping is dependent upon the mode shape and the maximum vibration stress in each mode. Although figure 6 shows that material damping is nonlinear, the material damping of the model will be identical to that of the prototype if (a) the mode shape is identical, (b) the model and prototype structures are made of the same material, and (c) $n_{\tilde{p}} = 1$. If the maximum stress is less than the endurance limit for both model and prototype structures, the resonant magnification resulting from material damping changes only slightly for different stress levels, obviating the need for $n_{\tilde{p}} = 1$.

An analysis performed by Greenspon, however, has shown that it is almost impossible to scale material damping perfectly (ref. 119). He assumed thermal relaxation to relate the internal friction to the temperature rise of material, and found that the thermal conductivity k_s and the specific heat c_s of the material must be scaled in accordance with

$$n_k = n_\ell (n_E/n_\rho)^{\frac{1}{2}} n_c \tag{30}$$

When the same material is used for model and prototype ($n_{ks} = n_{cs} = n_E = n_\rho = 1$), equation (30) is violated unless $n_\ell = 1$ (i.e., no length scaling). Even when different materials are used, in most cases they have almost the same speed of longitudinal waves (i.e., $n_E \approx n_\rho$). Thus, under these conditions, it would be fortuitous to find a model material that would satisfy equation (30). It should be noted that the scaling difficulty occurs in the heat conduction.

After the heat is conducted to the surface, it is transferred to the surrounding fluid by conduction and convection, and to the other surfaces and spaces by thermal radiation. For scaling the heat conduction across the layer of fluid adjacent to the structure, the model fluid must be selected to provide the same Reynolds number as the prototype fluid; that is,

$$(\rho_{fp} \dot{w}_p \ell_p / \mu_p) = (\rho_{fm} \dot{w}_m \ell_m / \mu_m) \tag{31}$$

where ρ_f and μ are the mass density and viscosity of the fluid, respectively, and $\dot{w}$ is the oscillatory velocity of the fluid at a point on the structural interface. Even so, the thermal conductivity k_f and specific heat c_f (at constant pressure) must also be scaled in accordance with equation (30). If the same fluid (usually air) is used for model and prototype, then $n_{k_f} = n_{c_f} = n_E = n_\rho = 1$, again violating equation (30) unless $n_\ell = 1$. It would be again fortuitous to find a model fluid that would satisfy equation (30). Thermal radiation will be scaled if all spatial relationships are scaled in accordance with n_ℓ and the following characteristics of the model structure and all adjacent surfaces are identical to those of the prototype: materials, temperature differences, emittances, and absorptances (ref. 120).

This scaling would be difficult to accomplish practically, even though the experimental data of figure 6 does not show the scaling to be as great a problem as is indicated by the theory.

Because friction damping is controlled by the kinetic coefficient of friction between the mated surfaces, it would appear on a theoretical basis that scaling should be no problem despite the fact that it is a predominant source of nonlinear vibration. Since the static friction must be overcome for slip or sliding to occur, (a) the static as well as the dynamic coefficient of friction for the model and prototype structures must be identical, and (b) the fluctuating pressure fields must be scaled in accordance with $n_{\tilde{\rho}} = 1$ (refs. 47 and 49). However, the first condition is usually impossible to achieve in practice. Acoustic radiation from the model and prototype will be identical if the spatial conditions and adjacent structures are scaled and if $(c_{ap}/c'_{Lp}) = (c_{am}/c'_{Lm})$ and $(\rho_{fp}/\rho_p) = (\rho_{fm}/\rho_m)$, where c_a is the speed of sound in the fluids; c'_L, the speed of longitudinal waves in the material; and ρ and ρ_f, the mass density of the structure and fluid, respectively. If the same material and fluid are used for the model and prototype, proper scaling should be achieved.

For viscoelastic damping, it can be shown that model and prototype have identical resonant magnifications if the model uses the same materials (metal and viscoelastic) as the prototype. To achieve proper scaling for air pumping, it is necessary that $(c_{ap}/c'_{Lp}) = (c_{am}/c'_{Lm})$ and $(P_{op}/P_{om}) = (E_p/E_m) = 1/n_\ell$, where P_o is the absolute ambient pressure. Unfortunately, it would be extremely difficult to satisfy the latter relationship, except under special circumstances, and impossible to satisfy if the same materials and fluid were used for the model and prototype. However, theoretically-determined corrections can be applied to model results to predict prototype performance accurately.

Scale models can also be used to predict fatigue behavior. Obviously the behavior is dependent upon the material, so that the model and prototype must be made of the same material (i.e., $n_E = n_\rho = 1$). Since the number of cycles to failure is dependent on the stress, the scale factor $n_{\tilde{p}} = 1$ must be used. If scaling is perfect, the time-to-failure T_f for model and prototype will be related by $T_{fp} = n_\ell T_{fm}$. However, fatigue tests performed by Gray on simple panels exposed to jet noise, using models of various scale factors n_ℓ, show imperfect scaling in the time to failure (ref. 121). From these tests, Gray observed by $T_{fp} = n_\ell^\lambda T_{fm}$, where $\lambda = 1/n_\ell^{0.2}$, indicating that his models produced conservative estimates for prototype-fatigue life. In most cases, this result can be explained by lack of scaling of the nonhomogeneity of the material (grain size, microscopic flaws, stress concentrations, etc.) between model and prototype. The effects of size on fatigue is discussed in reference 122.

Scale models are seldom used for other vibration failure mechanisms; for example, collision between adjacent structures, wear, and operational drift.

5.1.1.3 Assessment

To be of practical utility during the development of a space vehicle, a subscale structural model must provide the prediction of prototype performance with sufficient accuracy, with or without correction. A review of published literature on the comparison of model and prototype data shows that when the prototype was a highly complex structure, the model did not provide an adequate estimate of prototype performance, but when the prototype was fairly simple, the model did provide an adequate estimate. For example, acoustic noise was applied to various external panel sections of the highly complex Snark missile and two quarter-scale models (i.e., $n_\ell = 4$), and the vibration measured at many locations throughout the three structures (ref. 123.). The original model had many deficiencies in structural details, although most of the basic features of the prototype were properly scaled. The improved model was an attempt to correct most of the important deficiencies. Figure 22 shows a typical comparison of one-third-octave vibroacoustic-transfer functions (ratio of rms-vibration acceleration to rms-acoustic force) versus scaled frequency for these structures.

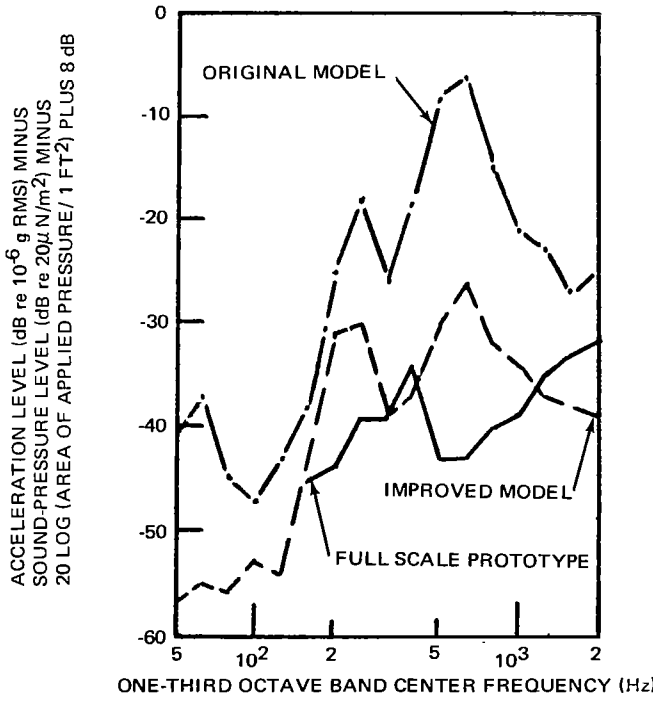

Figure 22. – Comparison of vibroacoustic-transfer functions for Snark missile structure and two one-quarter scale models.

The prediction produced by the original model was almost always in error, often by more than 20 dB. The improved model provided some improvement in accuracy, as shown in this typical figure; but the error was still too large (occasionally in excess of 20 dB and often in excess of 10 dB) to preclude its practical utility or to justify its cost. Another example of inaccuracies was observed between the Apollo boilerplate service module and its one-tenth scale model, shown in figure 23 (ref. 124). Great pains were taken to scale nearly all structural details in the model. Transonic flight data for the full-scale boilerplate were compared with wind-tunnel data for the model. Figure 24 shows a reasonably similar shape between the two normalized random strain spectra. Unfortunately, the model underpredicted the rms value of the strain by 8 dB during the most severe transonic period. On the other hand, the model underpredicted the rms acceleration of the flight prototype by only 2 dB. Unfortunately, the model missed the predominant frequency range by a factor of 2, as shown in figure 25. Reasons for the inaccurate predictions of the Snark and Apollo models are discussed in references 123 and 124. Similar results were noted on a Nimbus spacecraft at higher frequencies (ref. 125).

On the favorable side is the comparison of results for simple panels exposed to jet noise, mentioned previously in reference 121. Figure 26 shows the excellent prediction of the prototype-strain spectral density from the one-sixth-scale model data. Similarly, models of simple shells (cylindrical, conical, and hemispherical) have shown excellent estimates of prototype natural frequencies and mode shapes for lower-order modes. However, no effort has been made to determine the degree of complexity obtainable before prediction inaccuracies occur.

5.1.2. Vibration Tests

5.1.2.1 Test Classification and Philosophy

Laboratory vibration tests may be categorized as follows: (a) design development, (b) qualification, (c) acceptance, and (d) others. Design-development tests are performed to provide certain information to the designer regarding the modal characteristics of the structure (ref. 33), the vibration response to certain applied loadings, the adequacy of the design, and, in some cases, the vibration-failure mechanisms, locations, and levels. Qualification tests are performed on flight-quality hardware to demonstrate the adequacy of the design and fabrication methods for flight, usually before the first flight. Acceptance tests are performed on articles intended for flight usage to demonstrate that a predetermined minimum adequacy had been achieved during fabrication and assembly. Any of these may be performed as vibration tests combined with other loads and environments. Other tests include (a) reliability tests, to demonstrate the variation of the failure mechanism between items of hardware under prescribed types of loading; (b) fragility tests, to map the failure threshold perimeter under a variety of loadings or frequencies; and (c) certain interim tests between development and qualification. There is no common terminology used throughout the aerospace field to describe a particular type of test, so it is not uncommon in two different vehicle-development programs or in two different organizations to have two names for the same type of test.

(A) FULL-SCALE FLIGHT ARTICLE

(B) ONE-TENTH-SCALE MODEL

Figure 23. – Structural details of the Apollo boilerplate service module.

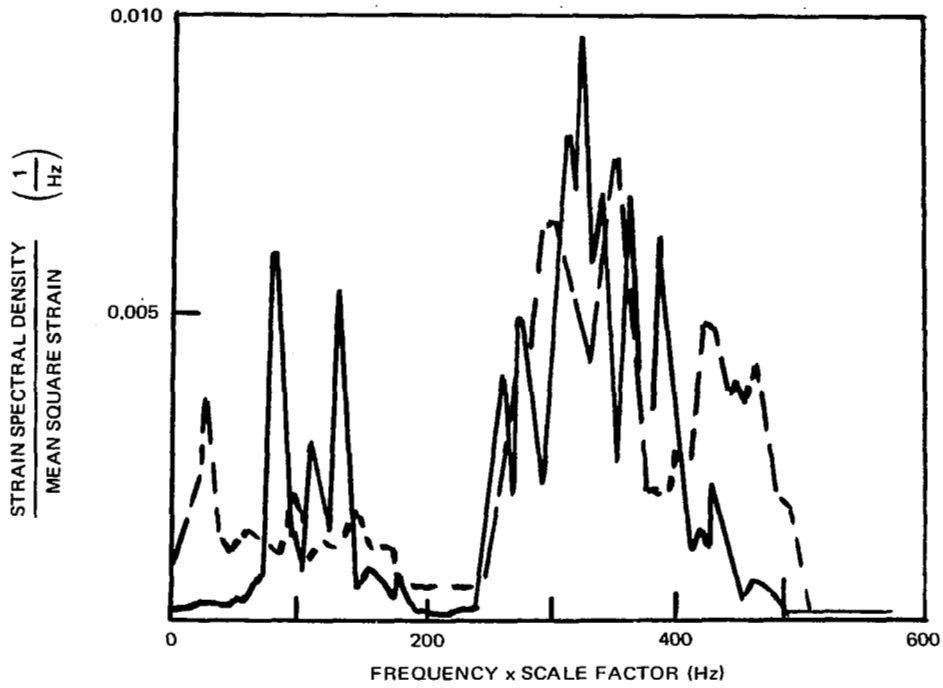

Figure 24. – Comparison of Apollo boilerplate service module vibration-strain spectra.

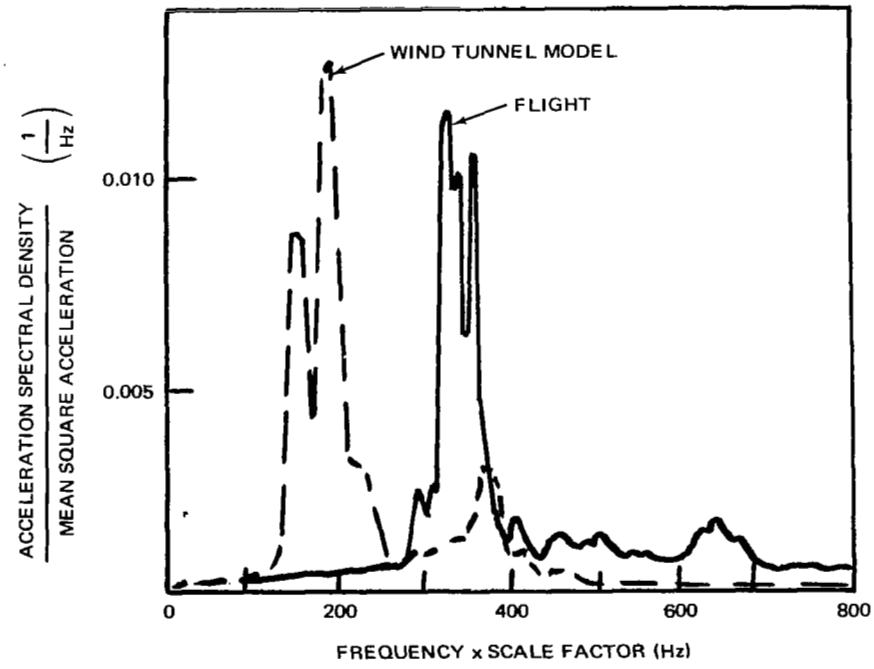

Figure 25. – Comparison of Apollo boilerplate service module vibration-acceleration spectra.

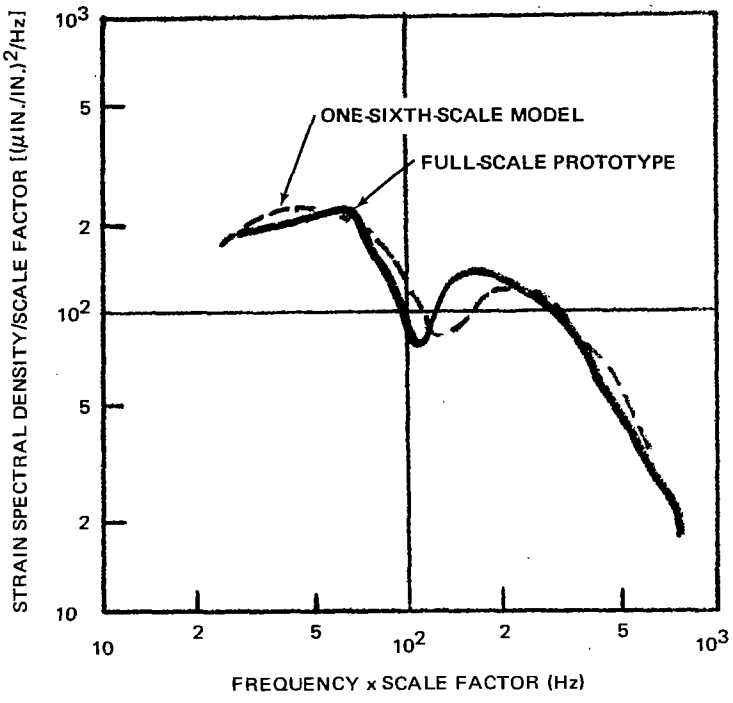

Figure 26. – Comparison of vibration-strain spectra for prototype and model panels excited by jet noise.

Usually, the selection of design-development tests and their test conditions are at the option of the designer and/or program management. Qualification tests are nearly always required by contract, with test conditions usually specified as somewhat more severe than those anticipated for flight. Qualification tests are often waived when the structures are too large to be tested. In these cases, the structures are often ''qualified'' by vibration analyses and/or tests on certain structural sections. Laboratory vibration-acceptance tests may or may not be required by the contract. If required, the test conditions must be selected with great care, since the test degrades the hardware by exposure before flight, while the flight adequacy is being demonstrated simultaneously. Hardware used for testing, other than acceptance testing, is never used for flight, except under unusually special circumstances.

Laboratory vibration tests are nearly always performed on equipment, sometimes on secondary structure (almost always with equipment items or dummies), and occasionally on primary structure.

The subject of equipment testing will be limited in this report to the discussion of design and test criteria. However, it is likely in the future that some equipment items may serve simultaneously as minor or major load-carrying members, so that this division may eventually disappear.

There is no uniform philosophy throughout the aerospace industry regarding the types of primary or secondary structures to be tested. Most spacecraft

contracts require vibration testing of the entire payload. For example, figure 27 shows the Ranger spacecraft excited by an electrodynamic shaker simulating the longitudinal vibration applied by the launch vehicle during the launch phase of the mission (ref. 126); figure 28 shows a similar test on the Gemini spacecraft (ref. 127). Figure 29 shows the Surveyor spacecraft excited by three electrodynamic shakers simulating the vibration applied by the three vernier rocket engines during the lunar-descent phase of the mission (ref. 128). The spacecraft is inverted to permit operation of the radar subsystem in the free field.

Only a few contracts require vibration testing of launch vehicles or large spacecraft because most are too large and too heavy to be tested conveniently or economically. In some cases, sections of the launch vehicle are tested; figure 30 shows the vibration-test setup for the thrust structure and aft skirt of the Saturn S-II stage (ref. 129). Eight hydraulic shakers excited the structure through a large fixture. Dummy engines and equipment, simulating the weight and center of gravity of the actual items, were used to provide a simulated loading for the primary and secondary structure of the section.

5.1.2.2 Test Facilities

There is a wide variety of test equipment available for performing laboratory vibration tests. The electrodynamic shaker is the most popular because of the ease of controlling the test. It is used mostly in the 5- to 2000-Hz frequency range, although the useful upper-frequency limit usually depends upon its force capacity and size. Electrodynamic shakers with force-generating capacities up to 30 000-lb rms are commercially available.

Hydraulic shakers are used mostly in the 0- to 500-Hz frequency range, although the useful upper-frequency limit is dependent upon the design features of the shaker, which vary widely, as well as on its force capacity and size. Hydraulic shakers with force-generating capacities up to 250 000-lb rms are commercially available.

Test systems for providing power and control to these shakers also vary widely. For performing sinusoidal vibration tests, a typical system has an electronic oscillator driving an electronic power amplifier through a gain-control circuit, as shown in figure 31. The power amplifier in turn drives the shaker (actually a translational motor) which is attached to the test fixture and test specimen.

In nearly all tests, a control accelerometer is attached to the test fixture at a point adjacent to the mounting point of the specimen. If there are two or more mounting points, the accelerometer is located adjacent to one of them. The accelerometer signal is either fed directly to the gain control circuit, so that the shaker is automatic-gain-controlled (AGC), or fed to a meter, which is read manually, and the gain-control circuit is then adjusted manually.

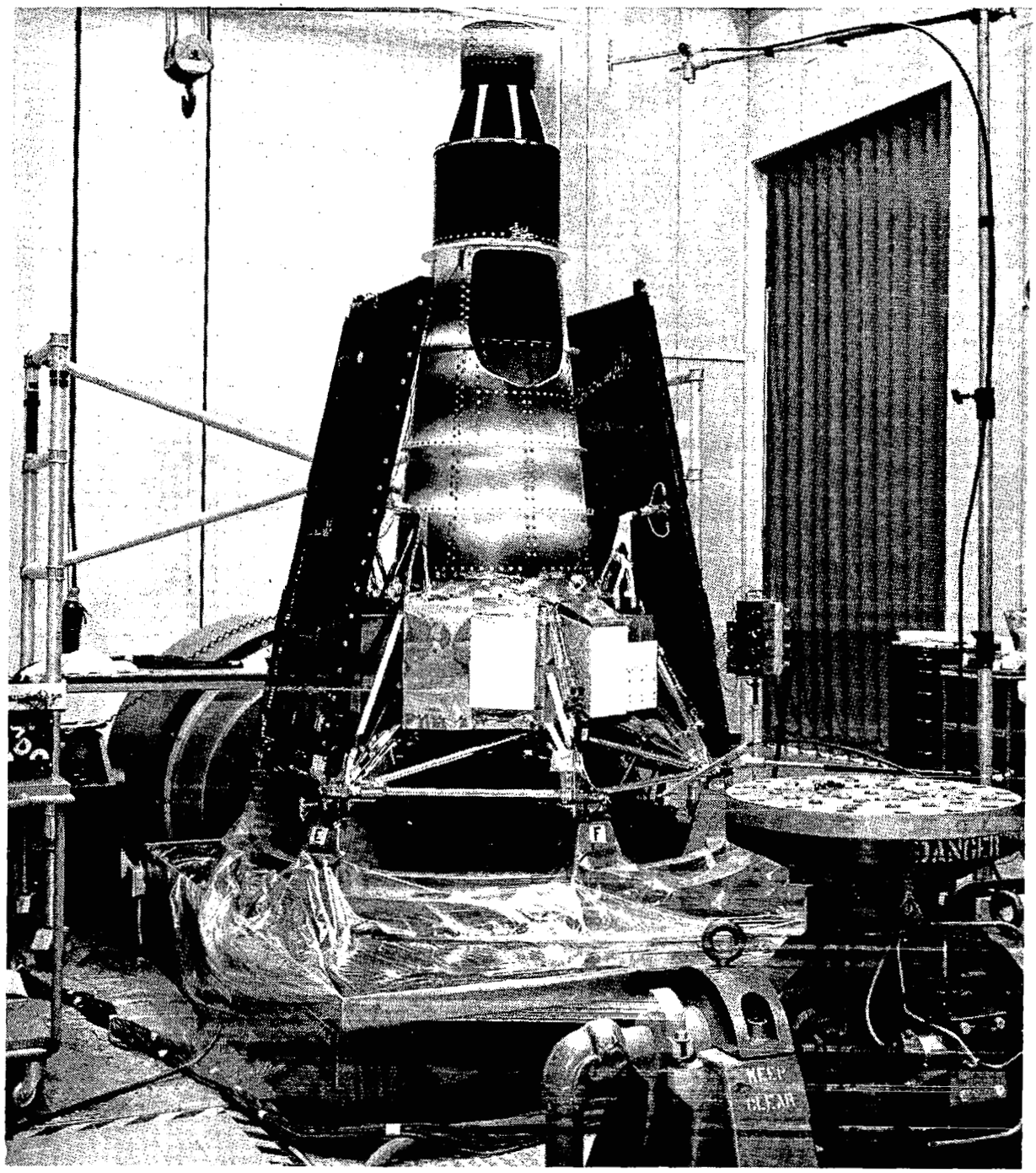

Figure 27.– Laboratory vibration test of the Ranger spacecraft.

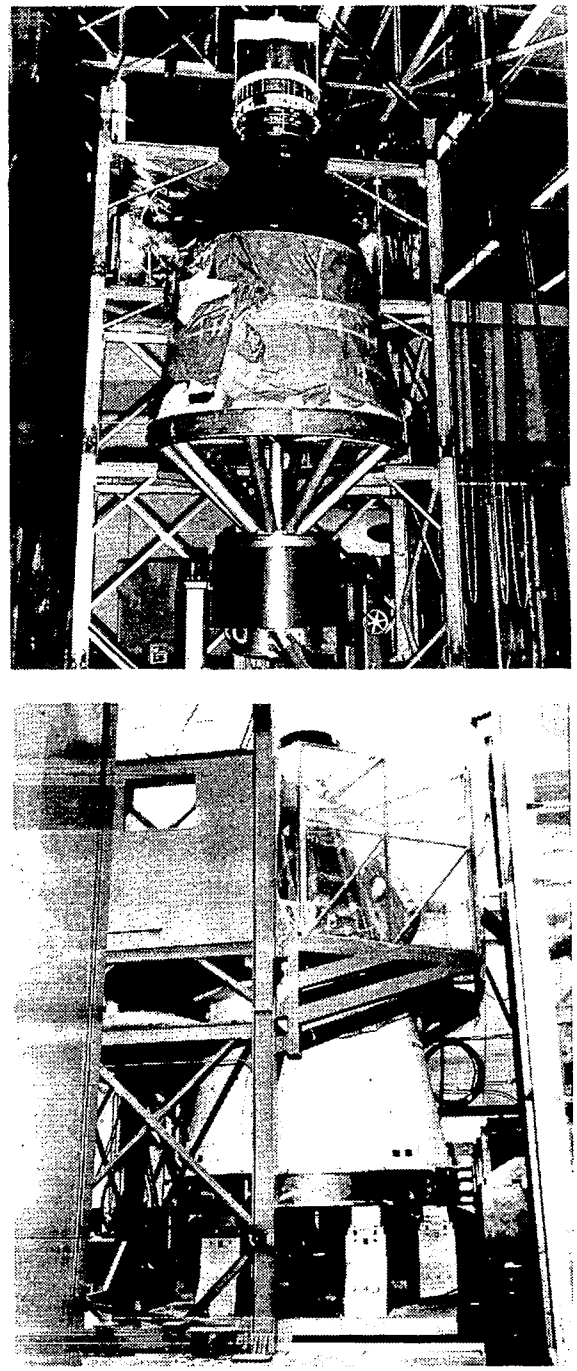

Figure 28.–Laboratory vibration tests of the Gemini spacecraft in the vertical and horizontal directions.

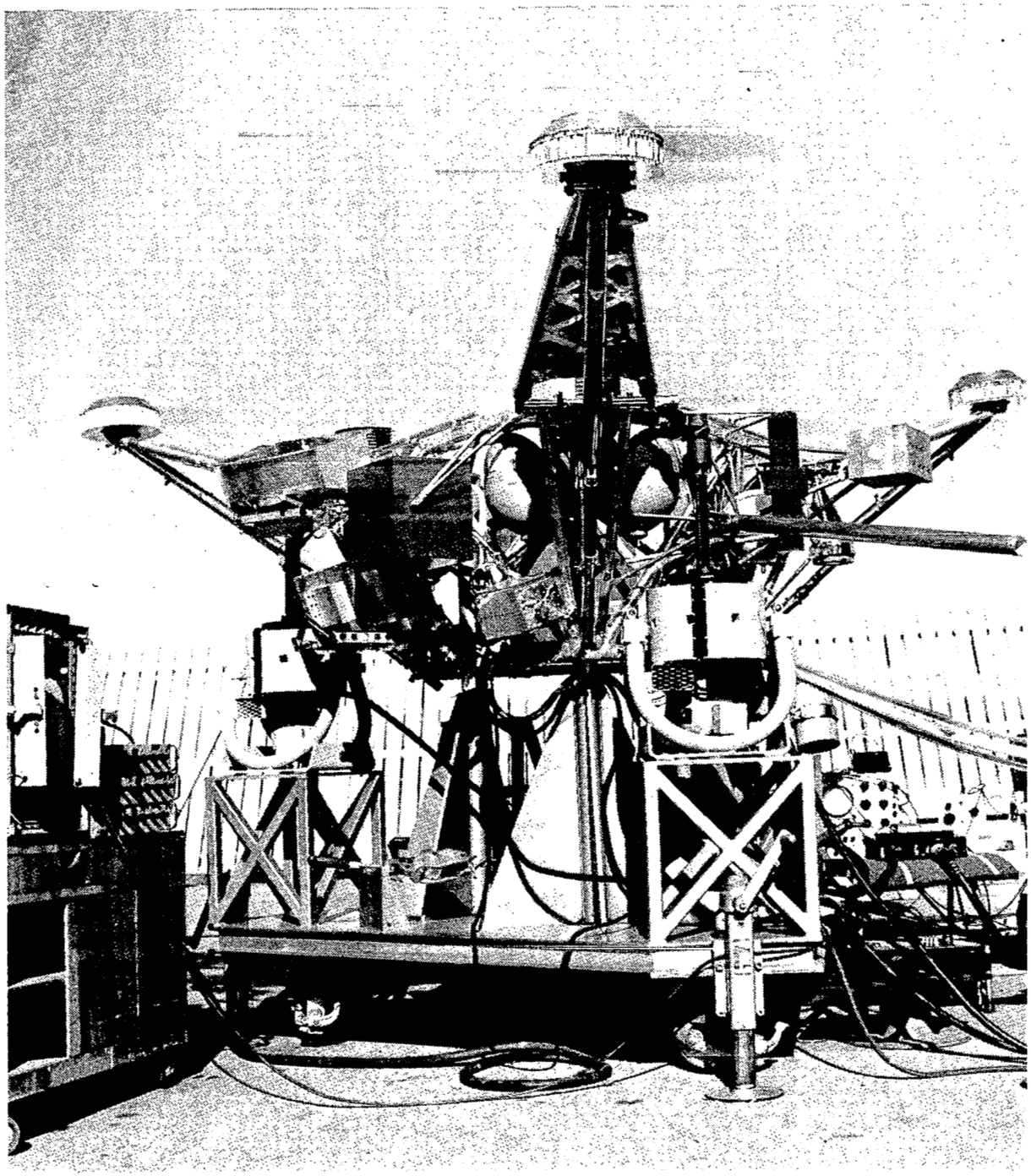

Figure 29.—Laboratory vibration test of the Surveyor spacecraft.

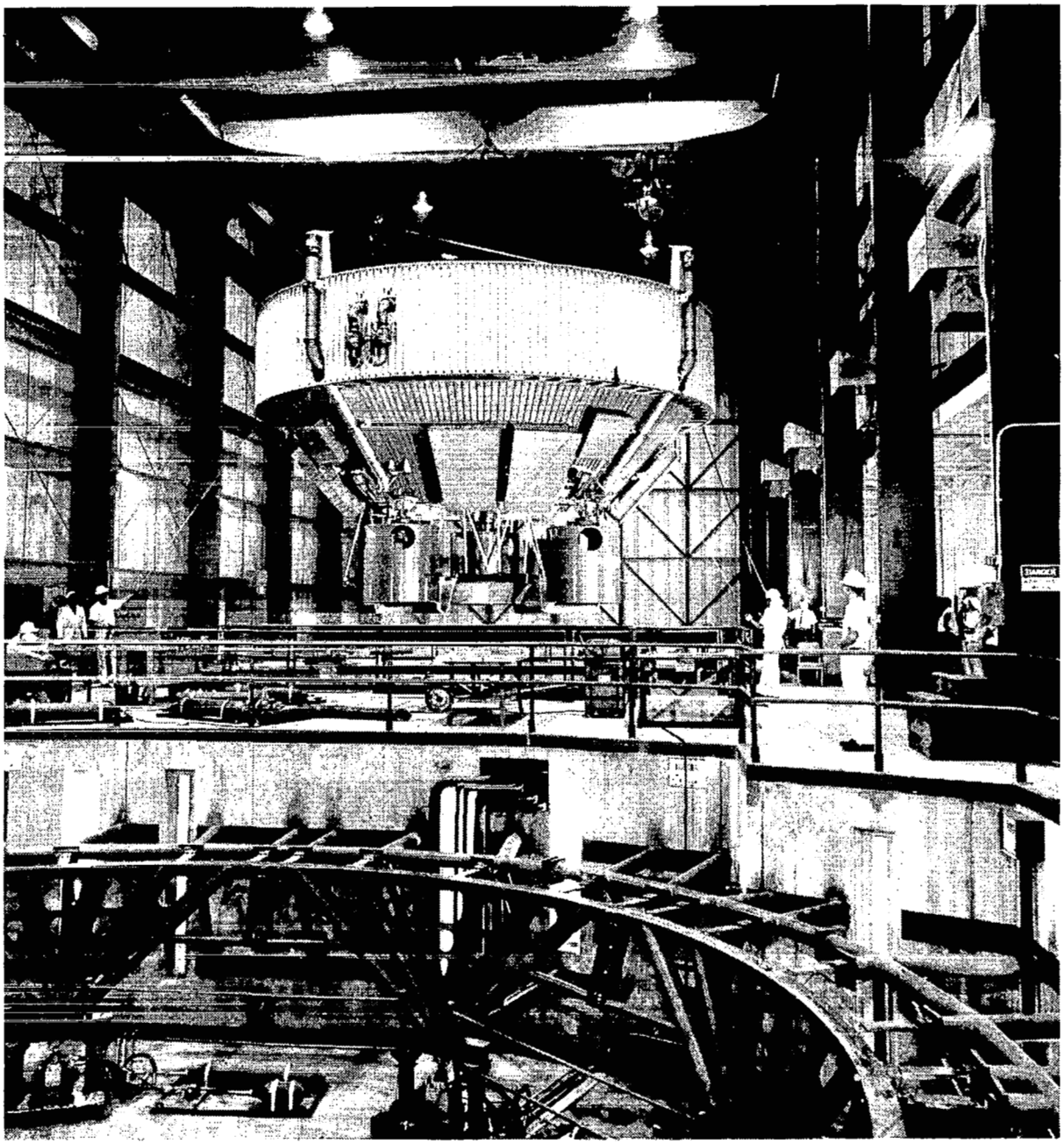

Figure 30.–Laboratory vibration-test facility of the thrust structure and aft skirt of the S-II stage, Saturn V launch vehicle.

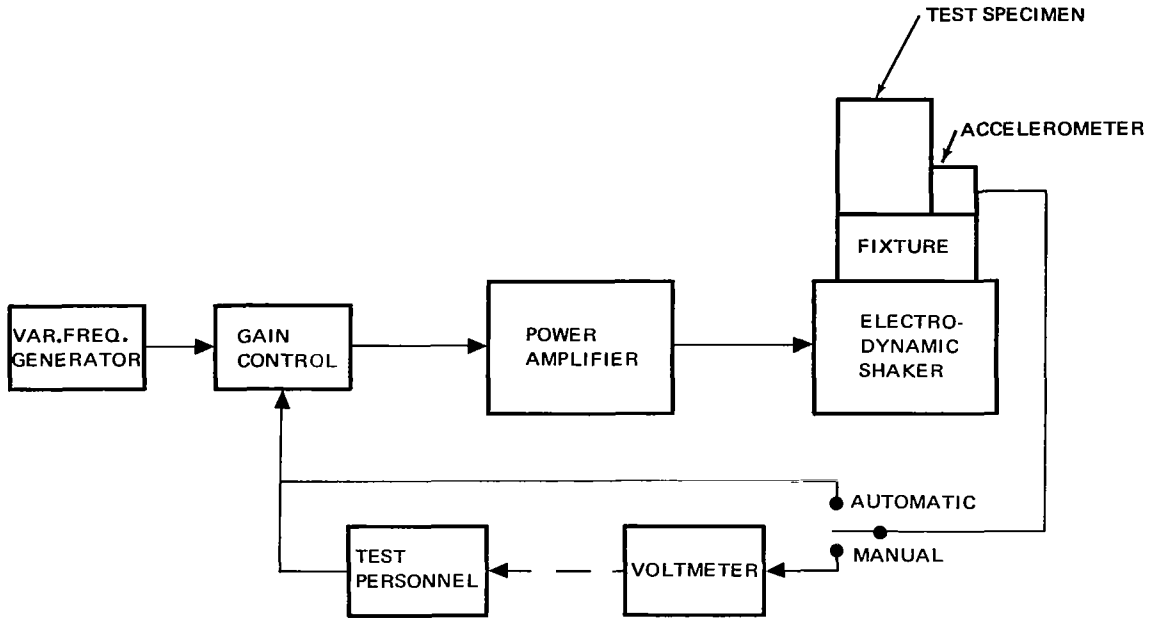

Figure 31.- Simplified schematic diagram of a typical system for performing sinusoidal-vibration tests.

To perform random-vibration tests, a typical system contains a random-noise generator driving an electronic power amplifier through a spectrum equalizer, which consists of a large number (usually 40 or 80) of contiguous bandpass filters, as shown in figure 32. Each filter covers a narrow band portion of the spectrum (usually 50 or 25 Hz). The gain of each filter is varied automatically by means of AGC, or manually. The output signals from all the filters are summed and fed to the power amplifier, which in turn drives the shaker, fixture, and specimen. The control accelerometer is attached to the fixture at a point adjacent to the specimen, as described previously. The accelerometer signal is fed to a spectrum analyzer, which consists of a set of filters that have bandpass frequencies identical to those in the spectrum equalizer. The signal from each filter in the analyzer is either fed to its respective equalizer circuit, controlling the equalizer gain by AGC, or fed to a meter (one of 40 or 80), which is read manually. The gain of all equalizer circuits is adjusted manually. These systems are obviously expensive. It must be noted that figures 31 and 32 show only the critical ''black boxes'' of the test equipment. In actuality, there are many additional items of equipment needed for control and overload protection.

5.1.2.3 Qualification-Test Requirements and Their Selection

Because of its contractual status, the qualification test is probably the most important type of vibration test performed during vehicle development. The intent of most qualification tests is to accept flight-adequate hardware

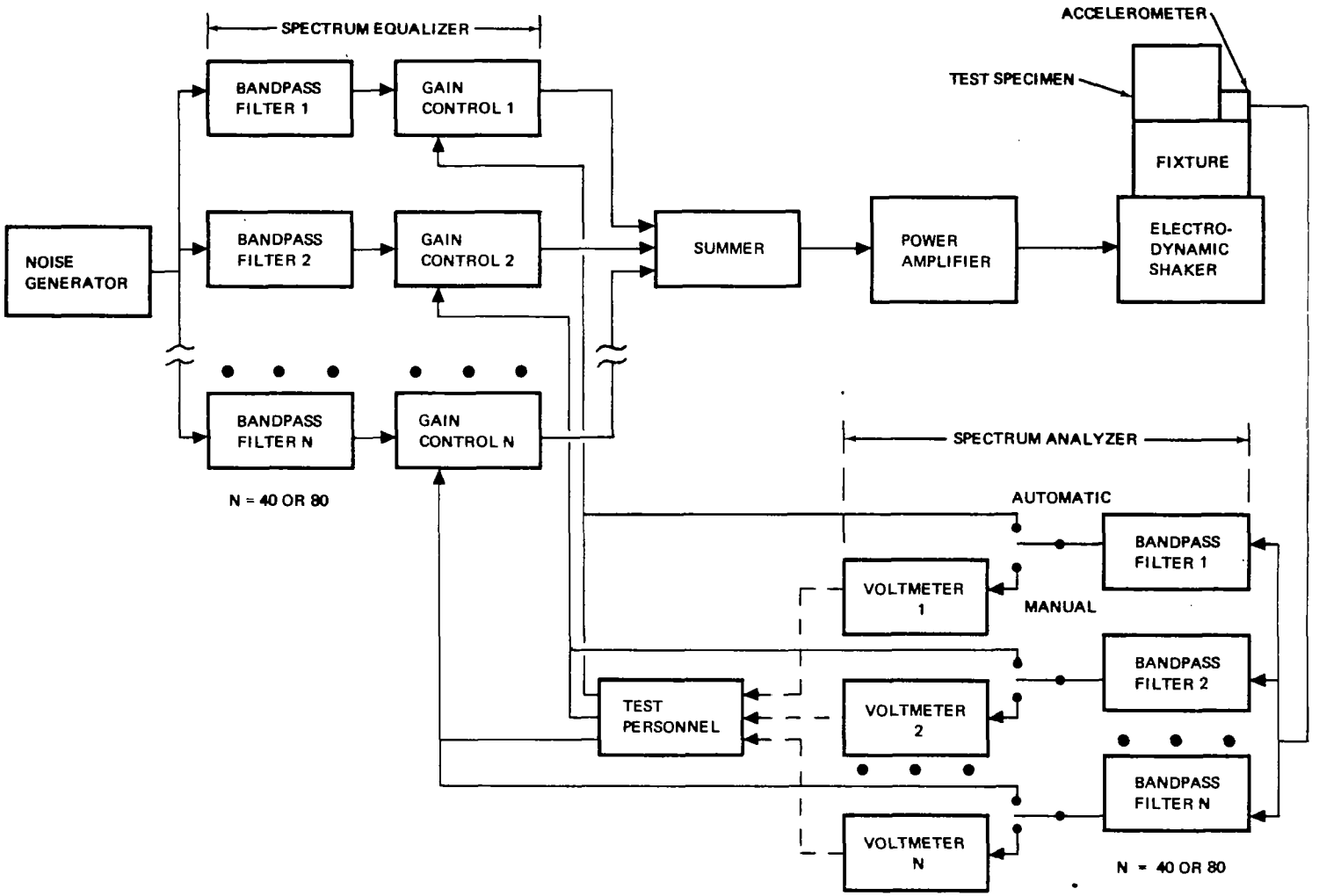

Figure 32.–Simplified schematic diagram of a typical system for performing random vibration tests.

and to reject flight-inadequate hardware. Short of actual flight test, it is impossible to achieve this goal in practice. Thus, it is necessary to consider the tradeoffs between undertesting and overtesting. Obviously, it is easy to avoid nearly all undertesting by increasing test levels until only the most rugged hardware survives. In this case, much of the hardware that is really adequate for flight must be redesigned and retested, often causing unnecessary weight increases and cost and schedule slippage. Many test specifications are written by personnel whose main assignment is to ensure high reliability and structural integrity, leaving to program management and other groups the weight, cost, and schedule problems resulting from overly conservative test levels (ref. 130). With this information, it is not surprising to find that there are many instances where program management has decided to fly space vehicles with hardware that has failed vibration-qualification tests.

The vibration problem that has probably been discussed in the aerospace industry more than any other over the years is that of the selection of qualification test levels and durations. The factors that should be considered in this selection include:

- The degree of similarity between the test and the flight configuration.
- The characteristics of the test facility.
- The method of controlling the test.
- The degree of confidence in the flight vibration predictions.
- The number of test specimens to be used in the qualification of each hardware item.
- The economic balance between the cost of possible flight failures and the cost of possible test failures.

The degree of similarity between test and flight configurations will have a major influence on the lowest frequency for which valid testing can be performed. Often, this frequency limit can be readily determined by comparing the modal characteristics at the lower resonance of the test specimen with the modal characteristics expected for the flight configuration. If these occur at significantly different frequencies, or if no similar mode shapes exist, no valid vibration testing is possible for these modes (ref. 131). For this reason, it is common practice to test a spacecraft by ''notching'' the vibration test level in the vicinity of its fundamental resonance.

Actually, an identical natural frequency or mode shape could exist only by coincidence because of the different mechanical impedance characteristics between the test fixture and the flight structure adjoining the hardware section under consideration. It is possible, however, to force the specimen to high levels at frequencies corresponding to the flight-resonant frequencies

and ''notch'' the levels at frequencies corresponding to the test-resonant frequencies and flight-antiresonant frequencies, if the shaker capacity is large enough and if the resonant characteristics of the flight configuration (usually not yet flown) are known with sufficient accuracy in the frequency range of interest. However, this is almost never done.

For smaller structures, such as the spacecraft shown in figure 27, it is common practice to vibrate the specimen by a single shaker through a test fixture. There are usually great pains taken to restrain the vibration motion of the shaker and fixture to a single direction, and to make the test fixture as rigid and as massive as the force limitations of the shaker permit. Such care helps avoid any contribution to the resonant behavior of the specimen by the fixture, except at higher frequencies. This is to be compared with the flight configuration where the adjoining structure is part of the resonant behavior, often allowing motion in all three orthogonal (mutually perpendicular) directions. This permits multidirectional resonance, and, in the case of most hardware that is attached to adjoining structure through two or more points of attachment, allows variation of amplitude and phase between attachment points throughout the frequency range. Thus, there is a considerable lack of simulation in using single-shaker restrained-motion vibration testing with rigid fixtures. Much of this problem can be reduced by using part of the flight structure adjoining the test specimen as a portion of the test fixture.

The variation between attachment points can often be improved by multiple shakers under separate control, but this increases the cost of testing. In addition, the shaker applies the vibration force in only one direction, whereas the flight excitation is applied in the three orthogonal directions simultaneously. Usually, it is assumed that vibration applied sequentially in each of three orthogonal directions for a specified time duration per direction has the same damage potential as vibration applied in all three directions simultaneously for the same duration. However, this assumption can only be valid for resonant behavior in one direction and by coincidence for multidirectional resonance.

As stated previously, most vibration tests are controlled from a signal generated by the control accelerometer, which is attached to the test fixture adjacent to the mounting point or to one of the mounting points. In the large majority of tests, the specimen interfaces with the fixture at several points or along lines or surfaces. Multidirectional resonant behavior of the test specimen (including rotation), which is coupled with fixture and shaker resonances at the higher frequencies, usually causes the vibration amplitude to vary between mounting points or along the interface. Since the control accelerometer senses motion at only one of these points, undertesting or overtesting usually occurs at the other mounting points, the magnitude of which depends on the mode shapes of the multidirectional resonances. To avoid this undertesting or overtesting during a sinusoidal vibration test, several control accelerometers (usually from three to six) can be used and their signals monitored simultaneously to select the lowest or highest amplitude for test control. Special test equipment is commercially available for implementing this selection automatically.

Another technique employs the averaging of the signals from the several accelerometers. Signal averaging may be used for sine or random vibration testing. Signal averaging may be performed in one of two ways: (1) instantaneous averaging and (2) time division multiplexing (TDM). Overtesting can occur with the instantaneous averaging technique in any mode when two of the control accelerometers are mounted at locations that are vibrating 180^{o} out of phase. This problem is especially acute when only two accelerometers are used, or when the out-of-phase accelerometers are vibrating at high amplitude relative to the other accelerometers. This problem may be avoided by using TDM, which samples the accelerometer signals in sequence to form a composite signal which is then used for manual or automatic test control. However, TDM is not without problems, such as the selection of sample time durations from one signal to the next, although these effects can be minimized (ref. 132). Special equipment is commercially available for implementing test control with TDM.

As seen from the time histories and the changes in the vibration spectra illustrated in figure 1, the flight vibration is nonstationary, especially for the period from liftoff through q_{max}. However, most presently available vibration test systems are capable of controlling stationary tests only. Thus, stationary testing is employed for nonstationary flight conditions. Several test techniques may be used, but all permit overtesting in the time and/or frequency domain. The most popular is the use of a vibration spectrum which envelopes the vibration spectra for the various prelaunch and mission events that exhibit high vibration (acceptance vibration testing, static firing, liftoff, transonic, q_{max}, stage-powered flight for hardware near engines, etc.). Often the time duration for this stationary laboratory test is selected to be the sum of the ''effective'' durations of these prelaunch and mission events. Thus, considerable overtesting may result compared to flight conditions. Overtesting can sometimes be minimized when qualification testing is performed by using several tests in sequence, each test representing a different phase of the mission or of prelaunch condition, and having a different vibration spectrum. However, this series of test setups, checkouts, etc., may be tedious to perform. In the future, special equipment or techniques will probably be available to permit nonstationary vibration testing. Two seem most likely: (1) the use of a nonstationary signal, which has been prerecorded onto magnetic tape that is fed directly to the kind of electronic power amplifier shown in figure 32 (using no AGC), after the system has been calibrated manually with a low-level white random spectrum; and (2) the use of an electronic programmer between the control accelerometer and AGC (fig. 32).

The degree of confidence in the flight-vibration prediction should also influence the selection of the qualification test levels and durations. Classical techniques of vibration prediction applied to a sophisticated representation of the flight structure and test specimen, discussed in Section 4.1, should permit a rather accurate selection of test levels up to a frequency where the representation becomes increasingly less accurate. At higher frequencies the test levels must be increased, usually in some arbitrary manner to avoid the possibility of undertesting. Similarly, the

statistical-energy analysis (SEA), discussed in Section 4.2, may be used for selecting qualification-test levels at higher frequencies. However, since SEA is less precise at high frequencies than classical techniques are at low frequencies, the test levels derived by SEA must be somewhat increased to avoid undertesting. The amount of the increase will also depend upon the degree of sophistication used in the structural representation. If sufficient detail is included, the test level should not be more than the SEA upper bound described previously, which was established by setting the structural damping to zero and utilizing only the coupling loss factor.

Extrapolation techniques (Sec. 4.3) are most often used for test level selection. The degree of confidence in the prediction will depend upon the similarity between the reference and the new vehicle, and how the reference vehicle data were grouped, and if applicable, statistically analyzed. If the reference and new vehicle structures are quite similar, it might be assumed that the vibration prediction would be quite accurate. However, as discussed previously in Section 4.3.2 on scaling methods, Condos and Butler found considerable differences between vibration predictions and subsequent measurements on a new vehicle, even when excellent similarity existed between the reference and the new vehicle, and the reference vehicle data were grouped into zones for similar location and type of structure. From this, as well as from similar experience on the uprated Saturn I launch vehicle, increased test levels to avoid the possibility of undertesting seem in order.

It would appear that a greater increase would be in order for frequency-response methods (Sec. 4.3.1), since even less similarity between vehicles is generally found. However, in all extrapolation methods, the number of measurements, the grouping of the data, and the type of statistical analysis (if used) often has a large influence on the vibration level predicted and thus on the resulting test level. In regard to the number of measurements, for example, Stevens compared eight vibration measurements made on Apollo-service-module external panels (considered simple aerospace structure) with the total population of 180 measurements made on these panels in the radial direction when the service module was acoustically tested (ref. 133). These eight measurements were selected because their locations corresponded with flight-measurement locations. Figure 33 shows that generally there was a 3-dB difference between random vibration spectral envelopes for the small and large number of measurements. This comparison has a direct bearing on the selection of test levels when only a small number of measurements are used for a zone of the reference vehicle in a particular direction.

In regard to data grouping, care is usually required (ref. 86). For example, for statistical analysis, it is common practice to put all vibration measurements for a particular zone of the reference vehicle into the same group, independent of the direction of the measurement. For structure exhibiting vibration predominantly in one direction, this type of data grouping can produce two effects on the test level. First, overtesting can occur in the two directions of lower vibration when the test level is selected on the basis of the entire population of three directional measurements. Second, overtesting can even occur in the direction of highest vibration if the test levels are selected on the basis of a statistical analysis which uses the

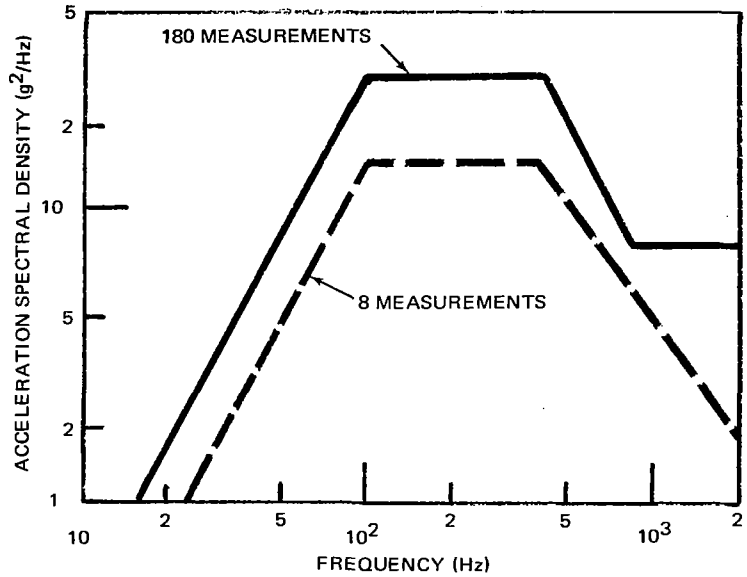

Figure 33.–Comparison of spectral envelope for 8 and 180 vibration measurements made on the external panels of the Apollo service module during acoustic testing.

mean value and standard deviation of the entire data population. A few data points for the two directions of lower vibration can cause a significant increase in the standard deviation without an equivalent decrease in the mean value. Thus, if the test level was based on a certain high probability level, such as the 95 percentile, a higher test level would be produced by using all measurements (independent of direction) than would be produced by using only measurements for the direction of highest vibration.

Although not often considered, the number of test specimens used for qualification testing should influence the selection of the test level. Of particular concern is the variation of the fragility level from specimen to specimen. Fortunately, the primary failure mechanism of primary and secondary structure is fatigue caused by response at the lower resonant frequencies. The fragility (time-to-failure) variation is often acceptable here because manufacturing tolerances can be reasonably controlled. The opposite is sometimes observed for equipment items, since the predominant fragility range can occur at the higher frequencies where manufacturing variations cannot be adequately controlled. This is because tolerances are usually controlled to mils (i.e., milli-inches), whereas relative vibration displacements often occur in the micro-inch range, and also occur where other failure mechanisms than fatigue, such as threshold crossings, may be dominant. When test specimens are

Error

An error occurred while processing this page. See the system log for more details.

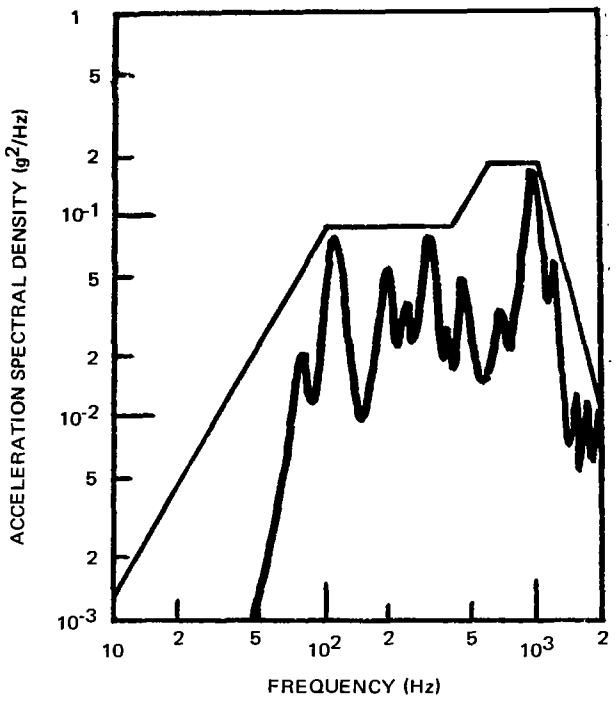

Figure 34.–Predicted vibration spectrum and a five-segment spectral envelope.

antiresonance (refs. 136 and 137). Thus, tolerances are usually specified for the test spectrum, often in the vicinity of ±3 dB for narrow-band analysis. If it is desired to avoid any possibility of undertesting, the test spectrum must be increased to match the lower tolerance. Then additional overtesting is produced at other frequencies. However, there has been much discussion regarding the necessity for this increase, since many test failures, as well as flight failures, are likely to occur at frequencies corresponding to antiresonances, as measured by an accelerometer on the test fixture or at the flight interface, although these antiresonances would not occur at identical frequencies (refs. 138 and 139).

Many of these problems may be avoided by using a test method developed by Curtis (refs. 140 and 141), sometimes called ''random on random''. Three high-level random vibration narrow-band ''spikes'' are applied simultaneously with a lower-level wideband random vibration spectrum, as shown in figure 35. Curtis suggests that (a) the levels for the wideband and narrowband portions be determined from the mean and 98% values, respectively, which are calculated from equation (15) in Section 4.3.1; (b) 12.5% bandwidths be used for the three narrow-band spectra; and (c) the ''spikes'' be stepped sequentially over a given frequency range (fig. 35), but never overlap. Of course, other variations are possible.

Undertesting can result when a possible failure is dependent upon simultaneous high-level excitation at two or more frequencies, which might occur in flight but is not programmed into the narrow-band sequence. Overtesting and/or

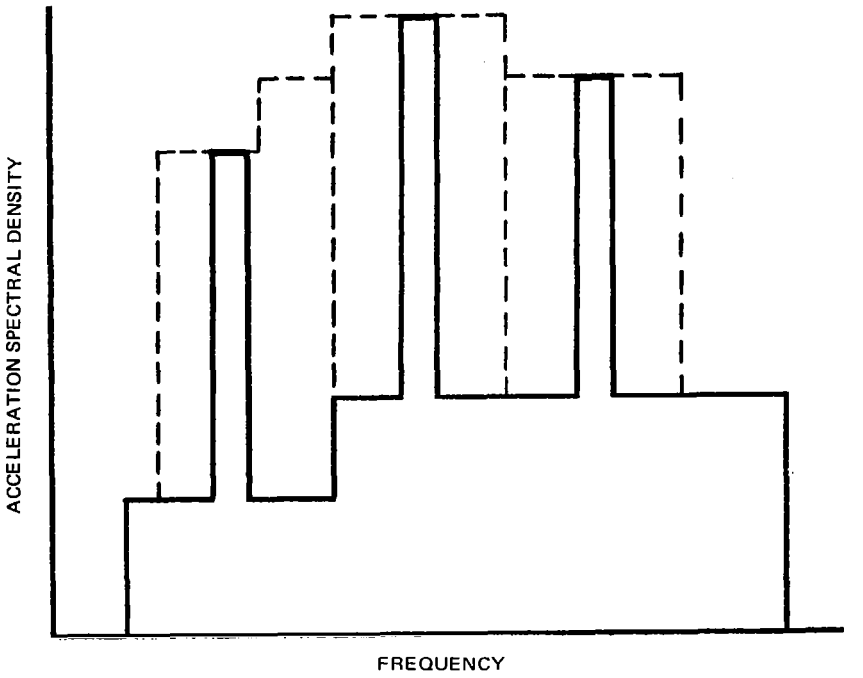

Figure 35. – Random vibration-test spectrum consisting of high-level narrow band "spikes" superimposed on lower-level wideband spectrum.

undertesting can also occur, depending upon the time duration of application of each narrow-band combination, as well as the wideband spectrum. However, Curtis reports good correlation between flight and laboratory results for equipment used in aircraft.

5.1.2.4 Alternatives for Insufficient-Force Capacity

If the test level is too high or the test specimen too heavy, the shaker's force capacity may be exceeded. The obvious solution is to use a larger shaker or multiple shakers. But in many cases, the largest commercially available shaker is already considered (for the frequency range desired) or spatial limitations preclude the use of a sufficient number of shakers. In these cases, alternate measures are required. First, the Curtis method should be considered, since a much lower rms acceleration is required, compared to that for the overall envelope of the high-level narrow-band ''spikes.'' Second, consideration should be given to using high-level narrow-band random vibration which is applied simultaneously at the predominant resonant frequencies of the test specimen for the desired time duration, with the surplus shaker capacity (if any) being used to produce a lower-level wideband random spectrum outside the resonant frequency ranges. A low-level sinusoidal resonance search may be used to establish the predominant resonant frequencies. Third, a narrow-band random spectrum swept across the frequency range may be used, as described by Booth and Broch (ref. 142). Finally, a sinusoid may be used for resonant dwell at the various resonant frequencies, or it may be swept across the frequency range. Some type of sine-random equivalence is

usually assumed (e.g., ref. 66), although it is unlikely that it can be achieved (ref. 143). Of these substitutes, the Curtis method is probably the most realistic; the random-at-resonance method, the most conservative; and swept random, swept sine, and sine dwell, the lowest in cost.

A completely different technique is to specify and control force, rather than control acceleration in vibration testing. Although this form of testing is harder to implement, and vibration force measurements are not normally made in flight, it is possible that much more realism may be achieved with force-control testing, thus avoiding undertesting and overtesting. Otts and his associates have demonstrated that random-force vibration testing can be implemented practically in the laboratory (refs. 144 and 145).

5.1.2.5 Acceptance-Test Requirements and Their Selection

Acceptance testing of articles to be used later for flight is seldom performed on structure, but is often performed on equipment items. Variations in structural integrity are usually small for structures, especially in the lower-order modes, so that qualification testing of an earlier specimen at higher levels (to avoid the possibility of undertesting), plus normal inspection of the flight-usage structure, should assure the adequacy of the structure for flight. On the other hand, there can be large variations in the structural integrity and operational performance of equipment, usually because the predominant response is in the higher-order modes. Thus, qualification testing at higher levels, plus normal inspection, will not necessarily assure flight adequacy. As stated previously, the test levels and durations must be selected with great care so that degradation resulting from preflight exposure is minimized while flight adequacy is being demonstrated.

Most of the problems found in the selection of qualification-test levels are also encountered in the selection of acceptance-test levels. However, the ''solutions'' to these problems are usually different. For qualification, a series of test inadequacies are usually countered by a series of test-level increases (i.e., overtesting), whereas for acceptance, the test inadequacies are usually judged equally for their effects on undertesting and overtesting. It should be remembered that the cost of an acceptance-test failure is almost always much less than the cost of a flight failure. It is not uncommon to find acceptance-test levels and durations specified as a certain percentage of qualification-test levels and durations. In some cases, stage static-firing tests (i.e., preflight acceptance firings of rocket engines in their stages) are used in lieu of laboratory acceptance tests. This is usually justified by assuming that there are fairly minor differences between flight and static-firing vibration levels, but this assumption is often violated. For example, for certain sections of the upper stage of a launch vehicle, the acoustic noise and the resulting equipment vibration from the upper-stage rocket engine(s) during static firing may be much less than the noise and vibration from the first-stage rocket engine(s) during liftoff.

Consideration must be given additionally to the differences in the cost between laboratory acceptance-test failures and static-firing failures. It is thus easy to see why acceptance tests are not always used and why there is no uniformity in acceptance-test level selection.

5.1.2.6 Design-Development Test Selection

There is a tremendous variety of design-development tests (DDT), since the major goal of these tests is usually to provide information to the designer and program management on the adequacy of the design and on the vibration characteristics of the hardware, in case the design is inadequate. These tests are usually performed quite early in the vehicle development so that program schedules are not affected if design changes are considered necessary. The test-to-failure technique is often used during design development to establish margins over flight and qualification-test conditions. Since they are performed to acquire design information, there is no stigma attached to a DDT failure. It is not uncommon to find that the first items off the production line are used for vibration DDT, since they often contain minor flaws, patches, etc., which make them unsuitable for other uses, but they are often still adequate for DDT purposes. Program management should consider DDT as an inexpensive tool in avoiding costly failures later in the program.

5.1.2.7 Assessment

It can be concluded from the preceding that it is impossible to perform a vibration test which, even under the best circumstances, avoids both overtesting and undertesting. Nevertheless, it is vitally important to any vehicle-development program that, despite this fact, the most realistic test conditions available under the circumstances be sought, and the best tradeoff of factors influencing the degree of undertesting or overtesting be selected. Arbitrary decisions concerning test techniques, levels, and durations can cause a considerable and sometimes an enormous unnecessary expense to the program in terms of reliability, schedule, and cost. For these reasons, little reliance should be placed on general specifications (ref. 146) purported to be applicable to every space vehicle.

5.1.3 Acoustic Tests

In the past, laboratory acoustic tests were used on an occasional basis to supplement qualification vibration testing of equipment. However, since two of the major causes of structural vibration are acoustic noise at liftoff and aerodynamic noise during the transonic and q_{max} regimes, it was a natural development to consider acoustic noise as a laboratory source of space-vehicle vibration. The Titan program was the first to utilize acoustic testing for the design development of vehicle structure subjected to acoustic noise (ref. 147). More recently, acoustic testing was used on the Apollo program (a) for qualification of equipment in lieu of qualification vibration testing, (b) for qualification of structure, and (c) for revision of vibration design and test requirements (refs. 148 through 152). Since the major objective of acoustic tests is to produce vibration in a large test specimen, it is common to call them vibroacoustic tests.

5.1.3.1 Test Facilities

The facilities used for these tests are many and varied. For example, figure 36 shows the OGO spacecraft on the flatbed of a truck located in an

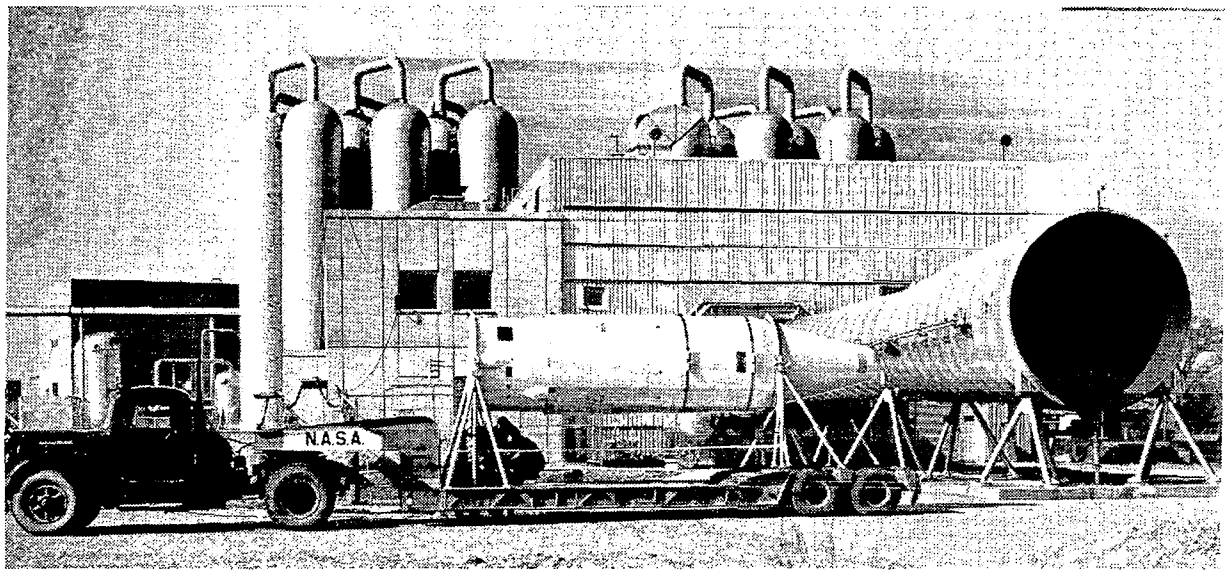

Figure 36.–Acoustic test of the OGO spacecraft near the discharge nozzle of a large blowdown wind tunnel.

open field near the discharge nozzle of a large blowdown wind tunnel (ref. 153). Here, the acoustic level and spectra are dependent upon (a) the mass and velocity of the discharge flow, (b) the distance from the nozzle exit to the test specimen, (c) the angle between the exhaust direction and an imaginary line connecting the nozzle exit with the specimen, and (d) climatic conditions.

A similar arrangement may also be used with a rocket engine as the noise source. However, if the acoustic test is intended to be performed as a ''free ride'' on a wind-tunnel or rocket-engine test, a great discrepancy may exist between the desired and the actual test duration. In figure 37, the S-II stage of the Saturn V launch vehicle is shown during its installation in a large reverberant test facility (ref. 154). The progressive test facility used for the acoustic tests of the Apollo lunar module and the command and service modules is shown in figure 38 (refs. 150, 155, and 156). In the latter case, the external structure is excited by acoustic noise which is propagated down 16 ducts, each duct having its own noise source. The 16 sources may be operated and controlled together, independently, or in any combination. These noise sources, and those used in the previously mentioned S-II tests, are air modulators. These devices work on the principle of exhausting high-pressure air through an orifice whose cross-sectional area is modulated by an electromagnet, which is controlled from an external electrical signal, usually a random-noise generator. In general, air modulators have limited spectrum range and control, usually from 50 Hz to 1 kHz, with a spectral maximum in the vicinity of 100 Hz. Noise generation above 1 kHz is usually determined by the ''unmodulated'' flow noise of the air through the orifice. Air modulators are commercially available in acoustic-power capacities up to 200 kW.

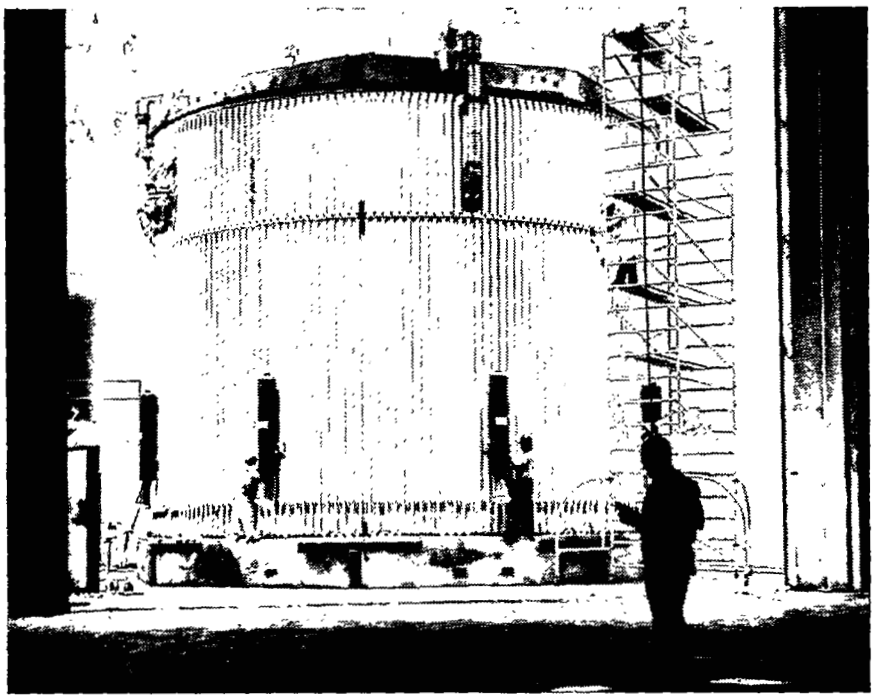

Figure 37.– Laboratory acoustic test of the thrust structure, aft skirt, and interstage of the S-II stage, Saturn V launch vehicle in a reverberant test facility.

5.1.3.2 Comparison With Vibration Tests

Although acoustic testing of space vehicles and large vehicle sections is still in its early development, a great many advantages have already been demonstrated over the vibration testing discussed in Section 5.1.2. If acoustic testing is performed on a large-enough section of the vehicle, so that the modal characteristics of the test specimen are similar to the modal characteristics of the flight configuration at the lowest frequency of interest, many of the following similarities with the flight configuration can often be achieved:

1. Similar (although not identical) vibration spectra at various locations throughout the specimen, except near where the specimen structurally interfaces with the acoustic facility.

2. Antiresonant behavior is allowed to occur at the attachment of heavy structural members, including equipment items, when these members exhibit resonant behavior (refs. 138 and 139).

3. Multidirectional resonances are allowed to occur.

4. The effects on the integrity of the structure and the performance of the equipment from vibration occurring simultaneously in the three orthogonal directions can be determined.

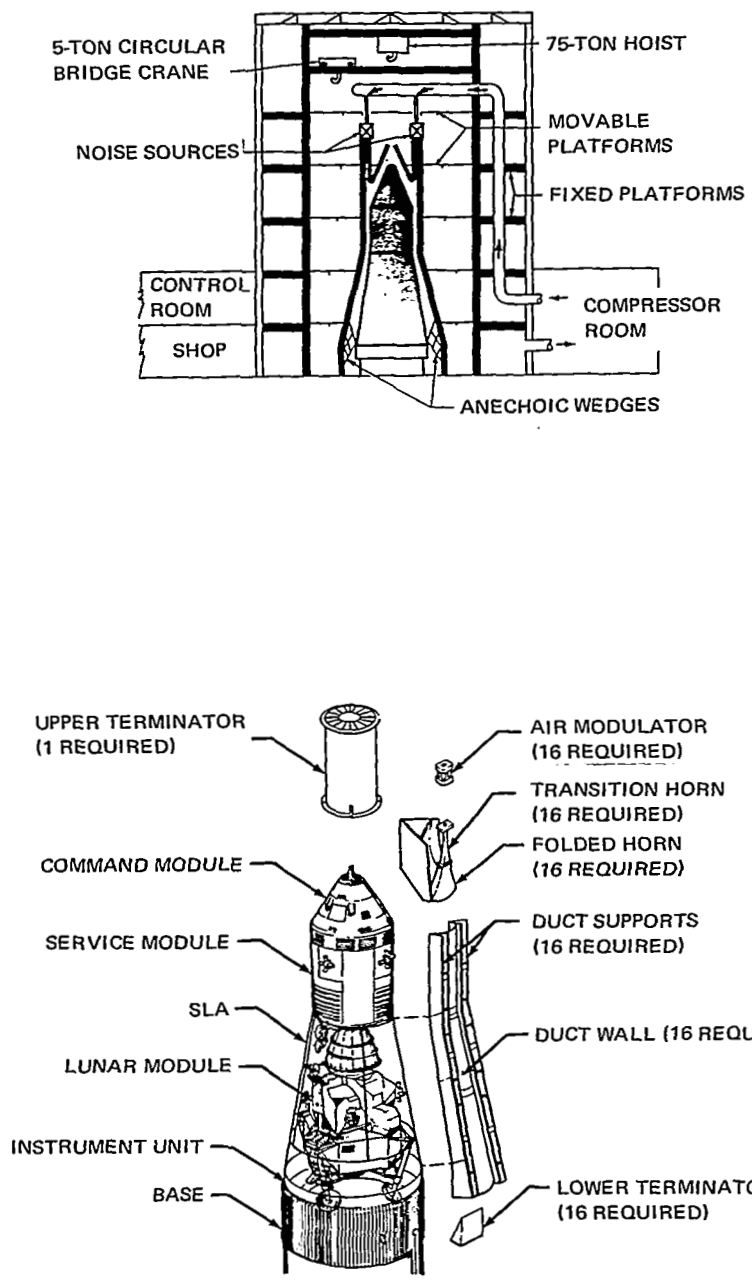

Figure 38.–Laboratory acoustic test of the Apollo spacecraft in a progressive test facility.

5. The specimen is not restrained to an arbitrary amplitude or phase at locations where the vibration forces are applied.

6. Combined vibration and acoustic loading can be applied to internal structures and equipment, which, under certain circumstances, can be made similar to flight conditions.

7. If test conservatism is desired, it can be applied simultaneously in all directions and more uniformly over the frequency range.

The major reasons for these improvements over vibration testing are (a) the ability to test a large and heavy structural specimen with a noise source of reasonable capacity, thus permitting the modal characteristics of the test specimen to be similar to those of the flight configuration over a wide frequency range; (b) the application of distributed loading over the external surface, rather than point-loading at one or more structural interfaces; and (c) fewer problems are encountered in selecting a reasonable acoustic-test spectrum than is found in selecting a reasonable vibration-test spectrum.

5.1.3.3 Test Requirements and Their Selection

In spite of the bright picture just described, there are several important limitations in utilizing acoustic testing for demonstrating structural adequacy and equipment performance. At present, one of the two major technical limitations is the inability to select the proper acoustic test spectrum which will accurately produce vibration spectra throughout the test specimen which are reasonably similar to space vehicle vibration spectra at equivalent locations, before flight vibration measurements are made. This limitation applies to all three forms of acoustic testing presently being performed: free field (fig. 36), reverberant (fig. 37), and progressive wave (fig. 38). Equations (2a) and (2b) from Section 4.1.2.2 can be used to describe this problem. At liftoff, the vehicle structure is subjected to the rocket-engine acoustic noise that is propagated over the vehicle, as described in Section 3. If the specimen were tested in a reverberant facility, a joint acceptance j^2_{ik} would probably be found that differed from that at liftoff, owing primarily to the difference in the cross-correlation functions $R_p(\xi,\xi',\tau)$ between liftoff and the acoustic test.

A progressive-wave or free-field test might provide sufficiently close longitudinal correlation, but probably would have some significant difference in the circumferential correlation. In addition, most progressive-wave ducts develop transverse standing waves that can couple with the vibration of the external structure above a certain frequency. This limitation is even more restrictive when the acoustic-test spectrum is to be selected to provide the same vibration spectra as the vehicle structure exposed to aerodynamic noise. In this case, the propagation speed for the acoustic test will generally be different from the aerodynamic-propagation speed, which, in addition, is increasing during the launch-and-ascent phase.

Near the locations where the vehicle cross-sectional area changes, local high, fluctuating pressures from the separated flow during flight often cause a large gradient of fluctuating pressure over the external structure. However, it is unnecessary in most cases to provide the same gradient or the highest local fluctuating-pressure level during the acoustic test since equation (2a) shows that the pressure distribution is integrated over the area of interest. Besides, at low frequencies, the cross-correlation coefficient for aerodyanamic noise is much less than the coefficient for acoustic noise, thus producing the lower vibration shown in figure 20 at $(f/f_1) < 1$.

At high frequencies, and in the frequency range near the ring frequency of the external structure, coincidence occurs (i.e., the propagation speed is equal to the wave speed of flexural waves in the structure), which causes an increase in the vibration response. Since the propagation speeds are different between flight and the acoustic test, the frequency ranges for this effect will not be identical (ref. 157).

Another factor influencing the proper selection of the acoustic test spectrum is the difference in the acoustic radiation (i.e., air damping) between the vehicle during flight and the specimen during the acoustic test. Radiation is one of the forms of damping influencing the value of ζ_i in equation (2b).

First, consider the space vehicle at liftoff. The external structure radiates sound externally to the free field (usually with little interference from the umbilical tower) and internally to the interior spaces. The external structure may be a payload shroud; a cylindrical or conical section enclosing a wide variety of equipment, as well as some primary and/or secondary structure; or a motor casing or tank for a solid or liquid propellant. Neglecting the latter, the external radiation from cylindrical shells is considerable for certain modes in the vicinity of the ring frequency, and for all modes above the coincidence frequency. References 53 through 56 describe the external radiation of unstiffened plates, cylindrical shells, and other surfaces. The internal acoustic radiation (for payload and equipment sections) is frequency-dependent (refs. 6 and 158 through 160).

At low frequencies, the internal space usually acts as an air ''spring'' or stiffness, so that the internal radiation is negligible unless there is leakage or venting through small openings. At frequencies corresponding to the lower ''air modes'' of the internal space, the internal radiation is usually small. Also, the air-mode natural frequencies and spatial distributions are greatly influenced by large internal objects, such as the payload, equipment items, and other internal structures. In addition, these items also vibrate, contributing to the internal noise. At frequencies sufficiently above these lower air modes, the internal space is reverberant, and the radiation is dependent on the average absorption coefficient of the walls of the space and the objects. If the internal space and configuration of the test specimen is identical or similar to that of the flight vehicle, the internal radiation should also be similar (refs. 81 and 161). However, the external radiation of both may or may not be similar, depending on the type of test facility used.

If acoustic testing is performed in a free field, such as illustrated in figure 36, the external radiation of the test specimen and the flight vehicle should be identical. If acoustic testing is performed in a sufficiently large reverberant facility, so that the fundamental modes of the external structure are sufficiently above the lower air modes of the test facility, the radiation will be dependent upon the average absorption coefficient of the facility walls and the external surface of the test specimen, and thus will be considerably different from that of free field (ref. 160). If acoustic testing is performed in a progressive-wave facility, the radiation difference will be dependent upon frequency and the cross-sectional area of the duct (ref. 162).

Second, consider the space vehicle in the transonic or q_{max} regime and its influence on the acoustic radiation. The external structure radiates sound externally through the boundary layer into a partial vacuum, so that the amount of external radiation is reduced compared to that at liftoff. If the internal space is partially or completely vented, the internal radiation is also reduced.

Another factor influencing the proper selection of the acoustic-test spectrum is the location of the microphone(s) for controlling and/or monitoring the test. Microphones placed near the test specimen may measure the radiation of the external structure, as well as the intended loading or reference pressure spectrum.

5.1.3.4 Assessment

Although there are many complications in determining the effects of the differences in the loading and radiation damping, and of the microphone locations, it is possible to determine these effects and to calculate the necessary adjustment to the acoustic-test spectrum. However, this has yet to be done in practice. Also, it is anticipated that this adjustment would produce a desired acoustic-test spectrum that would be highly shaped. Presently available noise sources provide a relatively smooth test spectrum, though, so that some conservatism would probably be produced. In the future, narrow-band noise sources, or even shakers attached directly to the external structure, may be used to reduce the conservatism.

Only the more obvious of the above factors are considered in the adjustment of the acoustic-test spectrum in testing performed to date. For example, a typical test may adjust for the differences in the joint acceptances simply by using the spatial-average flight-pressure spectrum for the acoustic test. Other factors are ''considered'' by increasing the acoustic test spectrum until sufficient conservatism is achieved. This practice notwithstanding, the resulting conservatism in the vibration spectra, as measured throughout the test specimen, is usually much less than the conservatism obtained during conventional vibration testing. Thus,acoustic testing of fairly large sections of space vehicles has the reputation of providing more realistic vibration-test conditions without the gross overtesting normally associated with vibration testing. It is expected that in the near future the substitution of acoustic testing for conventional vibration testing will be commonplace throughout the industry.

Acoustic testing can play an important role in vibration prediction for equipment. This is especially important in the mid- and higher-frequency range, where (a) classical analysis cannot be used, (b) statistical-energy analysis may provide too much spatial or spectral averaging, and (c) extrapolation methods are too inaccurate. Figure 39 shows á typical comparison of flight-vibration spectra with the original vibration design and test spectrum, and a vibration spectrum measured at the same location during an acoustic test. If acoustic testing can be performed early enough in the program, and if dummy equipment is used, greatly improved vibration criteria may be provided to equipment designers and subcontractors before the design is completed or qualification begins.

There are some important management problems that should be considered. The initial cost of a large reverberant or progressive-wave facility, such as shown in figure 37 or 38, is extremely high. The operational cost should however be nominal. Thus, a large capital outlay will be required if these types of facilities are not available. If the noise source is a blowdown wind tunnel or a rocket engine, the operational cost of these facilities may be considerable unless the acoustic test is a ''free ride'' on a wind-tunnel or engine test. In this latter case, the scheduling of the test may affect the acoustic-test schedule. Provisions must also be made for protecting the data-acquisition system from noise and climatic conditions. If operational equipment is included in the test, similar protection must be provided for the performance-monitoring equipment.

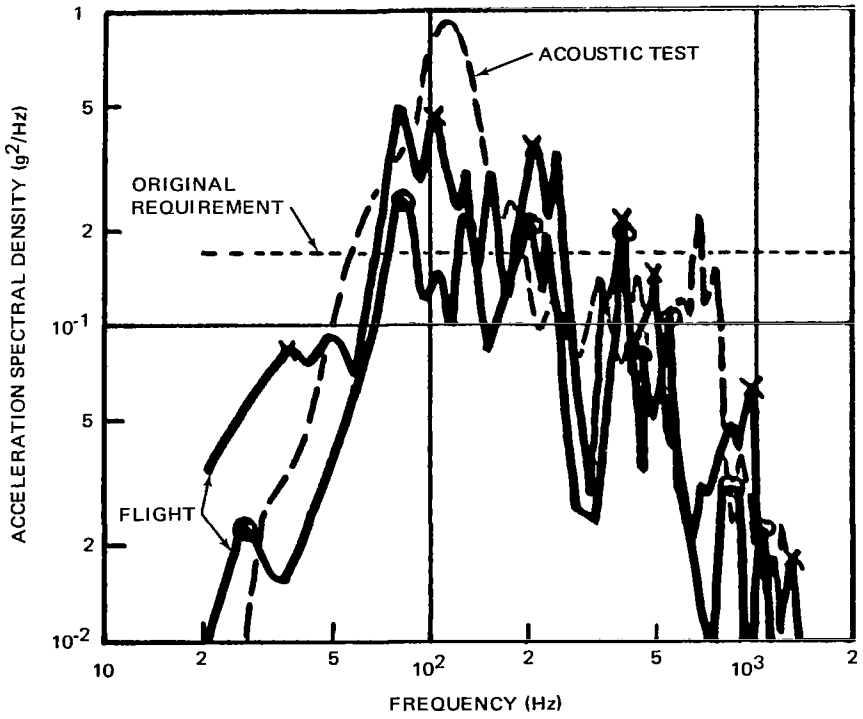

Figure 39.–Comparison of vibration spectra from acoustic test with flight and with original design and test requirement.

If acoustic testing is used in lieu of vibration testing for the qualification of equipment, certain subcontract management problems could arise that probably would not occur if conventional vibration qualification testing were performed completely under the control of the individual subcontractors. It is assumed that the acoustic testing would be performed by the prime contractor, or by others under his direction, because the prime contractor would probably be responsible for furnishing the structural-test specimen, arranging for or furnishing the use of the acoustic-test facility, and managing the scheduling of the equipment items to be supplied by the several subcontractors.

Problems of responsibility designation could arise if an equipment failure should occur during the acoustic test, and the subcontractor believes that the equipment item has been overtested or improperly monitored. Thus, sufficient operational, vibration, and internal acoustic measurements must be made so that equipment performance and the test environment may be adequately compared with the design and test criteria for the item. Also, the criteria should provide for the application of the combined vibration and acoustic environments of the item. Other potential problems, such as the pretest adjustment of the test spectrum to which the equipment item is exposed, are less significant for acoustic testing than for conventional vibration testing. If it takes several test runs to complete the vibroacoustic qualification of the several equipment items, owing to item scheduling problems or the necessity for redesign and retest, fatigue failure may develop in the structural-test specimen because of the long exposure time. This result should not imply a structural inadequacy of the vehicle. Usually, minor repairs can be made to the specimen between test runs. Unless a major structural element becomes fatigued, the repair should produce only minor changes to vibration spectra throughout the specimen.

Experience from the Apollo program has demonstrated that all these problems are nominal in comparison with the problems associated with conventional vibration testing, especially with its inherent overtesting to avoid the possibility of any undertesting. In addition, most major space vehicle contractors have large versatile acoustic facilities available for their use or have them in the planning stages (ref. 163).

Acoustic or vibration tests are seldom performed on structures containing propellants, since solid-rocket motor cases are usually unaffected by an external acoustic field, and liquid-filled tanks usually exhibit low vibration from the mass-loading effects of the liquid at the lower predominant frequencies (ref. 5).

5.1.4 Combined Environmental Testing

As described in Section 4.1.2.3, failures may occur under combined environments that may not occur when these same environments are applied sequentially. Since certain flight environments occur simultaneously, combined environmental testing is sometimes used for the laboratory qualification of space vehicle hardware. Various combinations of thermal, altitude (vacuum), sustained acceleration, vibration, and acoustic noise testing are most commonly used. In general, combined environmental effects are more difficult to predict on

equipment and its performance than on structure. For this reason, more combined environmental testing is performed on spacecraft and launch vehicle equipment than on launch vehicle structure.

The additional cost of combined environmental testing is usually rather nominal, with the possible exception of sustained acceleration testing on a centrifuge. Centrifuge testing often requires rather elaborate test facilities and instrumentation, especially when combined with other environments. However, these costs can often be justified when combined effects cannot be predicted on the basis of analysis and/or of sequential testing. The centrifuge facility shown in figure 40 is the launch phase simulator. In addition to applying a combination of sustained acceleration, vibration, acoustic noise, and vacuum to small- and medium-size hardware, this facility can be programmed to simulate the time-dependent changes in these environments and thereby reproduce the proper environmental combinations usually found during the launch-and-ascent phase (ref. 164).

5.2 FIELD TESTING

In the field-testing category are various nonlaboratory tests, such as rocket engine and stage or payload static firings used to demonstrate the operational performance of various space-vehicle subsystems before flight. If good planning is done early in the program, these tests can also be used to provide valuable data for predicting structural vibration or for revising earlier predictions.

Solid- and liquid-propelled rocket engines are usually designed and tested quite early in the vehicle-development program, sometimes as a lead item even before the prime vehicle contractors are selected. Because of this early scheduling, these tests can be invaluable in providing acoustic- and engine-vibration data which can be used for early vibration predictions. This is especially important when a rocket engine incorporates new design features that can affect acoustic noise and vibration generation, but has not been tested or instrumented previously. This normally includes engines with new types of combustion chambers or thrust vectoring, or with different propellants or expansion ratios. However, the use of the rocket-engine acoustic-noise data must take into consideration any differences in the test-stand and launch-pad configurations that may affect the noise generation or transmission, such as the design of the flame deflector.

Many of the components attached to the engine during the early firings are usually not of flight weight or configuration. In these cases, the spectral density $G''(f)$ of the vibration applied to a flight component can be predicted from the spectral density $G'(f)$ measured at the interface of the test-stand component with the engine, and from equation (26), where $Z_1(f)$, $Z_2'(f)$, and $Z_2''(f)$ are the mechanical (driving point) impedance of the engine, the test-stand component, and the flight component, respectively, as measured and/or predicted at the engine-component interface (ref. 105). However, most test-stand and flight components are sufficiently lightweight and small, so that test-stand vibration data obtained for these locations can usually be

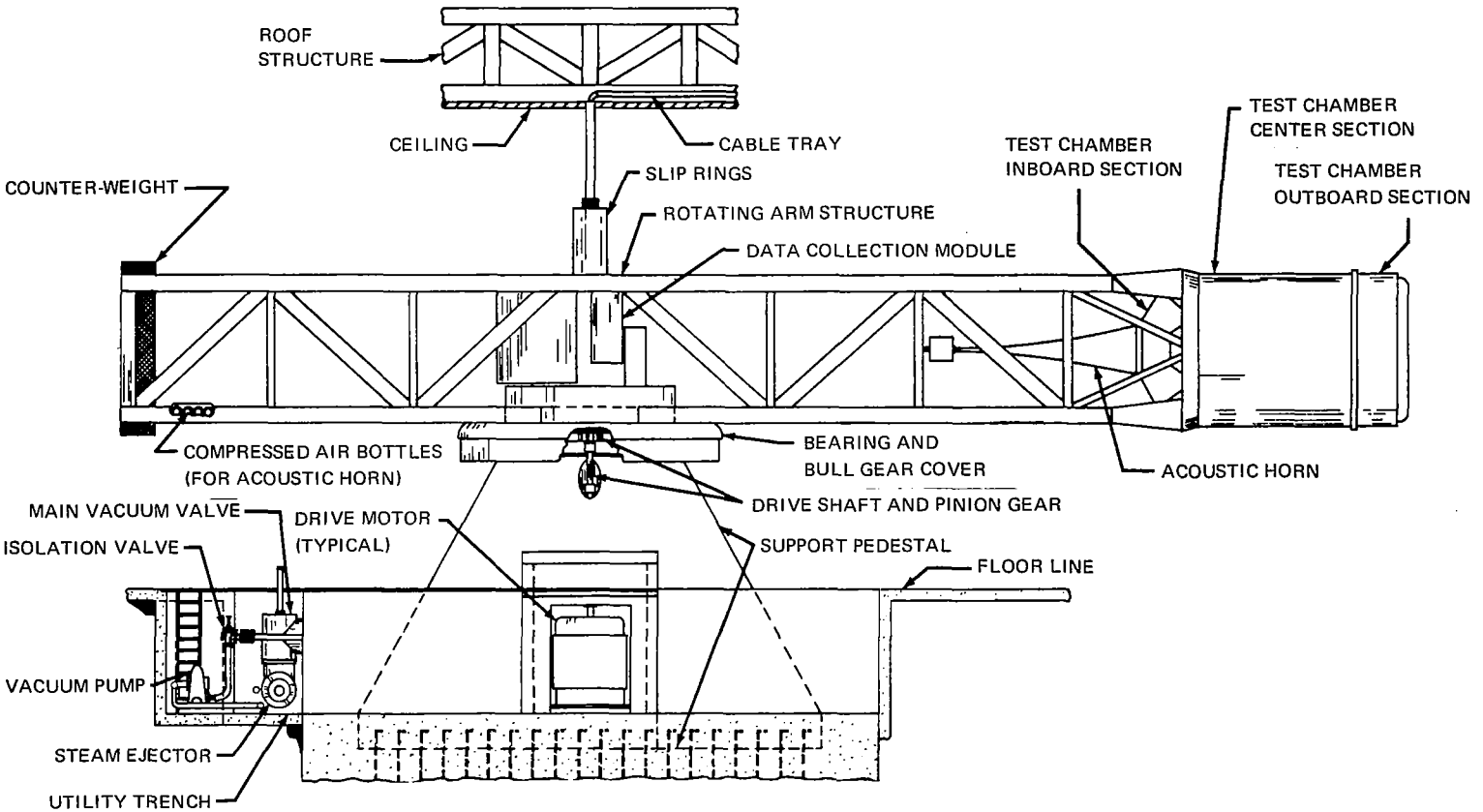

Figure 40. – Laboratory test facility for combined sustained acceleration-vibration-acoustic-noise-altitude environmental testing of space-vehicle hardware.

used for the flight components directly. Most rocket engines (and turbopumps for liquid engines) exhibit very high frequency vibration, so that it is not uncommon to measure vibration up to 20 kHz for these engines. The engines also transmit vibration mechanically to nearby sections of the vehicle. If they are included early enough in the test planning, vibration measurements can be made to determine the mechanical-vibration transmission from the engine(s). Mechanical-impedance measurements can be made and, together with the vibration measurements, used in equation (26) to predict the vibration of the space vehicle from this source.

Although they usually occur late in the program, static firings of the various stages of the vehicle can provide valuable preflight data. Generally, only stages with liquid-powered rocket engines are statically fired. If the stage is the first stage of the vehicle, and the flame deflector and tie-down configurations of the test stand are the same as those of the launch pad, the acoustic noise and structural vibration for the static firing should be almost identical to the noise and vibration at liftoff, except perhaps at the top of the stage (where the interface with the next stage or payload will probably not be properly simulated). Thus, except for the top, the static firing should provide the best definition of liftoff vibration throughout the stage.

If the flame deflector and tie-down configurations of the test stand differ from those of the launch pad, the static-firing noise and vibration must be extrapolated to account for the difference. For locations far from the engine(s), where the mechanically transmitted vibration is negligible, the vibration prediction may be accomplished by one of two methods. First, for a detailed correction of the data, the vibration measured during the static firing can be scaled in accordance with the differences in the joint acceptances and damping ratios, which must be calculated as described in Section 4.1.2.2. Even the structural vibration from aerodynamic noise can be predicted with reasonable accuracy when scaled in accordance with these differences. Second, for a gross correction of the data, the vibration measured during the static firing can be scaled in accordance with the differences in the spatial-average fluctuating pressures for liftoff, or, with an additional correction such as that shown in figure 20 for vibration caused by aerodynamic noise.

If the stage is an upper stage of the vehicle, the acoustic noise and structural vibration for the static firing will seldom be the same as (a) that produced by the first-stage engines during liftoff, (b) that observed during the transonic and q_{max} periods, or (c) that occurring during the powered flight of the upper stage, when in most cases, the only vibration is mechanically transmitted from the engines. At locations far from the engines, however, where the mechanical transmission is negligible, the vibration measured during the static firing can be scaled by methods described in the preceding paragraph to predict vibration of the upper-stage structure at liftoff, transonic, and q_{max} periods.

For locations near the upper-stage engines, it will be difficult to separate the relative contribution of acoustically-induced and mechanically-transmitted

vibration for the static firing. If knowledge of this relative contribution is required, special static-firing test facilities can be used if they are included in the planning early in the vehicle-development program. The following two test configurations must be implemented in sequence:

1. The engine(s) must be isolated from the remainder of the stage by taking the engine-thrust loads out through the test-stand structure, which is separated and isolated from the test-stand structure that supports the remainder of the stage, while all other connections between the stage and the engine(s) are made flexible.

2. The engine exhaust must be ducted away from the test stand for a considerable distance, so that the acoustic noise reaching the vehicle is negligible because of the great distance from the end of the duct to the vehicle.

The first test configuration will permit the determination of acoustically-induced vibration from the upper-stage engine(s), with only negligible contribution from the mechanically-transmitted vibration, whereas the second configuration will permit the opposite. For locations near the upper-stage engine(s), the first configuration will allow the acoustic and vibration data to be extrapolated to liftoff, transonic, and q_{max} conditions which occur during first-stage powered flight. The second configuration will allow the determination of mechanically-transmitted vibration for upper-stage powered flight.

It is not uncommon to use stage static firings as a form of vibroacoustic acceptance testing. The advantage of such testing is the performance evaluation of entire subsystems as they are exposed to combined structural vibration and acoustic noise, with the vibration occurring in three orthogonal directions simultaneously. The disadvantages are (a) in most cases, the acceptance vibration levels and durations are seldom found to be optimum, relative to the tradeoff between flight-adequacy demonstration and preflight degradation, as discussed in Section 5.1.2; and (b) major effect on the vehicle schedule may result if acceptance-test failures occur on the test stand, rather than in the laboratory. These advantages and disadvantages should be weighed carefully before static firings are designated for vibration- and acoustic-acceptance testing.

5.3 FLIGHT TESTING

The flight test is almost always used as the final demonstration of the adequacy of acoustic and vibration requirements. It is also the final demonstration of the structural adequacy and operational performance of the space vehicle. In case flight failure occurs, sufficient instrumentation must be onboard to determine the location of the failure and the probable cause. In too many cases, not enough instrumentation is provided, so that the failure location or probable cause is often not ascertained; then redesign must proceed on several fronts, usually at considerable cost and delay. Even with redesign, the real cause may not have been eliminated, which results in

more flight failures, higher costs and delays, and sometimes contract cancellation or lost national prestige. In light of the history of flight-test failures, it is surprising to note that some space-vehicle development programs are still managed on a ''success-oriented'' basis (i.e., few contingencies allowed for flight failures). This philosophy usually changes, though, with the first flight failure. In many cases, there is not sufficient instrumentation because too little space or weight has been allocated for it. This problem can be avoided by program-management insistence that all instrumentation requirements be submitted during the preliminary design phase, when instrumentation space and weight are usually designated. Other problems arise when the telemetry subsystem, generally used in the monitoring of subsystem performance, is inadequate.

A large number of vibration and aeroacoustic measurements are usually needed during flight test to (a) demonstrate the adequacy of the vibration and acoustic requirements, (b) help determine the probable cause in case of flight failure, and (c) provide data for the design of future space vehicles. Measurement requirements usually far exceed the capacity of the telemetry subsystem – a situation that appears to grow worse with each new program. The main reason is that most vibration and aeroacoustic measurements require a wide bandwidth (usually from 20 Hz to 2 kHz, and sometimes up to 10 kHz) and a large dynamic range (usually from 30 to 70 dB) (ref. 165). Often more than a hundred temperature, pressure, dc voltage, strain, flow, low-frequency acceleration, and guidance functions can be telemetered over the same rf bandwidth used to transmit one vibration or aeroacoustic measurement. Thus, the measurement requirements of the structural dynamicist are not usually received with enthusiasm by the instrumentation engineer.

The situation has improved slightly by recent changes in the Inter-Range Instrumentation Group (IRIG) Telemetry Standards (ref. 166), which allows more high-frequency channels through constant bandwidth fm/fm and the extension of proportional bandwidth fm/fm to higher frequencies. According to IRIG, single sideband am/fm and double sideband am/fm will be standardized in 1970, thus providing a major improvement in telemetering dynamic measurements. However, a major breakthrough in telemetry technology will be required to provide a capability which will satisfy most flight vibration-measurement requirements.

Other techniques can be employed to reduce the demand on the telemetry subsystem, including (a) onboard frequency analysis, where the rms or average output of a sweep or step-frequency analyzer is telemetered on a low-frequency channel; (b) onboard tape recording, where certain measurements are recorded during the periods of high vibration or aeroacoustic noise, and then telemetered later during a period of low vibration and noise; and (c) time division multiplexing, where certain measurements, usually from two to four, are sampled and telemetered in repeated sequence (e.g., 3 sec ''on'' and 9 sec ''off''). All these solutions, though, increase cost and onboard weight, and may permit some degradation in instrumentation reliability, so that all other possible solutions should be exhausted before these are considered. For example, in some cases a ''boilerplate'' spacecraft may be used during the early flight test of a launch vehicle. If the external aerodynamic

configuration of the boilerplate is identical to that of the actual spacecraft, aeroacoustic measurements should be made on the boilerplate and thus only vibration measurements will be required on the actual spacecraft.

Two other major flight-instrumentation problems are those of calibration error and electrical noise. A calibration error can occur when the various gain and attenuator settings actually used throughout the data-acquisition and -reduction process differ from those scheduled or appearing in the instrumentation engineer's or technician's notebook. Thus, it is not uncommon to have one or more cases where, for example, 8-g rms are measured during one flight and 80-g rms during another flight at the same mission phase and at the same location on the vehicle – with the instrumentation group often providing ''conclusive proof'' that both measurements were accurate!

Electrical noise in the form of ''spikes'' and random electrical voltages are also commonly observed on vibration and aeroacoustic measurements. This noise usually develops in the various signal conditioners, cables, or telemetry equipment, or in the ground recording facilities. Telemetry noise is usually caused by poor rf signal strength with distance, or interference from rocket-engine-exhaust products or hypersonic plasma effects. Most structural dynamicists experienced with flight-test data can distinguish random vibration and aeroacoustic noise from random electrical noise, except when the electrical noise is caused by an instrumentation component that is in itself sensitive to random vibration or aeroacoustic noise. Because of the high cost of flight vibration and aeroacoustic-noise measurements, it is certainly desirable to avoid these problems. For example, the likelihood of a calibration error, caused by an incorrect gain or attenuator setting, can be greatly reduced if an insert voltage or other ''end-to-end'' calibration is used, and if the ac calibration is applied immediately before flight and/or during periods of low flight vibration. The additional cost of ''end-to-end'' calibration equipment is usually negligible when compared to the overall cost of the measurements. Also, the ''end-to-end'' calibration signals may be used to set the gain and attenuation of the various instrumentation equipment, from the transducer signal conditioner in the vehicle to the frequency analyzer in the laboratory, thus reducing implementation costs.

The main reason for acquiring flight-test data is the need for determining the adequacy of design and test requirements. However, before flight measurements are compared with these requirements, the flight data should be scaled to represent worst-case conditions. For example, at liftoff the vibration should be scaled according to the difference between the measured and the highest-rated engine thrust and the difference between the measured and the highest expected acoustic-noise transmission characteristics resulting from climatic conditions (wind, ambient pressure, temperature, and humidity). For transonic and q_{max} periods, the vibration should be scaled according to the difference between the measured and the highest expected density and aerodynamic pressure. If sufficient measurements have been allocated to measure vibration at all locations of interest on the vehicle, some vibration and aeroacoustic measurements should be repeated on later flights to establish flight-to-flight variations. These should be considered when establishing worst-case conditions, unless the variance is so wide as to cause one to suspect the validity of the data.

If the requirements exceed the flight data by a considerable margin, and if redesign of structure or equipment is contemplated for later vehicles (as is often done), some weight reduction can often be realized by lowering the requirements without a significant sacrifice in flight adequacy or reliability. If the flight data exceed the requirements, then retesting and possibly some redesign should be performed to new requirements based on the flight data.

If the flight data are to be used in predicting the vibration for a new vehicle, it will probably be desirable to divide both reference and new vehicles into zones and perform a statistical analysis of the flight data for each zone, as described in Section 4.3.2. Depending on the similarity between the reference and the new vehicles, one of the scaling methods of Section 4.3.2, one of the frequency-response methods of Section 4.3.1, a modification of these, or a new method may be used for the vibration prediction.

If the new vehicle consists of a new spacecraft on a standard launch vehicle, and if the vibration is transmitted to the spacecraft predominantly through the mechanical path (as discussed in Section 4.2.3), the spectral density $G''(f)$ of the vibration applied to the new spacecraft can be predicted from the spectral density $G'(f)$ measured at the interface of the launch vehicle with the reference spacecraft, and from equation (26), where $Z_1(f)$, $Z_2'(f)$, and $Z_2''(f)$ are the mechanical (driving point) impedance of the launch vehicle, the reference spacecraft, and the new spacecraft, respectively (ref. 105).

6. OBJECTIVES OF SPACE-VEHICLE DESIGN DEVELOPMENT FOR VIBRATION

Certain objectives must be achieved to ensure that the space vehicle is properly designed to withstand structural vibration occurring during the various phases of the mission, in sequence and/or in combination with other loads and environments, without structural failure or degradation. In addition, design and test requirements for the various items of vehicle equipment must be selected to ensure their operational performance and structural integrity. To accomplish these objectives, the general tasks listed in the following paragraphs should be observed in every vehicle-development program:

- Applied Loading. The characteristics of the fundamental sources of vibration and the vibration loading applied to the structure should be determined by analysis and/or test for periods of the flight when high vibration is expected.

- Vibration Motion. The vibration motion of the structure due to the applied loading should be established by analysis and/or test.

- Vibration Stress. The stresses resulting from the vibration motion should be determined for critical locations of the vehicle by analysis and/or test.

- Allowable Stress. The allowable vibration stresses should be selected on the basis of the material properties, fabrication processes, time duration of the applied loading, and the effects of sequential and combined loads and environments (e.g., static loads, mechanical shock loads, thermal loads, humidity, propellant atmosphere) for critical locations of the structure.

- Structural Integrity. The integrity of the structure should be evaluated by comparing the resulting stresses with the allowable stresses, including consideration of the following: (a) the statistical variation and accuracy of determining the applied loading, the vibration motion and stress, and the failure mechanism; (b) the consequences of accepting an inadequate structure or rejecting an adequate structure; (c) the reliability goal, if one has been set; and/or (d) the desired confidence in the integrity of the structure.

- Equipment Requirements. Design and test requirements for vehicle equipment should be selected on the basis of (a) the determination of vibration motion due to the applied loading as outlined above, the determination of the equipment acoustic loading, the time duration of these loadings, and the accuracy of determining the applied loading, the vibration motion, and the equipment acoustic loading; (b) the statistical variation of the loading, motion, and the possible failure mechanisms; (c) the number of test specimens, the type of test to be performed (vibration or acoustic), the degree of simulation, and the method of test control; (d) the consequences of accepting an inadequate equipment item or rejecting an adequate

one; and (e) the reliability goal, if one has been set, and/or the desired confidence in the operational performance and structural integrity of the equipment.

Documentation. All analyses and tests should be clearly documented and available to customer representatives for examination and review. Design and test requirements should be supported by documentation showing their derivation.

7. RECOMMENDATIONS FOR IMPLEMENTING VARIOUS DESIGN, ANALYSIS, AND TESTING TECHNIQUES

All methods of design, analysis, and test described in Sections 4 and 5 have limitations of accuracy, cost, and/or timeliness to support program schedules and objectives. To provide a proper evaluation of structural integrity and an adequate selection of design and test requirements, in most programs it is necessary to apply several of these techniques during the various phases of vehicle development and to revise earlier predictions as later information becomes available. The selection of a particular technique is thus dependent upon the phase of vehicle development during which it is to be implemented. In this section certain techniques described in Sections 4 and 5 are suggested for implementation during specific phases of the vehicle-development program in order to satisfy the objectives listed in Section 6.

7.1 PRELIMINARY DESIGN PHASE

The evaluation of structural integrity should be initiated as soon as the preliminary vehicle configuration is selected; the initial determination of the structural characteristics is made on the basis of the static loading (engine thrust, vehicle acceleration, wind, etc.) and other loadings and environments (thermal, gusts, etc.).

First, the applied vibration loading should be described. For liftoff, the acoustic loading from the rocket engine(s) can be determined from data sources referenced in Section 3.1. For vehicles with very ''clean'' external configurations or for vehicle locations far removed from changes in the vehicle cross-sectional area, the aerodynamic fluctuating pressure loading at q_{max} can be determined from data sources referenced in Section 3.3. To determine the applied loading from aerodynamic noise or buffet during the transonic period for any vehicle, and at q_{max} for aerodynamically ''unclean'' vehicles, wind-tunnel tests must be used as discussed in Section 5.1.1. Usually, tests can be performed simultaneously with steady (i.e., static) aerodynamic-pressure measurements, so that close coordination between aerodynamicists and structural dynamicists should permit a considerable cost saving. Wind-tunnel tests are often performed during the early development phase of the program, but the detailed planning for these tests should be made during preliminary design. If rocket-engine development tests have been initiated, acoustic-noise measurements should be made to supplement or supersede the data referenced in Section 3.1. If not, planning should be made during preliminary design for the inclusion of acoustic measurements during the rocket engine test program. Also, vibration and mechanical impedance measurements to be used in the prediction of mechanically transmitted vibration should be made or planned during preliminary design, as discussed in Section 5.2. As an interim measure, vibration measurements from tests of an earlier engine should be used after they are scaled for differences in engine thrust, size, and other engine parameters. If the stage or payload is also subjected to static firing of its rocket engines, the applied loading for this condition should be determined.

Next, the vibration motion and stresses of the structure from the applied loading should be calculated. Since many or most of the structural details are lacking during preliminary design, it is often acceptable to represent the structure in these calculations by simplified mathematical models. This will permit an initial evaluation of the general adequacy of the overall structural design at little expense. This is especially important during early preliminary design when, in some programs, the structural design changes almost daily and a quick, inexpensive design evaluation is of great value. In the frequency range of the lower-order modes, the classical analysis discussed in Section 4.1 should be used to perform the initial evaluation. However, simplified representations of the joint acceptance and the arbitrary selection of damping may be used to reduce calculation costs, and equivalent isotropic representation may be made of composite construction. Certain structural sections may be represented as flat or curved plates, cylindrical or conical sections, simple trusses, and lumped mass, or as their lumped-parameter equivalents. The contribution of the higher-order modes should be calculated by the statistical-energy analysis discussed in Section 4.2, but since the predominant stresses will probably occur in the lower-order modes, it may not be necessary to consider higher-mode contribution during preliminary design. Since structural integrity is dependent upon the effects of all combined and sequential loads on the structure, close coordination between loads engineers, stress analysts, and structural dynamicists is essential to a good initial design of the vehicle.

Design and test requirements for vehicle equipment are usually needed as soon as the systems concept has been determined and preparations are made to solicit bids from subcontractors. If the requirements are to be submitted before the previously mentioned structural evaluation can be made, one of the extrapolation methods discussed in Section 4.3 and the test contingencies discussed in Sections 5.1.2 and 5.1.3 may be used to derive these requirements. As discussed in Sections 4.3.1 and 4.3.2, all extrapolation methods have serious deficiencies. Thus, it would appear advantageous to select more than one of these methods and use the most conservative prediction, since it is usually easier and less costly to reduce subcontractor requirements than to increase them. It is essential, however, that there be close coordination between the customer and the prime contractor's structural dynamicists concerning the selection of these requirements, so that the initial requirements are not ''cast in concrete'' for the remainder of the program, but are modified as better information becomes available. If the design and test requirements are to be submitted during or after the initial structural evaluation, classical analysis and statistical-energy analysis may be used in the frequency ranges of the lower- and higher-order modes, respectively, to derive these requirements in conjunction with the test contingencies discussed in Sections 5.1.2 and 5.1.3. It is also suggested that little reliance be placed on ''general'' specifications and other requirements that are not written or interpreted in terms of the specific mission or configuration of the space vehicle.

Design-development tests to provide early information to the designer regarding the adequacy of his structural design should be planned during preliminary design. Close coordination between designers and structural dynamicists is required to ensure that the proposed tests are likely to provide the desired information.

During preliminary design, recommendations should be submitted to the customer for major tests to be implemented during later phases of the program. It is suggested that vibration and acoustic measurements be planned for static firings of stage or payload rocket engines, as discussed in Section 5.2, as well as for flight tests, as discussed in Section 5.3. For new rocket-engine configurations, consideration should be given to performing model engine tests to acquire external acoustic data to improve or supersede the initial static firing or liftoff acoustic predictions. Until the problems observed with vibration models are resolved, it is suggested that model tests not be used to predict vibration.

Since the highest vibration usually occurs at liftoff and at transonic and q_{max} periods, it is highly recommended that acoustic tests of the vehicle or large vehicle sections be performed to demonstrate structural integrity and to improve the vibration prediction, as discussed in Section 5.1.3. Since these tests are usually among the major ground tests of the program, close coordination between the customer and the prime contractor's program management, structures, reliability, facilities, test, and structural dynamics groups is required, starting during preliminary design. As a major ground test, it is likely that it will be one of the main program constraints to flight testing. Also, it will probably be a major cost item to the program.

If the vehicle or section structure is one of the first items off the production line, and good planning and test program control is implemented, the early acquisition of test results can be achieved. If failures develop, early redesign can be implemented. If no failures occur and sufficient strain measurements are made, and if vehicle weight reduction is desired, early redesign based on experimental data can be implemented. If vehicle equipment is installed, the acoustic test may also serve as a combined vibration and acoustic-qualification test of the equipment items. If the test is performed before the actual equipment is available, dummy equipment should be installed. Vibration and acoustic measurements can then be used in the revision of the initial design and test requirements. In this case, it is suggested that two tests be performed: making use of dummies (1) to acquire early data for the revision of requirements, and (2) for the later qualification of the actual equipment.

A ground vibration test, as discussed in Section 5.1.2, is not recommended as a substitute for an acoustic test because of the difficulty in determining a reasonable vibration test spectrum. However, if mechanically transmitted vibration from the rocket engine(s) is expected to be a problem, then a ground vibration test is recommended to determine the effects on the structure, with shaker(s) used as the simulated source(s) of vibration. Engine vibration and mechanical impedance measurements can be used with equation (26) to determine the test spectrum. The engine-vibration test program should be planned during preliminary design. In certain cases, the same structural test specimen may be used for the acoustic test and the engine-vibration test.

It should be obvious from this discussion, then, that structural vibration planning should be started at the very beginning of the preliminary design phase. Also, it is apparent that sufficient flexibility should be allowed within the program to permit the application of improved definition of loads, vibration motion and stresses, failure mechanisms, and requirements to the vehicle design.

7.2 EARLY DEVELOPMENT PHASE

During the early development phase, great emphasis should be placed on the analytical effort. The evaluation of structural integrity, which was initiated during preliminary design, should be continued and refined during this phase. Since data from rocket-engine static firings, model-engine acoustic tests, and wind-tunnel tests provide better definition of the applied loading, and since the structural configuration becomes firm, the mathematical models and the classical analyses should be more detailed to provide improved vibration predictions. This is especially important if the earlier analyses showed that the vibration stresses approximated or exceeded the allowable stresses. Statistical-energy analyses of the structure should be performed and, together with the classical analysis, used to revise the initial design and test requirements for the equipment. Close coordination between designers and structural dynamicists will probably be required during this phase in order to resolve design problems as they arise.

Design-development tests, as discussed in Section 5.1.2, will probably be implemented during this phase. Structural dynamicists should be available to support the designer in the implementation of these tests and the interpretation of the results. Assistance may also be required to evaluate acoustic tests and wind-tunnel tests in order to ensure that the data are adequate for subsequent use. Also, support may be required for the later implementation of stage or payload static firing and acoustic (or vibration) tests, such as resolution of problems concerning the use of facilities or the selection of instrumentation and measurement locations.

7.3 LATE DEVELOPMENT PHASE

During late development, great emphasis should be placed on the experimental effort. Except for occasional revisions or refinements, the analytical evaluation of structural integrity should have been completed. Support to the designers concerning design problems and design-development test results should no longer be of major proportion. The major structural vibration tests are usually performed during this phase and will probably require a great deal of support from structural dynamicists. If proper planning has preceded them, ground acoustic (or vibration) tests and stage or payload static firings will probably provide a great deal of vibration and acoustic data that must be analyzed, validated, interpreted, and reported. Corrective action must be taken if failures occur. Test data should be scaled to account for any differences between these tests and flight. Redesign should be made for any marginal structures. The design and test requirements for equipment should be revised based on static firing results and on new flight predictions.

During this phase, qualification tests of equipment are also performed. If feasible, it is suggested that most vehicle equipment be qualified for combined vibration and acoustic noise by installing the equipment in the structural test specimen for acoustic testing, as discussed in Section 5.1.3. If not, conventional vibration testing must be used for qualification. Support may then be required from the customer and the prime contractor's structural dynamicists in the evaluation of test conditions, instrumentation, test results, and in the possible granting of waivers.

7.4 FLIGHT-TEST PHASE

Preceding flight testing, certain assistance may be required to verify to program management that with the successful completion of certain analyses and tests, the vehicle has demonstrated adequate structural integrity and that the equipment is qualified for vibration and aeroacoustic loading. Documentation is often required to support the verification. With the completion of the preceding analyses and tests, this verification should be made with confidence.

After each test flight, the flight vibration and aeroacoustic data should be reported and compared with the tests and analyses performed previously. If the mission parameters were not ''worst case'', the flight data should be scaled to worst-case conditions before this comparison. Structural integrity and the design and test requirements must be reevaluated, preferably before the next flight. Corrective action must be taken, as required, unless program management is willing to assume the risk of not incorporating these corrections.

In case of flight failure, usually several possible causes are suspected. Vibration is often one of them. Adequate flight-vibration measurements should therefore be programmed to support possible postflight-failure analysis.

Flight data should be carefully cataloged for later use, in case the space vehicle is selected for new missions or design changes are incorporated later in the program.

Finally, papers should be written for publication in the technical journals to make the valuable data and experience acquired on the program readily available for use in future space-vehicle design.

8. CONCLUDING REMARKS

The magnitude of the tasks outlined in the body of this report is expected to be considerable for most vehicle-development programs. For example, it is estimated that about 1.5% of the development costs for the Apollo spacecraft was associated with ensuring its structural integrity under aeroacoustic- and engine-induced vibration. Experience has also shown that failure to perform certain tasks can be a major source of risk to the successful development of the vehicle. Unfortunately, in many cases this risk can only be evaluated late in the program; that is, during flight test.

APPENDIX

INTERNAL FORCE-AND-MOMENT VIBRATION-RESPONSE EQUATIONS FOR STRUCTURES EXPOSED TO AEROACOUSTIC NOISE

A.1 FORCE-DISPLACEMENT AND MOMENT-DISPLACEMENT RELATIONSHIPS

Most failure-prone space vehicle structures are those with structural sections comprised of shallow shell elements (e.g., flat plates, cylindrical sections), such as shown in figure A-1. For these shell elements, reference 29 shows that the inplane force N_1, inplane shear force N_{12}, bending moment M_1, twisting moment M_{12}, and transverse shear force Q_1, (all per unit length) at location x in the X_2Z plane is

$$N_1(x,t) = \mathscr{D}[(u_1 + w/a_1) + \nu(v_2 + w/a_2)] \tag{A-1a}$$

$$N_{12}(x,t) = \frac{1}{2}\mathscr{D}(1 - \nu)(u_2 + v_1) \tag{A-1b}$$

$$M_1(x,t) = -D(w_{11} + \nu w_{22}) \tag{A-1c}$$

$$M_{12}(x,t) = D(1 - \nu)w_{12} \tag{A-1d}$$

$$Q_1(x,t) = -D(w_{111} + w_{122}) \tag{A-1e}$$

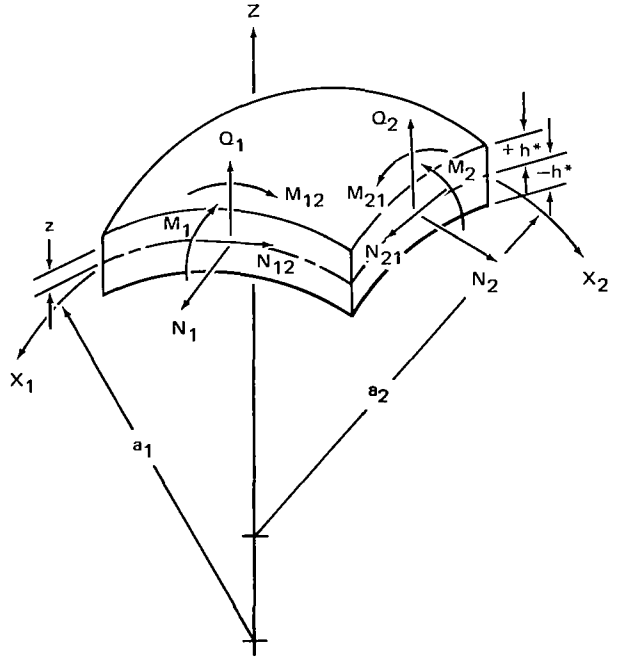

Figure A-1.—Forces and moments on a shallow shell element.

where u, v, and w are the instantaneous displacements (at location x) in X_1, X_2, and Z directions, respectively; and a_1 and a_2, the radii of curvature in the X_1Z, and X_2Z planes, respectively. The partial spatial derivations are as follows:

$$u_1 = \partial u/\partial x_1 \qquad w_{11} = \partial^2 w/\partial x_1^2$$

$$u_2 = \partial u/\partial x_2 \qquad w_{22} = \partial^2 w/\partial x_2^2$$

$$v_1 = \partial v/\partial x_1 \qquad w_{12} = \partial^2 w/\partial x_1 \partial x_2$$

$$v_2 = \partial v/\partial x_2 \qquad w_{111} = \partial^3 w/\partial x_1^3$$

$$w_{122} = \partial^3 w/\partial x_1 \partial x_2^2$$

Similar equations may be derived for forces N_2, and N_{21}, and Q_2, and for moments M_2 and M_{21} in the X_1Z plane. For an isotropic shell, the inplane and flexual rigidities are

$$\mathscr{D} = Eh/(1 - \nu^2) \tag{A-2a}$$

$$D = Eh^3/12(1 - \nu^2) \tag{A-2b}$$

while for a honeycomb sandwich shell (ref. 167), with face sheets having the same material and thickness

$$\mathscr{D} \simeq 2E_2h_2 \tag{A-2c}$$

$$D \simeq 2E_2h_1^2h_2/(1 - \nu_2^2) \tag{A-2d}$$

where E, h, and ν are Young's modulus, thickness, and Poisson's ratio for the isotropic shell, respectively; E_2, h_2 and ν_2, Young's modulus, thickness, and Poisson's ratio for each face sheet, respectively; and h_1, the half thickness of the core for a honeycomb shell. The instantaneous stresses are related to the various forces and moments by

$$N_1(x,t) = \int_{-h^*}^{+h^*} S_{11}(1 + z/a_2)dz \tag{A-3a}$$

$$N_{12}(x,t) = \int_{-h^*}^{+h^*} s_{12}(1 + z/a_2)dz \qquad \text{(A-3b)}$$

$$M_1(x,t) = \int_{-h^*}^{+h^*} s_{11}z(1 + z/a_2)dz \qquad \text{(A-3c)}$$

$$M_{12}(x,t) = \int_{-h^*}^{+h^*} s_{12}z(1 + z/a_2)dz \qquad \text{(A-3d)}$$

$$Q_1(x,t) = \int_{-h^*}^{+h^*} s_{13}z(1 + z/a_2)dz \qquad \text{(A-3e)}$$

For an isotropic shell, $h^* = 1/2$; for a honeycomb shell, $h^* = h_1 + h_2$.

A.2 FORCE-AND-MOMENT SPECTRAL DENSITIES BASED ON SPATIAL DERIVATIVES

Similar to equation (A-2) the force-and-moment spectral densities for location x in the X_2Z plane at each frequency f due to a spatially distributed applied random loading are

$$\begin{aligned} G_{N_1}(x,f) = \mathscr{D}^2 \Big\{ & G_{u_1}(x,f) + \nu^2 G_{v_2}(x,f) \\ & + \left[a_1^{-2} + (2\nu/a_1a_2) + (\nu/a_2)^2 \right] G_w(x,f) \Big\} \\ & + 2\mathscr{D}^2 \Big\{ \left[a_1^{-1} + (\nu/a_2) \right] \left[G_{u_1w}(x,f) + \nu G_{v_2w}(x,f) \right] \\ & + \nu G_{u_1v_2}(x,f) \Big\} \end{aligned} \qquad \text{(A-4a)}$$

$$G_{N_{12}}(x,f) = \frac{1}{4}\mathscr{D}^2(1 - \nu)^2 \left[G_{u_2}(x,f) + G_{v_1}(x,f) + 2G_{u_2v_1}(x,f) \right] \qquad \text{(A-4b)}$$

$$G_{M_1}(x,f) = D^2\left[G_{w_{11}}(x,f) + \nu^2 G_{w_{22}}(x,f) + 2\nu G_{w_{11}w_{22}}(x,f)\right] \qquad \text{(A-4c)}$$

$$G_{M_{12}}(x,f) = D^2(1-\nu)^2 G_{w_{12}}(x,f) \qquad \text{(A-4d)}$$

$$G_{Q_1}(x,f) = D^2\left[G_{w_{111}}(x,f) + G_{w_{122}}(x,f) + 2G_{w_{111}w_{122}}(x,f)\right] \qquad \text{(A-4e)}$$

All spectral density terms on the right-hand side of equations (A-4) are expressible in the form

$$G_t(x,f) = A^2 G_{pr}(f) \sum_{i=1}^{N}\sum_{k=1}^{N} \frac{\phi_i^t(x)\phi_k^t(x)H_i^*(f)H_k(f)j_{ik}^2(f)}{(2\pi)^4 f_i^2 f_k^2 M_i M_k} \qquad \text{(A-5)}$$

where the relationships between the product of the mode shape derivatives $[\phi_i^t(x)\phi_k^t(x)]$ and their spectral densities $G_t(x,f)$ are given in table A-I. In this table, $\psi_i(x)$, $\varphi_i(x)$ and $\phi_i(x)$ are the mode shapes in the i^{th} mode and in the X_1, X_2, and Z directions, respectively. Thus, with the appropriate substitutions of table A-I into equation (A-5) and the subsequent substitution of these into the equations of (A-4), the spectral densities for the forces N_1, N_{12}, and Q_1, and moments M_1 and M_{12} can be calculated. Spectral-density equations for forces N_2, N_{21}, and Q_2, and moments M_2 and M_{21} in the X_1Z plane can be similarly calculated. Rms forces and moments can then be calculated from equation (5b), and rms stresses from the equations of (A-3).

It is apparent a considerable amount of calculation is required to determine forces and moments, which is unfortunate when the importance of these quantities to the determination of structural integrity is considered. In certain cases, these calculations can be reduced somewhat by ignoring all terms in equation (A-4) that are multiplied by ν^2, since $\nu \approx 0.3$ for most aerospace metals. However, care must be exercised since other terms (i.e., not multiplied by ν^2) may be small at certain locations, and so cause appreciable unconservative errors.

In most modal analyses, approximate methods are used to derive mode shapes. While an adequate approximate analysis can provide a reasonable estimate of the mode shape, a large error may be found in the spatial derivatives appearing

APPENDIX

TABLE A-I.-RELATIONSHIPS BETWEEN SPECTRAL DENSITIES AND MODE SHAPE DERIVATIVES

$G_t(x,f)$	$\phi_i^t(x)\phi_k^t(x)$
$G_{u_1}(x,f)$	$[\partial\psi_i(x)/\partial x_1][\partial\psi_k(x)/\partial x_1]$
$G_{v_2}(x,f)$	$[\partial\varphi_i(x)/\partial x_2][\partial\varphi_k(x)/\partial x_2]$
$G_w(x,f)$	$\phi_i(x)\phi_k(x)$
$G_{u_1}(x,f)$	$[\partial\psi_i(x)/\partial x_1]\phi_k(x)$
$G_{v_2 w}(x,f)$	$[\partial\varphi_i(x)/\partial x_2]\phi_k(x)$
$G_{u_1 v_2}(x,f)$	$[\partial\psi_i(x)/\partial x_1][\partial\varphi_k(x)/\partial x_2]$
$G_{u_2}(x,f)$	$[\partial\psi_i(x)/\partial x_2][\partial\psi_k(x)/\partial x_2]$
$G_{v_1}(x,f)$	$[\partial\varphi_i(x)/\partial x_1][\partial\varphi_k(x)/\partial x_1]$
$G_{u_2 v_1}(x,f)$	$[\partial\psi_i(x)/\partial x_2][\partial\varphi_k(x)/\partial x_1]$
$G_{w_{11}}(x,f)$	$[\partial^2\phi_i(x)/\partial x_1^2][\partial^2\phi_k(x)/\partial x_1^2]$
$G_{w_{22}}(x,f)$	$[\partial^2\phi_i(x)/\partial x_2^2][\partial^2\phi_k(x)/\partial x_2^2]$
$G_{w_{11}w_{22}}(x,f)$	$[\partial^2\phi_i(x)/\partial x_1^2][\partial^2\phi_k(x)/\partial x_2^2]$
$G_{w_{12}}(x,f)$	$[\partial^2\phi_i(x)/\partial x_1\partial x_2][\partial^2\phi_k(x)/\partial x_1\partial x_2]$
$G_{w_{111}}(x,f)$	$[\partial^3\phi_i(x)/\partial x_1^3][\partial^3\phi_k(x)/\partial x_1^3]$
$G_{w_{122}}(x,f)$	$[\partial^3\phi_i(x)/\partial x_1\partial x_2^2][\partial^3\phi_k(x)/\partial x_1\partial x_2^2]$
$G_{w_{111}w_{122}}(x,f)$	$[\partial^3\phi_i(x)/\partial x_1^3][\partial^3\phi_k(x)/\partial x_1\partial x_2^2]$

in table A-I. Thus, in certain cases, forces and moments (and subsequent stresses) calculated by equations (A-4) and (A-5) may be in error by several orders of magnitude, especially for M_1, M_{12}, and Q_1, which are functions of second and third spatial derivatives (ref. 25). However, an alternate technique, which is summarized in Section A.3, can provide adequate estimates of vibration stresses even when approximate methods of modal analysis are used.

A.3 FORCE-AND-MOMENT SPECTRAL DENSITIES BASED ON EXTERNAL AND INERTIAL LOADING

This technique is an extension of the modal displacement and modal acceleration methods of reference 24. The instantaneous internal force or moment P at location x due to instantaneous forces F applied at locations $\tilde{x}$ is

$$P(x,t) = \sum B_p(x,\tilde{x})F(\tilde{x},t) \tag{A-6a}$$

where $B_p(x,\tilde{x})$ can account for the effects of redundance if the structure is redundant (ref. 25). The force F has two components:

$$F(\tilde{x},t) = F_e(\xi,t) - F_{\ddot{w}}(\tilde{x},t) \tag{A-6b}$$

where F_e and $F_{\ddot{w}}$ are the external force and the inertial force, respectively. For a distributed loading on a distributed structure:

$$P(x,t) = \int_A B_p(x,\underline{\xi})p(\underline{\xi},t)d\underline{\xi} + \int_S B_p(x,\underline{\tilde{x}})\rho(\underline{\tilde{x}})h(\underline{\tilde{x}})\ddot{w}(\underline{\tilde{x}},t)d\underline{\tilde{x}} \tag{A-7}$$

where $p(\xi,t)$ is the instantaneous external pressure at location ξ. For an isotropic shell of uniform thickness, the surface density is

$$[\rho(\tilde{x})h(\tilde{x})] = \rho h \tag{A-8a}$$

whereas for a sandwich shell

$$[\rho(\tilde{x})h(\tilde{x})] = 2(\rho_1 h_1 + \rho_2 h_2) \tag{A-8b}$$

Under random external loading, the force or moment spectral density is

$$G_P(x,f) = G_{P_p}(x,f) + G_{P_{\ddot{w}}}(x,f) + G_{P_pP_{\ddot{w}}}(x,f) + G_{P_{\ddot{w}}P_p}(x,f) \tag{A-9a}$$

where

$$G_{P_p}(x,f) = \iint_A B_P(x,\underline{\xi})B_P(x,\underline{\xi}')G_p(\underline{\xi},\underline{\xi}',f)d\underline{\xi}d\underline{\xi}' \qquad \text{(A-9b)}$$

$$G_{P_{\ddot{w}}}(x,f) = \iint_S B_P(x,\underline{\tilde{x}})B_P(x,\underline{\tilde{x}}')[\rho(\underline{\tilde{x}})h(\underline{\tilde{x}})][\rho(\underline{\tilde{x}}')h(\underline{\tilde{x}}')]$$

$$(2\pi f)^4 G_w(\underline{\tilde{x}},\underline{\tilde{x}}',f)d\underline{\tilde{x}}d\underline{\tilde{x}}' \qquad \text{(A-9c)}$$

and where $G_p(\xi,\xi',f)$ is given in equation (3) and $G_w(\tilde{x},\tilde{x}'f)$ is given in equation (2), substituting $[\phi_i(\tilde{x})\phi_k(\tilde{x}')]$ for $[\phi_i(x)\phi_k(x)]$. It is reasonable to assume that the external loading and the response in any mode is uncorrelated, so that

$$G_{P_p P_{\ddot{w}}}(x,f) = G_{P_{\ddot{w}} P_p}(x,f) = 0 \qquad \text{(A-9d)}$$

Since P may be any force or moment, such as those expressed in equations (A-1) and (A-3), the force and moment spectral densities may be obtained from repeated solutions of equations (A-9). For example, the bending-moment spectral density at location x in the X_2Z plane can be found when B_{M_1} is substituted for B_P:

$$G_{M_1}(x,f) = \iint_A B_{M_1}(x,\underline{\xi})B_{M_1}(x,\underline{\xi}')G_p(\underline{\xi},\underline{\xi}',f)d\underline{\xi}d\underline{\xi}'$$

$$+ \iint_S B_{M_1}(x,\underline{\tilde{x}})B_{M_1}(x,\underline{\tilde{x}}')[\rho(\underline{\tilde{x}})h(\underline{\tilde{x}})][\rho(\underline{\tilde{x}}')h(\underline{\tilde{x}}')]$$

$$(2\pi f)^2 G_w(\underline{\tilde{x}},\underline{\tilde{x}}',f)d\underline{\tilde{x}}d\underline{\tilde{x}}' \qquad \text{(A-10)}$$

The transfer function B_P between the internal forces or moments, and the applied force, given in equation (A-6a), can be obtained from static-stress analysis, and in fact is normally calculated by stress analysts for static-load analysis. However, the magnitude of the task is still considerable because B_P must be obtained for every combination of potential failure location x and location $\tilde{x}$ of the structure (or location ξ of the structure exposed to the external-pressure field). Thus, it is apparent that the calculation of stresses is considerably more complex and expensive than the calculation of displacements or accelerations.

A.4 ASSESSMENT

Examination of equations (A-9) shows that they contain no spatial derivatives. Thus, when approximate methods of modal analysis are used, appreciably greater accuracy may be expected from the use of equations (A-9) than from equations (A-4), especially for the calculation of the spectral densities for moments M_1, M_{12}, M_2, and M_{21}, and forces Q_1 and Q_2, which are functions of second and third derivatives.

REFERENCES

1. Potter, R.C.; and Crocker, M J.: Acoustic Prediction Methods for Rocket Engines, Including the Effects of Clustered Engines and Deflected Exhaust Flow. NASA CR-566, 1966.

2. Bond, D.A.: Summary of Model and Full-Scale Acoustic Data for Prediction of Missile Lift-Off Noise Environments. The Shock and Vibration Bull. No. 34, P. 4, Feb. 1965, pp. 123-131. (Available from DDC as AD 460002.)

3. Anon.: Specialists' Meeting of the Mechanism of Noise Generation in Turbulent Flow. AGARD Repts. 448-469, Apr. 1963.

4. Eldred, K.M.; Roberts, W.H.; and White, R.W.: Structural Vibrations in Space Vehicles. WADD TR 61-62, Dec. 1961. (Available from DDC as AD 273334.)

5. Dyer, I.: Estimation of Sound-Induced Missile Vibration. Random Vibration. (Edited by S.H. Crandall). John Wiley & Sons, Inc., 1958, ch. 9.

6. Franken, P.A.; and Kerwin, E.M.; et al.: Methods of Flight Vehicle Noise Prediction. WADC TR 58-343. Vol. I, Nov. 1958, and Vol. II, Sept. 1960. (Available from DDC as AD 205776 and AD 260995, respectively.)

7. White, P.H.: Estimation of Structural Response to Aeroacoustic Loads. SAE Paper no. 660721, Oct. 1966.

8. Crocco, L.; and Cheng, S.I.: Theory of Combustion Instability in Liquid Propellant Rocket Motors. AGARDograph 8, Butterworth Scientific Publications, 1956.

9. Zinn, B.T.; and Crocco, L.: Periodic Finite Amplitude Oscillations in Slowly Converging Nozzles. Astronautica Acta, vol. 13, nos. 5 and 6, Aug. 1968, pp. 481-488.

10. Hart, R.W.; and McClure, F.T.: Theory of Acoustic Instability in Solid-Propellant Rocket Combustion. Proc. Tenth Intern. Symp. on Combustion, Combustion Institute, Aug. 1964, pp. 1047-1066.

11. Culick, F.E.C.: Acoustic Oscillations in Solid Propellant Rocket Chambers. Astronautica Acta, vol. 12, no. 2, Mar. 1966, pp. 113-126.

12. Ailman, C.M.: On Predicting Fluctuating Pressures at a Wall Beneath a Turbulent Boundary Layer. J. Acoust. Soc. Amer., vol. 41, no. 6, June 1967, p. 1583(A). (Also MDC Paper no. 4331.)

13. Bies, D.A.: A Review of Flight and Wind Tunnel Measurements of Boundary Layer Pressure Fluctuations and Induced Structural Response. NASA CR-626, 1966.

14. Jones, G.W.; and Foughner, J.T.: Investigation of Buffet Pressures on Models of Large Manned Launch Vehicle Configurations. NASA TN D-1633, 1963.

15. Rainey, A.G.: Progress on the Launch-Vehicle Buffeting Problem. J. Spacecraft Rockets, vol. 2, no. 5, May 1965, pp. 289-299.

16. Speaker, W.V.; and Ailman, C.M.: Spectra and Space-Time Correlations of the Fluctuating Pressures at a Wall Beneath a Supersonic Turbulent Boundary Layer Perturbed by Steps and Shock Waves. NASA CR-486, 1966.

17. Black, T.J.: An Analytical Study of the Measured Wall Pressure Field Under Supersonic Turbulent Boundary Layers. NASA CR-888, 1968.

18. Ailman, C.M.; and Hopkins, A.S.: Narrow Band Cross-Correlation Analysis of Fluctuating Pressures Beneath a Turbulent Boundary Layer. NASA CR-1066, 1968.

19. Coe, C.F.; and Rechtien, R.D.: Scaling and Spatial Correlation of Surface Pressure Fluctuations in Separated Flow at Supersonic Mach Numbers. Proc. AIAA Structural Dynamics and Aeroelasticity Specialist Conf., Apr. 1969.

20. Robertson, J.E.: Characteristics of the Static- and Fluctuating-Pressure Environments Induced by Three-Dimensional Protuberances at Transonic Mach Numbers. Rept. WR 69-3, Wyle Labs., June 1969.

21. Saunders, H.: Prediction of the Sound Pressure Levels of the Aft Section of a Blunt Nose Body in a Turbulent Boundary Layer. Proc. Inst. Envir. Sci., 1968, pp. 73-77.

22. Menkes, E. G.; and Houbolt, J.C.: Evaluation of Aerothermoelasticity Problems for Unmanned Mars-Entry Vehicles. J. Spacecraft Rockets, vol. 6, no. 2, Feb. 1969, pp. 178-184.

23. Smith, F.A.; and Benedetti, F.J.: Prediction of Re-Entry Vibration. The Shock and Vibration Bull. No. 35, P. 7, Apr. 1966, pp. 9-18.

24. Bisplinghoff, R.L.; Ashley, H.; and Halfman, R.L.: Aeroelasticity. Addison-Wesley Pub. Co. Inc., 1955.

25. Hurty, W.C.; and Rubinstein, M.F.: Dynamics of Structures. Prentice-Hall, Inc., 1964.

26. Przemieniecki, J.S.: Theory of Matrix Structural Analysis. McGraw-Hill Book Co., Inc., 1968.

27. Pestel, E.C.; and Leckie, F.A.: Matrix Methods in Elastomechanics. McGraw-Hill Book Co. Inc., 1963.

28. Timoshenko, S.P.: Vibration Problems in Engineering. Third ed., D. Van Nostrand Co., 1955.

29. Nowacki, W.: Dynamics of Elastic Systems. John Wiley & Sons, Inc., 1963.

30. Kalnins, A.: Dynamic Problems of Elastic Shells. Appl. Mech. Rev., vol. 18, no. 11, Nov. 1965, pp. 867-872.

31. Forsberg, K.: A Review of Analytical Methods Used to Determine the Modal Characteristics of Cylindrical Shells. Proc. Seventh Intern. Aero. Cong., June 1965. (Also NASA CR-613, 1966.)

32. Anon.: Proceeding of the Conference on Matrix Methods in Structural Mechanics. AFFDL-TR-66-80, 1966. (Available from DDC as AD 646300.)

33. Anon.: Natural Vibration Modal Analysis. NASA SP-8012, NASA Space Vehicle Design Criteria (Structures), Sept. 1968.

34. Lin, Y.K.: Probabilistic Theory of Structural Dynamics. McGraw-Hill Book Co., Inc., 1967.

35. Lyon, R.H.: Empirical Evidence for Nonlinearity and Directions for Future Work. J. Acoust. Soc. Amer., vol. 35, no. 11, Nov. 1963, pp. 1712-1721. (Also NASA TN D-1872, 1963.)

36. Caughey, T.K.; and O'Kelly, M.E.J.: Classical Normal Modes in Damped Linear Dynamic Systems. J. Appl. Mech. vol. 32E, no. 3, Sept. 1965, pp. 583-588. (Discussion by Y.K. Lin, J. Appl. Mech, vol. 33E, no. 2, June 1966, pp. 471-472.)

37. Caughey, T.K.; and O'Kelley, M.E.J.: Effect of Damping on the Natural Frequencies of Linear Dynamic Systems. J. Acoust. Soc. Amer., vol. 33, no. 11, Nov. 1961, pp. 1458-1461.

38. Wang, M.C.; and Uhlenbeck, G.E.: On the Theory of Brownian Motion II. Rev. Mod. Physics, vol. 17, nos. 2 and 3, Apr. and July 1945, pp. 323-342 [Also Selected Papers on Noise and Stochastic Processes (Edited by N. Wax), Dover Publications, Inc. pp. 113-132.]

39. Robson, J.D.: Introduction to Random Vibration. Elsevier Pub. Co., 1964.

40. Bendat, J.S.; and Piersol, A.G.: Measurement and Analysis of Random Data. John Wiley & Sons, Inc., 1966.

41. White, R.W.: Theoretical Study of Acoustic Simulation of In-Flight Environments. The Shock and Vibration Bull. No. 37, P. 5, Jan. 1968, pp. 55-75. (Available from DDC as AD 667230.)

42. Schweiker, J.W.; and Davis, R.E.: Response of Complex Shell Structures of Aerodynamic Noise. NASA CR-450, 1966.

43. Lagerquist, E.R.; and Jacobs, L.D.: Random-Vibration Analysis System for Complex Structures: Engineering User's Guide. AFFDL-TR-68-43, P. 1, Nov. 1968. (Available from DDC as AD 845604.)

44. Tsurusaki, K.; and Wallace, F.S.: Random-Vibration Analysis System for Complex Structures: Computer Program Description. AFFDL-TR-68-43, P. 2, Jan. 1969. (Available from DDC as AD 849017.)

45. MacNeal, R.H.; and McCormick, C.W.: NASTRAN Computer Program for Structural Analysis. SAE Paper no. 690612, Oct. 1969,

46. Rommel, B.A.; and Wacker, G.F.: Computer Solution of the Response of Complex Structure to Random Excitation. J. Acoust. Soc. Amer., vol. 47, no. 1, P. 1, Jan. 1970, p. 102(A).

47. Lazan, B.J.; and Goodman, L.E.: Material and Interface Damping. Shock and Vibration Handbook (Edited by C.M. Harris and C.E. Crede). Vol. II, McGraw-Hill Book Co. Inc., 1961, ch. 36.

48. Lazan, B.J.: Damping of Materials and Members in Structural Mechanics. Pergamon Press, 1968.

49. Metherill, A.F.; and Diller, S.V.: Instantaneous Energy Dissipation Rate in a Lap Joint - Uniform Clamping Pressure. J. Appl. Mech., vol. 35E, no. 1, Mar. 1968, pp. 123-128.

50. Goodman, L.E.; and Klumpp, J.H.: Analysis of Slip Damping with Reference to Turbine Blade Vibration. J. Appl. Mech., vol. 23, no. 3, Sept. 1956, pp. 421-429.

51. Smith, P.W.; and Lyon, R.H.: Sound and Structural Vibration. NASA CR-160, 1965.

52. Lyon, R.H.; and Maidanik, G.: Statistical Methods in Vibration Analysis. AIAA J., vol. 2, no. 6, June 1964, pp. 1015-1024.

53. Smith, P.W.: Response and Radiation of Structural Modes Excited by Sound. J. Acoust. Soc. Amer., vol. 34, no. 5, May 1962, pp. 640-647.

54. Manning, J.E.; and Maidanik, G.: Radiation Properties of Cylindrical Shells. J. Acoust. Soc. Amer., vol. 36, no. 9, Sept. 1964, pp. 1691-1698.

55. Chertock, G.: Sound Radiation From Vibrating Surfaces. J. Acoust. Soc. Amer., vol. 36, no. 7, July 1964, pp. 1305-1313.

56. Chertock, G.: A Fortran Program for Calculating the Sound Radiation From a Vibrating Surface of Revolution. DTMB Rept. 2083, Dec. 1965. (Available from DDC as AD 627745.)

57. Ross, D.; Ungar, E.E.; and Kerwin, E.M.: Damping of Plate Flexural Vibrations by Means of Viscoelastic Laminae. Structural Damping (Edited by J.E. Ruzicka). ASME, 1959, pp. 49-87.

58. Maidanik, G.: Energy Dissipation Associated with Gas-Pumping in Structural Joints. J. Acoust. Soc. Amer., vol. 40, no. 5, Nov. 1966, pp. 1064-1072.

59. Crandall, S.H.; and Mark, W.D.: Random Vibration in Mechanical Systems. Academic Press, 1963.

60. Anon.: Metallic Materials and Elements for Flight Vehicle Structures. MIL-HDBK-5, Aug. 1962.

61. Gohn, G.R.; Hardrath, H.F.; and Peterson, R.E.: Fatigue of Metals. Mat. Res. and Stds., vol. 3, no. 2, Feb. 1963, pp. 105-139.

62. Manson, S.S.; Fatigue: A Complex Subject – Some Simple Approximations. Exper. Mech., vol. 5, no. 7, July 1965, pp. 193-226.

63. Christensen, R.H.; and Bellinfante, R.J.: Some Considerations in the Fatigue Design of Launch and Spacecraft Structures. NASA CR-242, 1965.

64. Swanson, S.R.: Random Load Fatigue Testing: A State of the Art Survey. Mat. Res. and Stds., vol. 8, no. 4, Apr. 1968, p. 11-44.

65. Corten, H.T.; and Dolan, T.J.: Cumulative Fatigue Damage. Intern. Conf. on Fatigue of Metals, Session 3, Paper no. 2, ASME, Nov. 1956.

66. Miles, J.W.; and Thomson, W.T.: Statistical Concepts in Vibration. Shock and Vibration Handbook (Edited by C.M. Harris and C.E. Crede.) Vol. I, McGraw-Hill Book Co. Inc., 1961, ch. 11.

67. Davis, P.J.: Gamma Function and Related Functions. Handbook of Mathematical Functions (Edited by A. Abramowitz and I.A. Stegun). Natl. Bur. Stds., Appl. Math. Series 55, Government Printing Office, 1964, ch. 6.

68. Pierson, K.: Tables of the Incomplete Gamma Function. Cambridge University Press, 1948.

69. Freudenthal, A.M.: Fatigue of Structural Metals under Random Loading. Symposium on Acoustical Fatigue, STP 284, ASTM, 1961.

70. Broch, J.T.: Effects of Spectrum Non-linearities Upon the Peak Distribution of Random Signals. Bruel and Kjaer Tech. Rev. no. 3, 1963.

71. Broch, J.T.: Peak Distribution Effects in Random Load Fatigue. Bruel and Kjaer Tech. Rev. no. 1, 1969.

72. Barnoski, R.L.: The Maximum Response of Distributed Structures with Rectangular Geometry to Random Excitation. J. Sound and Vibration, vol. 7, no. 3, May 1968, pp. 333-350.

73. Crandall, S.H.; Chandiramani, K.L.; and Cook, R.G.: Some First-Passage Problems in Random Vibration. J. Appl. Mech., vol. 33E, no. 3, Sept. 1966, pp. 532-538.

74. Lyons, W.C.; and Tuler, F.R.: Failure Mechanisms in Materials and Structures Subjected to Short-Time Loading. Proc. Inst. Envir. Sci., 1969, pp. 78-91.

75. Smits, T.I.: Wear-Dependent Failure Rates and System Wearout Reliability Prediction Under Nongaussian Random Loading. Proc. Inst. Envir. Sci., 1969, pp. 98-108.

76. Sargent, D.: Dynamic Effects of Vibration on Guidance and Control System Performance. Proc. Inst. Envir. Sci., 1969, pp. 109-120.

77. Piersol, A.G.: Study of the Interaction of Combined Static and Dynamic Loads. J. Sound and Vibration, vol. 7, no. 3, May 1968, pp. 319-332.

78. Heller, R.A.: Reliability Through Redundancy. Proc. Inst. Envir. Sci., 1969, pp. 121-127.

79. Lyon, R.H.: Random Noise and Vibration in Space Vehicles. Shock and Vibration Monograph 1, Shock and Vibration Information Center, DOD, 1967.

80. Ungar, E.E.: Fundamentals of Statistical Energy Analysis of Vibration of Vibrating Systems. AFFDL-TR-66-52, April 1966. (Available from DDC as AD 637504.)

81. Manning, J.E.; Lyon, R.H.; and Scharton, T.D.: The Transmission of Sound and Vibration to a Shroud-Enclosed Spacecraft. NASA CR-81688, Oct. 1966. (Also BBN Rept. 1431.)

82. Maidanik, G.: Response of Ribbed Panels to Reverberant Acoustic Fields. J. Acoust. Soc. Amer., vol. 34, no. 6, June 1962, pp. 809-826.

83. Scharton, T.D.; and Yang, T.M.: Statistical Energy Analysis of Vibration Transmission into an Instrument Package. SAE Paper no. 670876, Oct. 1967.

84. Chandiramani, K.L.; Widnall, S.E.; Lyon, R.H.; and Franken, P.A.: Structural Response to Inflight Acoustic and Aerodynamic Environments. NASA CR-88211, June 1966. (Also BBN Rept. 1417.)

85. Barnoski, R.L.; Piersol, A.G.; Van Der Laan, W.F.; White, P.H.; and Winter, E.F.: Summary of Random Vibration Prediction Procedures. NASA CR-1302, 1969.

86. Piersol, A.G.: The Development of Vibration Test Specifications for Flight Vehicle Components. NASA CR-234, 1965.

87. Mahaffey, P.T.; and Smith, K.W.: Method for Predicting Environmental Vibration Levels in Jet Powered Vehicles. Noise Control, vol. 6, no. 4, July 1960, pp. 20-26. (Also The Shock and Vibration Bull. No. 28, P. 4, Aug. 1960, pp. 1-14. Available from DDC as AD 244857.)

88. Brust, J.M.; and Himelblau, H.: Comparison of Predicted and Measured Vibration Environments for Skybolt Guidance Equipment. The Shock and Vibration Bull. No. 33, P. 3, Mar. 1964, pp. 231-280. (Available from DDC as AD 435514.)

89. White, R.W.; Bozich, D.J.; and Eldred, K.M.: Empirical Correlation of Excitation Environment and Structural Parameters with Flight Vehicle Vibration Response. AFFDL-TR-64-160, Dec. 1964. (Available from DDC as AD 610482.)

90. Curtis, A.J.: A Statistical Approach to Prediction of the Aircraft Flight Vibration Environment. The Shock and Vibration Bull. No. 33, P. 1, Feb. 1964, pp. 1-13. (Available from DDC as AD 348503.)

91. Franken, P.A.: Sound-Induced Vibrations of Cylindrical Vehicles. J. Acoust. Soc. Amer., vol. 34, no. 4, Apr. 1962, pp. 453-454.

92. Winter, E.F.; and Van Der Laan, W.F.: Recommended Procedures for Predicting Random Vibration Environments in MSFC Aerospace Vehicles. MAC Rept. 504-19, Sept. 1967.

93. Callahan, J.A.: Gemini Spacecraft Flight Vibration Data and Comparison with Predictions. The Shock and Vibration Bull. No. 35, P. 7, Apr. 1966, pp. 67-76. (Available from DDC as AD 633096.)

94. Curtis, A.J.; and Tinling, N.G.: Success and Failure with Prediction and Simulation of Aircraft Vibration. The Shock and Vibration Bull. No. 39, P. 6, Mar. 1969, pp. 77-92.

95. Clevenson, S.A.: Lunar Orbiter Flight Vibrations with Comparisons to Flight Acceptance Requirements and Predictions Based on a New Generalized Regression Analysis. The Shock and Vibration Bull. No. 39, P. 6, Mar. 1969, pp. 119-132.

96. Hunt, F.V.: Stress and Strain Limits on the Attainable Velocity in Mechanical Vibration: J. Acoust. Soc. Amer., vol. 32, no. 9, Sept. 1960, pp. 1123-1128.

97. Ungar, E.E.: Maximum Stresses in Beams and Plates Vibrating at Resonance. Trans. ASME, J. Eng. Ind., vol. 82B, no. 1, Feb. 1962, pp. 149-155.

98. Crandall, S.H.: Relation between Strain and Velocity in Resonant Vibration. J. Acoust. Soc. Amer., vol. 34, no. 12, Dec. 1962, pp. 1960-1961.

99. Condos, F.M.; and Butler, W.: A Critical Analysis of Vibration Prediction Techniques. Proc. Inst. Envir. Sci., 1963, pp. 321-326.

100. Barrett, R.E.: Techniques for Predicting Localized Vibration Environments of Rocket Vehicles. NASA TN D-1836, 1963.

101. Barrett, R.E.: Statistical Techniques for Describing Localized Vibration Environments in Rocket Vehicles. NASA TN D-2158, 1964.

102. Runyan, H.L.; Morgan, H.G.; and Mixson, J.S.: Role of Dynamic Models in Launch Vehicle Development. Experimental Techniques in Shock and Vibration (Edited by W.J. Worley), ASME, Nov. 1962, pp. 55-69.

103. Abramson, H.N.; and Nevill, G.E.: Some Modern Developments in the Application of Scale-Models in Dynamic Analysis. Use of Models and Scaling in Shock and Vibration (Edited by W.E. Baker), ASME, Nov. 1963, pp. 1-15.

104. Ezra, A.A.: Scaling Laws and Similitude Requirements for Valid Scale Model Work. Use of Models and Scaling in Shock and Vibration (Edited by W.E. Baker), ASME, Nov. 1963, pp. 57-64.

105. Belsheim, R.O.; and Young, J.W.: Mechanical Impedance as a Tool for Shock or Vibration Analysis. NRL Rept. 5409, Feb. 15, 1960. (Available from DDC as AD 234227.)

106. Schloss, F.: Inherent Limitations of Accelerometers for High-Frequency Vibration Measurements. J. Acoust. Soc. Amer., vol. 33, no. 4, Apr. 1961, p. 539.

107. Brooks, G.W.: Experimental Techniques and Apparatus. The Dynamic Behavior of Liquids in Moving Containers (Edited by H.N. Abramson), NASA SP-106, 1966, pp. 170-197.

108. Sutherland, L.C.; and Morgan, W.V.: Use of Model Jets for Studying Acoustic Fields Near Jet and Rocket Engines. Noise Control, vol. 6, no. 3, May 1960, pp. 6-12.

109. Bies, D.A.; and Franken, P.A.: Notes on Scaling Jet and Rocket Noise. J. Acoust. Soc. Amer., vol. 33, no. 9, Sept. 1961, pp. 1171-1173.

110. Wiley, D.R.; and Seidl, M.G.: Aerodynamic Noise Tests on X-20 Scale Models. AFFDL-TR-65-192, Vols. I and II, Nov. 1965.

111. Seide, P.; Weingarten, V.I.; and Morgan, E.J.: The Development of Design Criteria for Elastic Stability of Thin Shell Structures. AFBMD/TR-61-7, Dec. 31, 1960.

112. Budiansky, B.; and Hutchinson, J.W.: A Survey of Some Buckling Problems. AIAA J., vol. 4, no. 9, Sept. 1966, pp. 1505-1510.

113. Fung, Y.C.; and Sechler, E.E.: Instability of Thin Elastic Shells. Structural Mechanics (Edited by J.N. Goodier and N.J. Hoff), Pergamon Press, 1960, pp. 115-168.

114. Schloss, F.: Recent Advances in the Measurement of Structural Impedance. SAE Paper no. 426B, Oct. 1961. (Also DTMB Rept. 1584, Jan. 1963.)

115. Himelblau, H.; and Schloss, F.: Measurement of Mechanical Admittance or Impedance. Design of Vibration Isolation Systems, SAE Doc. AE-3, Pergamon Press, App. 3.7, 1961.

116. Benedetti, F.J.; and Brown, D.: A Digital System for Mechanical Impedance Measurement. SAE Paper no. 752B, Sept. 1963.

117. Hixson, E.L.: Mechanical Impedance and Mobility. Shock and Vibration Handbook, Vol. I, (Edited by C.M. Harris and C.E. Crede), McGraw-Hill Book Co. Inc., 1961, ch. 10.

118. Remmers, G.M.; and Belsheim, R.O.: Effects of Technique on Reliability of Mechanical Impedance Measurement. The Shock and Vibration Bull. No. 34, P. 3, Dec. 1964, pp. 37-58. (Available from DDC as AD 460001.)

119. Greenspon, J.E.: Modeling of Spacecraft under Random Vibration. NASA CR-132, 1964.

120. Jones, B.P.: Theory of Thermal Similitude with Applications to Spacecraft – A Survey. Astronautica Acta, vol. 12, no. 4, July 1966, pp. 258-271.

121. Gray, C.L.: Study in the Use of Structural Models for Sonic Fatigue. ASD TR 61-547, Apr. 1962. (Available from DDC as AD 277186.)

122. Grover, H.J.; Gordon, S.A.; and Jackson, L.R.: Fatigue of Metals and Structures. Govt. Print. Office, 1954, ch. 8.

123. White R.W.; Eldred, K.M.; Roberts, W.H.; and Finwall, P.E.: Investigation of a Method for the Prediction of Vibratory Response and Stress in Typical Flight Vehicle Structure. ASD-TDR-62-801 (and Supp. I), Aug. 1963 (and Apr. 1964). (Available from DDC as AD 416784 and 600234 respectively.)

124. Doggett, R.V.: Comparison of Full-Scale and Model Buffet Response of Apollo Boilerplate Service Module. NASA TM X-1202, 1966.

125. Carden, H.D.; and Herr, R.W.: Vibration Studies on a Simplified 1/2-Scale Model of the Nimbus Spacecraft. The Shock and Vibration Bull. No. 33, P. 2, Feb. 1964, pp. 57-71. (Available from DDC as AD 432931.)

126. Wiksten, D.B.: Dynamic Environment of the Ranger Spacecraft: I through IX (Final Report). Rept. JPL TR 32-909, Jet Propulsion Lab., Calif. Inst. Technol., May 1, 1966.

127. Daiber, J.R.; and Noonan, V.S.: The Vibration Design Approval and Acceptance Test Program for the Gemini Spacecraft – Component, Module and Whole Vehicle Testing. The Shock and Vibration Bull. No. 35, P. 2, Jan. 1966, pp. 139-146. (Available from DDC as AD 628599.)

128. Curtis, A.J.; Abstein, H.T.; and Varga, R.J.: On the Use of Multiple (Multi-Point) Random Excitation with Application to Surveyor Spacecraft Tests. The Shock and Vibration Bull. No. 35, P. 2, Jan. 1966, pp. 49-74. (Available from DDC as AD 628599.)

129. Schock, R.W.; Everitt, J.M.; and Seat, J.R.: Saturn S-II, S-IVB, and Instrument Unit Subassembly and Assembly Vibration and Acoustic Evaluation Programs. The Shock and Vibration Bull. No. 37, P. 5, Jan. 1968, pp. 117-137. (Available from DDC as AD 667230.)

130. Blake, R.E.; and Baird, W.S.: Derivation of Design and Test Criteria. Proc. Inst. Envir. Sci., 1969, pp. 128-138.

131. Eldred, K.M.: Vibroacoustic Environmental Simulation for Aerospace Vehicles. The Shock and Vibration Bull. No. 37, P. 5, Jan. 1968, pp. 1-11. (Available from DDC as AD 667230.)

132. Usher, T.: Average Control for Sinusoidal- and Random-Vibration Testing. J. Acoust. Soc. Amer., vol. 41, no. 4, Apr. 1967, pp. 840-849.

133. Stevens, C.L.: Vibration Response of Apollo Shell Structure to Acoustic and Aerodynamic Noise. Proc. Inst. Envir. Sci., Apr. 1967, pp. 619-627.

134. Blake, R.E.: A Method for Selecting Optimum Shock and Vibration Tests. The Shock and Vibration Bull. No. 31, P. 2, Mar. 1963, pp. 88-97. (Available from DDC as AD 403814.)

135. Choi, S.C.; and Piersol, A.G.: Selection of Test Levels for Space Vehicle Component Vibration Tests. ASQC, J. Elect. Div., vol. 4, no. 3, July 1966, pp. 3-9.

136. Forlifer, W.R.: The Effects of Filter Bandwidth in Spectrum Analysis of Random Vibration. The Shock and Vibration Bull. No. 33, P. 2, Feb. 1964, pp. 273-278. (Available from DDC as AD 432931.)

137. Curtis, A.J.: Concepts in Vibration Data Analysis. Shock and Vibration Handbook, (Edited by C.M. Harris and C.E.Crede) Vol. II, McGraw-Hill Book Co. Inc., 1961, ch. 22.

138. Vigness, I.: Instrumentation, Analyses, and Problems Concerning Shock and Vibration. Structural Mechanics, (Edited by J.N. Goodier and N.J. Hoff), Pergamon Press, 1960, pp. 506-532.

139. Vigness, I.: Field Measurements, Specifications, and Testing, Random Vibration, Vol. II, (Edited by S.H. Crandall), MIT Press, 1963, ch. 8.

140. Curtis, A.J.; Herrera, J.G.; and Witters, R.F.: Combined Broadband and Stepped Narrowband Random Vibration. The Shock and Vibration Bull. No. 35, P. 2, Jan. 1966, pp. 33-47. (Available from DDC as AD 628599.)

141. Curtis, A.J.; and Herrerra, J.G.: Random Vibration Test Level Control Using Input and Test Item Response Spectra. The Shock and Vibration Bull. No. 37, P. 3, Jan. 1968, pp. 47-60. (Available from DDC as AD 667228.)

142. Booth, G.B.; and Broch, J.T.: Analog Experiments Compare Improved Sweep Random Tests with Wide Band Random and Sweep Sine Tests. The Shock and Vibration Bull. No. 34, P. 5, Oct. 1964, pp. 67-82. (Available from DDC as AD 461200.) (Also Bruel and Kjaer Tech. Rev. No. 3, 1965.)

143. Brust, J.M.: Determination of Fragility to Meet Random and Sinusoidal Vibration Environment. SAE Paper no. 430A, Oct. 1961.

144. Otts, J.V.: Force Controlled Vibration Tests: A Step Toward Practical Application of Mechanical Impedance. J. Envir. Sci., vol. 8, no. 5, Oct. 1965. (Also The Shock and Vibration Bull. No. 34, P. 5, Feb. 1954, pp. 45-53. Available from DDC as AD 461200.)

145. Otts, J.V.; and Hunter, N.F.: Random-Force Vibration Testing. The Shock and Vibration Bull. No. 37, P. 3, Jan. 1968, pp. 61-74. (Available from DDC as AD 667228.)

146. Anon.: Environmental Test Methods. MIL-STD-810B, June 15, 1967.

147. McGregor, H.W.; Dinicola, D.; Williamson, H.; Otera, J.M.; Pitsker, J.R.; and Condos, F.M.: Acoustic Problems Associated with the Underground Launching of a Large Missile. The Shock and Vibration Bull. No. 29, P. 4, June 1961, pp. 317-335. (Available from DDC as AD 259522.)

148. Peverley, R.W.: Vibroacoustic Test Methods for Vibration Qualification of Apollo Flight Hardware. The Shock and Vibration Bull. No. 37, P. 5, Jan. 1968, pp. 153-166. (Available from DDC as AD 667230.)

149. Newbrough, D.E.; Colonna, R.A.; and West, J.R.: Development and Verification of the Vibration Test Requirements for the Apollo Command and Service Modules. The Shock and Vibration Bull. No. 37, P. 5, Jan. 1968, pp. 89-103. (Available from DDC as AD 667230.)

150. Newbrough, D.E.; Bernstein, M.; and Baird, E.F.: Development and Verification of the Apollo Lunar Module Vibration Test Requirements. The Shock and Vibration Bull. No. 37, P. 5, Jan. 1968, pp. 105-115. (Available from DDC as AD 667230.)

151. Stevens, R.A.; Allen, H.C.; and Pratt, H.K.: Vibration Qualification of Flyaway Umbilical by Acoustic Test Method. Proc. Inst. Envir. Sci., 1967, pp. 437-442.

152. Chirby, A.E.; Stevens, R.A.; and Wood, W.R.: Apollo CSM Dynamic Test Program. The Shock and Vibration Bull. No. 39, P. 2, Feb. 1969, pp. 105-121.

153. Alfonsi, P.J.: The Vibration Response of an Orbiting Geophysical Observatory Spacecraft Full-Scale Structural Model to a Simulated Launch Acoustic Environment. NASA TM X-55640, 1966. (Supersedes NASA/GSFC Rept. X-320-66-353. Available from NASA as N67-15543.)

154. Murray, F.M.: Operational Characteristics of a 100,000-Cubic-Foot Acoustic Reverberant Chamber. The Shock and Vibration Bull. No. 37, P. 5, Jan. 1968, pp. 13-24. (Available from DDC as AD 667230.)

155. Wren, R.J.; Dorland, W.D.; and Eldred, K.M.: Concept, Design and Performance of the Spacecraft Acoustic Laboratory. The Shock and Vibration Bull. No. 37, P. 5, Jan. 1968, pp. 25-54. (Available from DDC as AD 667230.)

156. Dorland, W.D.; Wren, R.J.; and Eldred, K.M.: Development of Acoustic Test Conditions for Apollo Lunar Module Flight Certification. The Shock and Vibration Bull. No. 37, P. 5, Jan. 1968, pp. 139-152. (Available from DDC as AD 667230.)

157. Lyon, R.H.: Boundary Layer Noise Response Simulation with a Sound Field. Acoustical Fatigue in Aerospace Structures. (Edited by W.J. Trapp and D.M. Forney) Syracuse Univ. Press, 1965, ch. 10.

158. Lyon, R.H.: Noise Reduction of Rectangular Enclosure with One Flexible Wall. J. Acoust. Soc. Amer., vol. 35, no. 11, Nov. 1963, pp. 1791-1797.

159. Beranek, L.L.: The Transmission and Radiation of Acoustic Waves in Solid Structures. Noise Reduction, McGraw-Hill Book Co. Inc., 1960, ch. 13.

160. Beranek, L.L.: Acoustics. McGraw-Hill Book Co. Inc., 1954.

161. Manning, J.E.; and Koronaios, N.: Experimental Study of Sound and Vibration Transmission to a Shroud-Enclosed Spacecraft. NASA CR-96144, Aug. 1968.

162. Eldred, K.M.: Problems in the Laboratory Qualification of Structures and Equipment Exposed to Intense Acoustic Environments. Proc. Inst. Envir. Sci., 1964, pp. 321-332. (Also Bozich, D.J.: Radiation Damping of Panels Mounted in Ducts, Rept. WR 64-4, Wyle Labs., June 1965.)

163. Bianchi, R.A.; Bradshaw, R.T.; Farrell, J.H.; and Reed, F.E.: Survey and Evaluation of Sonic Fatigue Testing Facilities. ASD-TR-61-185, Mar. 1962. (Available from DDC as AD 277124.)

164. Kirchman, E.J.; and Arcilesi, C.J.: Advanced Combined Environmental Test Facility. The Shock and Vibration Bull. No. 37, P. 3, Jan. 1968, pp. 175-192. (Available from DDC as AD 667228.)

165. Subcommittee G-5.9 on Telemetry Requirements, SAE Committee G-5 on Aerospace Shock and Vibration: Desired Telemetry System Characteristics for Shock, Vibration and Acoustic Measurements. Proc. International Telemetering Conference. Vol. II, 1966, pp. 232-253.

166. Telemetry Working Group, Inter-Range Instrumentation Group: Telemetry Standards. IRIG Doc. 106-66, rev. Mar. 1966.

167. Anon: Composite Construction for Flight Vehicles. Part III-Design Procedures, Rev. Oct. 1962.